University of Alberta

Activity of Nanocrystalline Gold and Silver Alloys

by

Kevin Robert Unrau

A thesis submitted to the Faculty of Graduate Studies and Research

in partial fulfillment of the requirements for the degree of

Master of Science

in

Chemical Engineering

Department of Chemical and Materials Engineering

Spring 2012

Edmonton, Alberta

Abstract

Gold and silver dressing alloys were created by DC magnetron sputtering and compared with pure silver nanocrystalline dressings using conventional biological and physical characterization techniques. While the gold/silver dressings were weaker antimicrobials than the pure silver nanocrystalline structures, the addition of gold reduces the minimum crystallite size from 17 to 4 nm. This increases the number of grain boundary atoms from 12 to 40% which could augment the anti-inflammatory properties of the dressings. The formation of gold oxide (Au_2O_3) could be responsible for the observed decrease in crystallite size. Increasing the oxygen content of the dressings increased antimicrobial potency and dressing longevity. The oxygen tended to be combined in O-O bonds rather than Ag-O bonds. Heat treatment reduced both the antimicrobial and longevity parameters of the dressings. Sterilization by electron beam irradiation was determined to preserve the antimicrobial and longevity properties of the dressing the best.

Acknowledgements

First and foremost, I would like to acknowledge my supervisor Dr. Robert Burrell for his support and direction over the duration of this Master's project. His knowledge of silver, guidance and facilities have been indispensible for completing this project.

I would also like to thank the following people for their respective contributions to this project: Dr. William McCaffrey for lab space to complete the biological testing, Dr. Dimitre Kapruzov of ACSES for help with x-ray photoelectric spectroscopy and energy-dispersive x-ray-spectroscopy analysis, Shiraz Merali of Chemical Engineering for his assistance with atomic absorption spectroscopy, Dr. Loredana Dorobantu for her assistance with atomic force microscopy, Dr. Patricia Nadworny for teaching me biological testing methods and providing me with analysis software and especially my summer students Marion Cavanagh, On Kwan Cheng, Warren Chung and Tracy Wang who all contributed significantly to both the log reduction and corrected zone of inhibition data presented in this thesis.

Table of Contents

List of Tables

List of Figures

Nomenclature

AAS	Atomic Absorption Spectroscopy
AFM	Atomic Force Microscopy
Ag_x	Silver or silver/gold dressing where x is the weight percent of the target the dressing was sputtered with
Atm%	Atomic Percentage
CZOI	Corrected Zone of Inhibition
d/w	De-ionized Water
DC	Direct Current
EDS	Energy-Dispersive X-ray-Spectroscopy
ICP	Inductively Coupled Plasma
MS	Mass Spectroscopy
SEM	Scanning Electron Microscopy
SPS	Sodium Polysorbate (Thioglycolate) Solution
XPS	X-ray Photoelectric Spectroscopy
XRD	X-ray Diffraction

Chapter 1 – Introduction, Motivation, Scope and Experimental Plan

Introduction

Silver has a long history of medicinal use [1] and nanocrystalline silver dressings have been researched extensively due to their antimicrobial and anti-inflammatory properties. [2,3,4] These dressings are widely used in clinical settings because of their ease of use, longevity and clinically proven effect of reducing healing times versus conventional alternatives. [5] A commercial nanocrystalline silver dressing (Acticoat®) is composed of nanocrystals of silver deposited by direct current (DC) magnetron sputtering. This deposition technique creates a high surface area structure which is thought to aid in the release of ionic silver and contribute to the number of grain boundary silver atoms which allow for the release of Ag^0. [6] While antimicrobial properties are attributed to the ionic silver species the anti-inflammatory properties are thought to be a result of the release of inert silver. [4]

Similarly to silver, gold and gold complexes have also been extensively used in medicine [7,8] and both their antimicrobial and anti-inflammatory properties have been demonstrated. [9,10] Furthermore, (DC) magnetron sputtering deposition of gold has resulted in fabric coatings that are antimicrobial *in vitro*. [9] Nanocrystalline gold has also been researched for its application to oxidation reaction catalysis [11] and nanocrystalline semi-conductors [12], but these materials are more correctly called gold nanoparticles for, as Tjong and Chen (2004) define the terms, nanocrystalline materials are "polycrystalline bulk materials with grain sizes in the nanometer range" while nanoparticles are "ultrafine dispersive particles with diameters below 100nm." [13]

Table 1.1 shows relevant properties of gold and silver. Both elements form face-centered cubic (FCC) crystal structures and have similar lattice constants and atomic radii. This would suggest that they should replace each other one-to-one in a crystal lattice. This principle has been supported where the co-reduction of chlorauric acid ($HAuCl_4$) and silver nitrate ($AgNO_3$) yielded alloyed nanocrystals.[14] Furthermore, it is important to note that gold is significantly more electronegative then silver – 2.54 on the Pauling scale compared to 1.93.

Table 1.1. Atomic parameters of gold and silver.

	Crystal Structure	Lattice Parameter (nm) [14]	Ionization Energy (kJ/mol) [15]	Electronegativity (Pauling Scale) [15]	Atomic Radius (pm) [15]
Gold	FCC	0.408	923	2.54	146
Silver	FCC	0.409	758	1.93	144

The sputtering process itself is a physical vapour deposition technique where atoms are condensed (one-by-one or in small clusters) on a surface from a low pressure vapour phase. A schematic of the technique is shown in Figure 1.1.

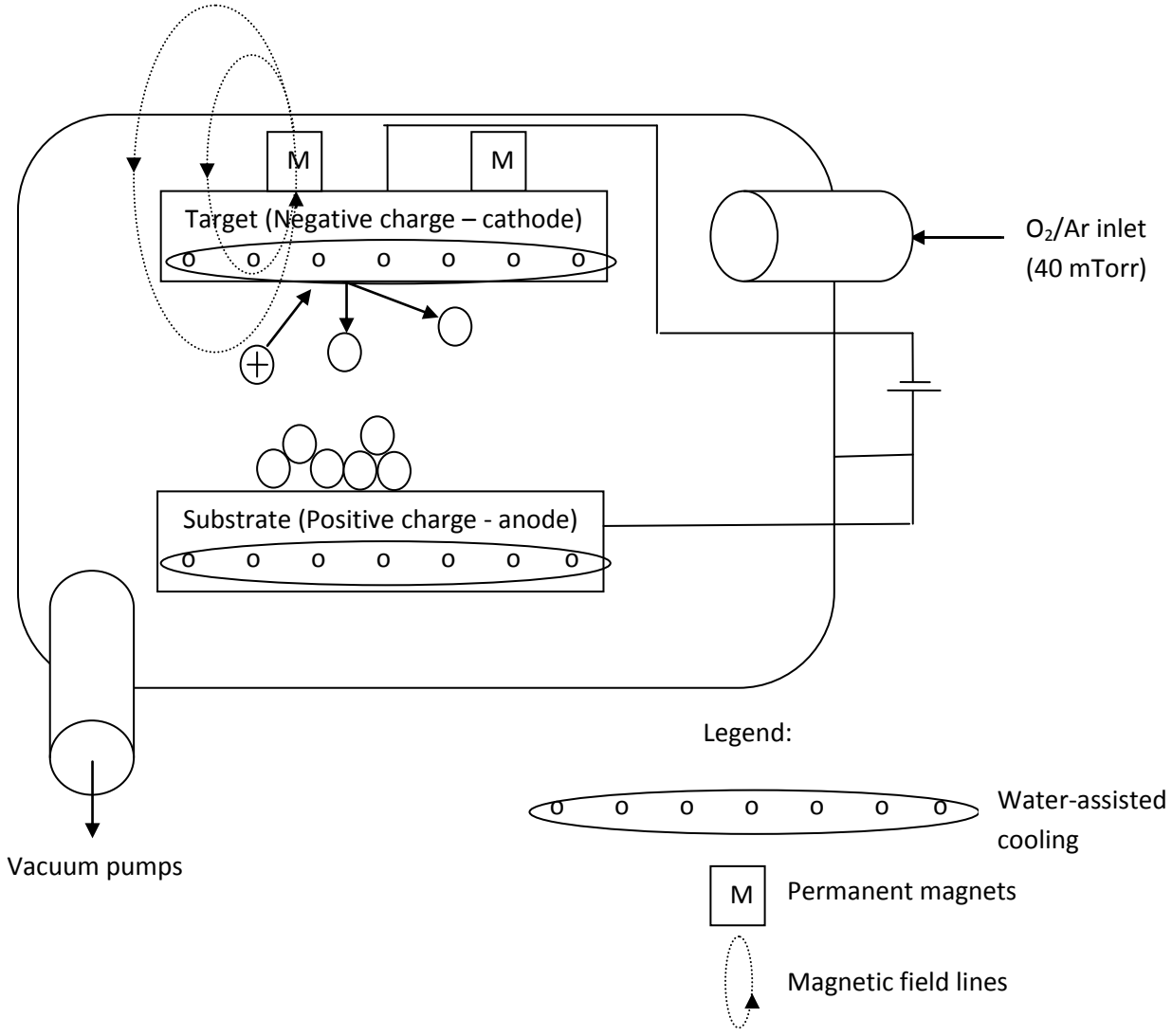

Figure 1.1. A schematic of a planar diode magnetron sputtering system.

In this process a vacuum pump maintains the environment at a low pressure while oxygen and argon flow rates can be specified to control the gas composition and pressure in the sputtering chamber. A voltage applied from the cathode to ground creates an ionized gas (Ar^+ and a complex oxygen mixture). This plasma is magnetically confined by the permanent magnets and attracted towards the negatively charged target through electrostatic interactions. At the target surface, a ballistic collision results in the ejection of atoms from the target crystal lattice. The ejected atom is usually not the atom struck by the initial collision, but a series of energy transfers between atoms in the crystal lattice result in the ejection of an atom a few angstroms away. [16] The vast majority of ejected atoms are not in cluster form and are in the netural oxidation state (the fraction of charged atoms or particles sputtered from a clean, pure metal is around 10^{-4}); however, the number of charged particles can be increased by sputtering with a target that has two species with different electronegativities. [17] The amount of material that is ejected from the target is dependent on the sputtering yield of the material on the target which is a function of how tightly the individual atoms are bound to their nearest neighbour.

Figure 1.2 shows the sputtering yield (in atms per ion impact) versus ion energy of an argon-based sputtering process. While silver is preferentially sputtered at ion energies below 3900 eV, gold is preferentially sputtered above this value. Data for Figure 2 was adapted from Bunshah 1994. [16]

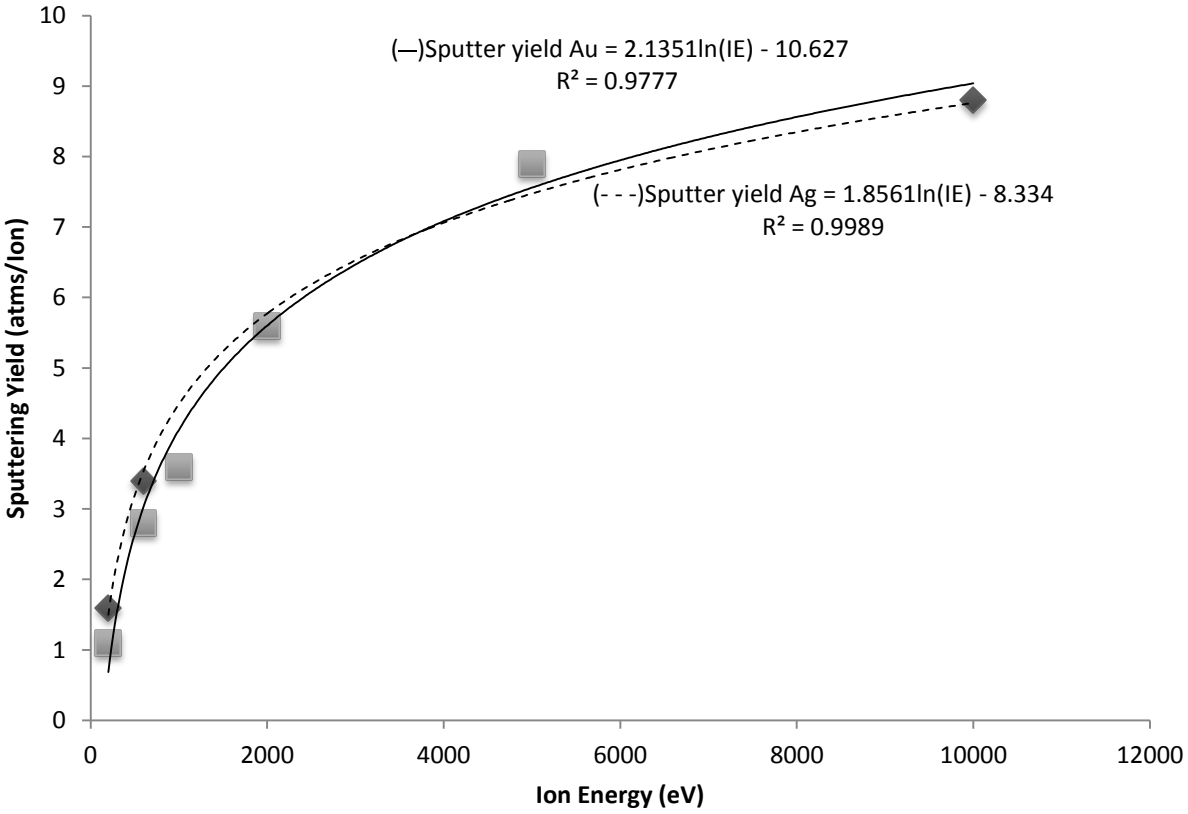

Figure 1.2. Sputtering yields of gold and silver at various ion energies.

After ejection from the target the atom can travel in a relatively straight line of sight (directional sputtering) or with more of a diffusive motion (diffusional sputtering) towards the target where it condenses on the substrate. Silver atoms are known to interact with oxygen in the plasma and gas phases creating silver oxide and other silver oxygen complexes. The silver oxide is thought to be responsible for pinning the silver nanostructure creating the dressing's columnar appearance. This is evidenced by silver sputtering in the absence of oxygen which results in a relatively planar film deposited on the substrate.

One characteristic of the Extreme Sputtering Machine at the University of Alberta is that the targets can be removed to sputter with target of different compositions. To do this, the target and backing plate must be heated in a 220^{o}C furnace so that the solder connection melts and the target can

be slid relative to the backing plate. New solder can be placed between the new target and the backing plate and melted in the furnace such that a continuous joint is made.

Traditionally, nanocrystalline silver dressings are sputtering in 4% oxygen (the balance argon) for 30 minutes. This creates a film about 900 nm thick and has 3 mg of silver per inch squared. [18] The silver film has usually been sputtered on high density polyethylene (HDPE) mesh. A single piece of rayon/polyester non-woven gauze is placed between the two HPDE sputtered layers to create a water absorbent layer since the sputtered dressing is highly hydrophobic. This increases the contact between the bacteria-laden wound exudates and the dressing while silver ions and clusters are released into solution.

After fabrication, dressings are sterilized using 25 kGy of electron-beam (E-beam) irradiation. This sterilization treatment achieves a sterility assurance level of 10^{-6}. Bioburden testing of these samples showed that 16 Colony Forming Units remained in roughly $3x10^{6}$ in^{2} of sterilized dressing. (personal communications, Dr. Burrell).

Motivation and Scope

It has been established that nanocrystalline silver is an effective antimicrobial and anti-inflammatory agent. [2,4,18] Since it is also known that gold also has these properties, the central question of this report is whether gold/silver nanocrystalline alloys can be produced that rival or surpass the properties of nanocrystalline silver. There were two limitations imposed on this study to limit the scope of the project. Firstly, only alloys were tested and not pure sputtered gold. While scientifically relevant, sputtering pure gold was determined to be cost prohibitive and therefore not studied in this report. Secondly, only the antimicrobial properties of the dressing were studied in addition to the chemical and physical characterization of the dressing. This limitation was placed on the study as *in vivo* characterization of the dressings was determined to be too extensive for a Master's thesis.

From the central question posed above and the following limitations, the following questions were developed:

1) Can nanogold/silver alloys be created?

2) Are they effective antimicrobials? If so, for how long?

3) How does the physical structure (morphology, composition, etc.) of the dressing compare to that of nanocrystalline silver?

4) How does the dissolution rate of the dressing compare to that of nanocrystalline silver?

5) How do these chemical and physical properties change when exposed to heat?

6) How do these chemical and physical properties change when the dressings are sputtered with different oxygen levels?

7) Can we sterilize these dressings without a significant change in their chemical, physical and biological properties?

Experimental Plan

Table 1.2 shows the experimental plan that was developed based on the guiding questions above and the imposed limitations. It is formatted such that the question is first, followed by the techniques used to evaluate the questions and finally the thesis chapter where the answer of the question is given.

Table 1.2. Experimental questions and approaches to solve those questions.

1) Can nanogold/silver alloys be created?	Techniques: DC Magnetron Sputtering and Scanning Electron Microscopy (SEM). Chapter: 2
2) Are they effective antimicrobials? If so, for how long?	Techniques: Log Reduction (LR) and Corrected Zone of Inhibition (CZOI) Chapter: 2
3) How does the physical structure (morphology, composition, etc.) of the dressing compare to that of nanocrystalline silver?	Techniques: X-ray Diffraction (XRD), X-ray Photoelectron Spectroscopy (XPS), Atomic Force Microscopy (AFM), SEM and Energy Dispersive X-ray Spectroscopy (EDS) Chapter: 2
4) How does the dissolution rate of the dressing compare to that of nanocrystalline silver?	Techniques: Atomic absorption spectroscopy (AAS) and Inductively Coupled Plasma (ICP) Chapter: 2
5) How do these chemical and physical properties change when exposed to heat?	Techniques: XRD, XPS, EDS, AFM, LR and CZOI Chapter : 3
6) How do these chemical and physical properties change when the dressings are sputtered with different oxygen levels?	Techniques: DC Magnetron Sputtering, XRD, XPS, EDS, AFM, LR and CZOI Chapter : 3

7) Can we sterilize these dressings without a significant change in their chemical, physical and biological properties?	Techniques: DC Magnetron Sputtering, Ethylene Oxide (EO) Sterilization, Gamma (γ) Sterilization, Electron beam (E-beam) Sterilization, LR and CZOI Chapter : 4

References

1. Chopra I. **The increasing use of silver-based products as antimicrobial agents: a useful development or a cause for concern?.** *Journal of Antimicrobial Chemotherapy.* 2007;59:587-90.

2. Bhol KC, Schechter PJ. **Effects of Nanocrystalline (NPI 32101) in a Rat Model of Ulcerative Colitis.** *Dig Dis Sci.* 2007;52:2732-42.

3. Poon VKM, Burd A. **In vitro cytotoxicity of silver: implication for clinical wound care.** *Burns.* 2004;30:140-147.

4. Nadworny PL, Landry BK, Wang J, Tredget EE, Burrell RE. **Does nanocrystalline silver have a transferable effect?.** *Wound Repair and Regerenation.* 2010;18:254-265.

5. Huang Y, Li X, Liao Z, Zhang G, Lui Q, Tang J, Peng Y, Liu X, Luo Q. **A randomized comparative trial between Acticoat and SD-Ag in the treatment of residual burn wounds, including safety analysis.** *Burns.* 2007;33:161-166.

6. Fan F, Bard AJ. **Chemical, Electrochemical, Gravimetric, and Microscopic Studies on Antimicrobial Silver Films**. *Journal of Physical Chemistry B.* 2002;106:279-287.

7. Mody VV, Siwale R, Singh A, Mody HR. **Introduction of metallic nanoparticles**. *J Pharm Bioallied Sci.* 2010;2(4):282-89.

8. Messori L, Marcon G. **Gold Complexes in the Treatment of Rheumatoid Arthritis.** In: Sigel A, Sigel H, editors. *Metal Ions in Biological Systems.* Volume 41. CRC Press; 2004: Chapter 9.

9. Scholz J, Nocke G, Hollstein F, Weissbach A. **Investigations on fabrics coasted with precious metals using the magnetron sputter techniques with regard to their anti-microbial properties.** *Surface & Coatings Technology.* 2005;192: 252-256.

10. Zainali K, Baas J, Jakobsen T, Danscher G, Soballe K. **Particulate gold as an anti-inflammatory mediator in bone allograft – An animal study.** *J Biomedical Materials Research A.* 2010;95A: 956-63.

11. Hutchings GJ. **Nanocrystalline gold and gold palladium alloy catalysts for chemical synthesis.** *Chem. Commun.* 2008;10:1148-64.

12.Zhang J, Gao Y, Alvarez-Puebla RA, Buriak JM, Fenniri H. **Synthesis and SERS Properties of Nanocrystalline Gold Octahedra Generated from Thermal Decomposition of $HAuCl_4$ in Block Copolymers.** *Adv. Mater.*2006;18:3233-37.

13. Tjong SC, Chen H. **Nanocrystalline materials and coatings.** *Materials Science and Engineering* 2004, 45:1-88.

14. Link S, Wang L, El-Sayed A. **Alloy Formation of Gold-Silver Nanoparticles and the Dependence of the Plasmon Absorption on Their Composition.** *J. Phys. Chem. B.* 1999;103: 3529-33.

15. Knovel.com. New York: Knovel Corporation; 2010 [cited 2 December 2011]. Available from: http://www.knovel.com/web/portal/periodic_table.

16. Bunshah RF, McGuire GE, Rossnagel SM, editors. Handbook of Deposition Technologies for Films and Coatings. Second ed. Park Ridge (NJ): Noyes Publications; 1994.

17. Cuomo JJ, Gambino RF, Harper JME, Kuptsis JD, Weber JC. **Significance of negative ion formation in sputtering and SIMS analysis.** Vac. Sci. Technol. 1978;15:281-288.

18. Wright JB, Hansen DL, Burrell RE. **The Comparative Efficacy of Two Antimicrobial Barrier Dressings: In-vitro Examination of Two Controlled Release Silver Dressings.** *Wounds.* 1998;10:179-188.

Chapter 2 – Nanogold/silver Dressing Fabrication and Analysis

Introduction

Studies have demonstrated that nanocrystalline silver is an effective antimicrobial [1,2] and numerous reports have characterized the physical and chemical properties of this dressing. [3,4] Due to the extensive literature concerning gold as an effective anti-inflammatory [5-7] and antimicrobial [8,9] agent, it was questioned whether its incorporation into a nanosilver dressing would augment the nanocrystalline silver dressing's properties. The feasibility of this study was supported by the remarkably similar physical properties of gold and silver atoms (atomic size, crystal structure, etc.).

While this Chapter focuses on quantifying the physical and chemical properties of gold/silver dressings, the data obtained will be necessary to begin to quantify new silver and gold species that may be created on or released from these dressings. Due to the sputtering deposition process which condenses atoms one-by one, the silver structure is in a highly energized state because of the large number of grain boundaries and material defects. Both of these are properties of nanocrystalline structured materials are thought to contribute to the release of Ag^0 in cluster form. Furthermore, a study by Fan and Bard (2002) supports the hypothesis that higher oxidation state species of silver are present in the dressing and able to be released into the wound environment. [10] While specifying how the addition of gold will affect the concentrations and actions of the ionic silver, cluster-form silver and silver oxide compounds is out of the scope of this project, it will be useful to use clues derived from the biological and physical assays to hypothesize how the addition of gold affects the silver release profile.

This preliminary chapter seeks to show that nanocrystalline gold/silver dressings can be created reproducibly and characterize these dressings using conventional biological and physical techniques.

Materials and Methods

All materials were purchased from Fisher Scientific Inc. unless otherwise indicated.

Dressing Fabrication:

Acticoat® was purchased commercially (Acticoat®, Smith and Nephew Inc., Largo, Fl). Since gold dressings are not available on the market, all other gold and silver dressings were produced by batch sputtering in our in-house Extreme sputtering machine at the University of Alberta. A base pressure of $2x10^{-5}$ Torr and an aquatrap temperature of 200 K were obtained before the system was sealed from the pump and a leak test was preformed. A leak rate of less than 1 mTorr per minute was considered acceptable. The silver and gold/silver alloys were then sputtered onto high density polyethylene mesh. The targets had a variable weight percent silver with the balance gold. The five targets employed in the study were: all silver (Ag_{100}), 80wt% silver (Ag_{80}), 50wt% silver (Ag_{50}) and 35 wt% silver (Ag_{35}). The nomenclature Ag_{100}, Ag_{80}, Ag_{50} and Ag_{35} will hereafter be used to refer to the dressings created from these targets unless otherwise specified. For clarification, a dressing will be called Ag_{80} because it was sputtered with a target that had 80wt% silver, not because the dressings contains 80wt% silver. While targets with gold were treated as experimental groups, the Ag_{100} dressing was used as a control for Acticoat® to ensure the sputtering process was similar since both products are produced by sputtering 100% Ag. The working pressure of the sputtering machine was 40 mTorr (4% O_2 with the balance Ar). The dressings were sputtered using a constant current of 0.9 A. This resulted in an applied voltage of 300 ± 10 V between the target and substrate (ground). After each dressing was sputtered, the full mesh was removed from the sputtering machine and the sample directly under the middle of the target (a total of $10in^2$ per batch) was immediately cut from the HDPE mesh, placed in sterile bags and stored in the dark at 4^oC.

Log Reduction:

To quantify the bactericidal properties of each of the dressings, log reduction analysis was performed in triplicate using the same method as Taylor et al 2005. [3] To obtain bacteria in the log-phase growth, first 2 to 3 isolated colonies of *Pseudomonas aeruginosa* (ATCC 27317, Cedarlane, ON), *Staphylococcus aureus* (ATCC 25923, Cedarlane, ON) or *Proteus mirabilis* (ATCC 25933, Cedarlane, ON) were used to inoculate a flask containing 100 mL of tryptic soy broth (TSB) and the flask was incubated overnight in a rotary shaker at 37°C and 120 rpm. The next morning, one milliliter of this culture was used to inoculate another 100 mL of TSB and incubated for 4 hours under identical conditions. Experimental groups were prepared as follows. An aseptically-cut 1 in^2 (6.45 cm^2) piece of dressing was placed coated-side up on a sheet of plastic (3 cm^2) in an inverted Petri dish lid and inoculated with 0.3 mL of the log phase bacteria. The inoculated dressing was covered with another layer of plastic followed by the upright Petri dish bottom to apply pressure. The inoculated dressings were incubated for 30 mins at 37°C. After incubation, the dressing was immediately placed in 2.7 mL of sodium polysorbate solution (SPS) containing 3.0g of NaCl, 0.050g of sodium thioglycolate, 0.50mL of Tween 20 and 0.050g of sodium thiosulphate in 50 mL of deionized water. This solution was used to inactivate the metal ions in the experimental groups and aid in bacterial recovery. By placing the dressing in the SPS, a 1 in 10 dilution was realized. The mixture was then vigorously mixed with a vortex in order to recover bacteria and inactivate noble metals. For control groups, 0.3 mL of the log-phase bacteria was used directly to inoculate 2.7 mL of SPS. The resulting experimental and control solutions were serially diluted to 10^{-6} and 10^{-8} respectively by transferring 0.1 mL to 0.9 mL of phosphate buffered saline (PBS) five times and mixing with a vortex between transfers. Three 20 μL drops of each dilution were pipetted onto tryptic soy agar (TSA), incubated at 37°C for 24 h and then individual colonies were counted. The CFUs from the control groups were used to determine the $\log_{10}$ of bacteria in the original inoculum while the CFUs from the experimental groups were used to calculate the $\log_{10}$ of surviving bacteria. These two values were

subtracted to yield the log reduction number. Additionally, silver nitrate or gold chloride dressings were made by pipetting 0.25 mL of log phase bacteria with 0.05 mL of $AgNO_{3(aq)}$ or $AuCl_{3(aq)}$ solutions on a three-layered dressing consisting of the same materials as the other dressings tested (i.e. mesh-gauze-mesh). 1.5 mg of $AgNO_3$ or $AuCl_3$ was added (after dissolution in de-ionized water (dH_2O)) to yield final concentrations of 0.5% of gold chloride or silver nitrate. These values were chosen as this level of silver has been shown to be effective in reducing wound contamination in clinical settings. [11] Controls of SPS were also completed to ensure the solution was not toxic to the microorganisms. Sample calculations for calculating amount of $AgNO_3$ or $AuCl_3$ to add are shown in Appendix 2A.

Corrected Zone of Inhibition (CZOI):

The revised form of the Kirby-Bauer assay was used to assess the dressing longevity. [12] *Pseudomonas aeruginosa* was grown to log phase as described for the log reductions. An aseptically-cut 1 in^2 piece of each dressing was placed coated-side down in the center of an inoculated plate and moistened to saturation with 0.3 mL of dH_2O. The plates were covered with their Petri dish lid and incubated overnight at 37°C. The dressings were transferred to a new log-phase bacteria lawn daily. If the dressings appeared dry, they were moistened with 0.1 mL of dH_2O. A total of six transfers were made over a period of seven days. Every day, the zones of bacterial inhibition were measured in two perpendicular directions. The dressing width was subtracted from the zone width for both directions and their results were averaged to yield the CZOI values. Tests were performed in triplicate.

A second set of log reductions was completed on dressings which had been subjected to three days of CZOI testing.

Scanning Electron Microscopy (SEM)/ Atomic Force Microscopy (AFM):

SEM and AFM analysis was used to image the surface microstructure and determine the roughness of the dressing samples, repectively. SEM testing was completed at the Alberta Centre for Surface Engineering and Sciences (ACSES). A JAMP 9500F auger microprobe was used to image

subsections of a $1in^2$ dressing sample by SEM. SEM images were taken between 10μm and 100nm scales. AFM images were taken to confirm SEM images and calculate the roughness of the dressings. For roughness calculations, a 25 nm^2 image was obtained at using an Olympus 160TS tip. MFD-3D from Asylum Research (Santa Barbara, CA), controlled by IGOR PRO software (Wavemetrics, Portland, OR), calculated the roughness on three $1nm^2$ subsections of the image located at (0.5nm,0.5nm), (2.5nm,2.5nm) and (4.5nm,4.5nm). These values were then averaged to give an average roughness for the dressing sample. The roughness was calculated by the RMS roughness given in Figure 2.1.

$$R_{rms} = \sqrt{\frac{\sum_{i=1}^{n}(z_i - z^-)^2}{n}}$$

Figure 2.1. RMS Roughness formula for calculating roughness using the AFM height retrace.

Energy Dispersive X-ray Spectroscopy (EDS):

EDS was used to analyse the bulk dressing composition since the separation of the XRD peaks led to high error when deconvolution was attempted. While this technique is not typically used for bulk concentration, the samples in this study are less than 900 nm thick and the penetration depth of the X-rays is on the order of micrometers permitting bulk analysis via this tecnique. EDS was completed on a $20mm^2$ oxford x-max detector attached to a VEGA3 SEM at ACSES. A working distance of 10.0 mm was used and a dead time of 40% was acquired by increasing the beam intensity to between 15 and 17 nA before data acquisition began. A copper signal was omitted from the data as copper tape was used to adhere the sample to the target holder. When carbon tape was used instead of copper tape it was noticed that the copper signal disappeared and the carbon signal increased. Peak significance was ensured by verifying that the fit index for the peak was less than 10. For gold peaks a fit index of up to 15 was accepted as dissolution data showed that the data was still reliable. This check is shown in Appendix 2B.

X-ray Diffraction (XRD):

Gold and silver dressings were analysed by XRD using a RIGAKU rotating anode XRD system in the Chemical and Materials Engineering Department at the University of Alberta. The dressings were scanned from 10 to 110 $^{o}2\theta$ in continuous mode using a step size of 0.05$^{o}2\theta$. A copper anode was used at a voltage of 40 KV and current of 110mamps. Minimum crystallite sizes were determined by the Scherrer method. [13] The values for minimum crystallite size were obtained by averaging the minimum crystallite size calculated from peaks at 44 and 64.5 $^{o}2\theta$. The Scherrer equation in Figure 2.2 was used for this calculation. In this equation, τ is the crystallite size, K is the shape factor and was assumed to be 0.9, λ was 1.54nm with a Cu anode, β is the full width at half maximum in $^{o}2\theta$ and θ is the width the peak spans in $^{o}2\theta$.

$$\tau = \frac{K\lambda}{\beta \cos\theta}$$

Figure 2.2. The Scherrer Equation for determining minimum crystallite size.

X-ray Photoelectric Spectroscopy (XPS):

Dressings were analysed by XPS at the ACSES facility. To obtain the spectra, an Axis 165 spectrometer (Kratos Analytical) with a monochromatic Al Ka source was used at a power of 210W. The samples were analysed at 3 x 10^{-10} Torr and a normal take off angle. The pass energy of 160eV was used for the survey spectra and a pass energy of 20 eV was used for the high-resolution spectra. Spectra were analysed using linear background corrections and Gauss/Lorentz approximations in CasaXPS software (Version 2.3.15© 1999-2009 Neal Fairley). The peaks were calibrated to a C1s signal at 284.8eV. The deconvolution of XPS peaks was considered acceptable when the Chi squared value was less than 50 without the RMS fitting option. No constraints were placed on the peaks when fitting them with the CasaXPS software.

Atomic Absorption Spectroscopy (AAS):

The release of silver into dH_2O and ammonium hydroxide (NH_4OH) were studied with AAS at the University of Alberta using methods similar to those of Wright et *al.* [12] For de-ionized water samples, one in^2 of dressing was placed in 10mL of de-ionized water for 24 hours at room temperature. After 24 hours, the dressing was removed with forceps and allowed to drip back into the vial for 10 s. The 10mL of water and dissolved silver was then acidified with 10 mL of nitric acid acidification solution (18% nitric acid/1.8% tartaric acid). The acidification prevented silver precipitation before analysis. No filtration was required as no visible particulate silver was present in the solutions. For the NH_4 samples, 1 in^2 of dressing was placed in 10mL of 20.0g/L ammonium hydroxide for 3 minutes. The samples were also acidified with 10 mL of acidification solution. Both water and NH_4OH samples were submitted for total silver analysis on a Varian 220 FS double beam Atomic Absorption Spectrophotometer. A lean air-acetylene flame and a silver hollow cathode lamp (λ = 328.1 nm) were used with this spectrophotometer. Samples were diluted if the silver concentration was greater than the upper limit of the calibration plot (5.0ppm). The results were then corrected for the applied dilution factor.

Inductively Coupled Plasma – Mass Spectroscopy (ICP-MS):

Gold release was too small to be measured by AAS, so ICP was used as it can provide a much more accurate measurement. dH_2O dissolutions were made by submersing 1 in^2 of dressing in 10mL of de-ionized water for 24 hours at room temperature. After 24 hours, the dressing was removed with forceps and allowed to drip back into the vial for 10 s. The 10mL of water and gold was then acidified with 10 mL of aqua regia. The aqua regia is known to dissolve gold and precipitate silver. Furthermore, dissolution of 1 in^2 of dressing into 20 mL of aqua regia was used to determine the total amount of gold in the dressing samples. Both the dH_2O dissolution and the total gold digest were measured in the University of Alberta's Radiogenic Isotope Facility using a Perkin Elmer Elan6000 quadrupole ICP-MS. A

calibration plot up to 300 ppm was created using a gold standard stock solution of 1000ppm. dH_2O samples were diluted by a factor of 10 and aqua regia dissolution samples were diluted by a factor of 1000 before measurement. The dilution factor was re-applied after analysis.

Statistics:

One way ANOVA with Tukey-Kramer Multiple Comparisons were performed using GraphPad Instat version 3.10. For log reductions, only trials with exact numbers (i.e. not greater than numbers) were statistically analysed. This method was also used to test for statistical significance in the CZOI, AFM and dissolution (AAS and ICP) data.

Results

Log Reduction:

Table 2.1 summarizes the log reduction results of the different dressing alloys using three different bacteria strains. A log reduction of 3 or greater is considered bactericidal. [1] A greater than symbol is used when the observed log reduction was beyond the upper limit which could be measured by the test. In this case statistics and interpretations cannot be made on the data point except for noting that the dressing is highly antimicrobial to this specific organism. While all dressings recorded a complete kill for *S. aureus* and *P. aeruginosa*, only Acticoat®, Ag_{100} and Ag_{80} were bactericidal when challenged with *P. mirabilis*.

Table 2.1. Log Reductions of silver/gold dressings against different bacteria. Shown as log reduction number ± standard deviation.

	S. aureus	*P. aeruginosa*	*P. mirabilis*
Acticoat	≥ 4.32	≥ 4.65	4.78 ± 0.05
Ag100	≥ 4.32	≥ 4.65	≥ 6.65
Ag80	≥ 5.03	≥ 5.01	4.02 ± 0.05
Ag50	≥ 5.01	≥ 5.01	2.29 ± 0.15
Ag35	≥ 5.03	≥ 5.08	1.67 ± 0.17

Log reductions on Table 2.2 were conducted after the dressings has been exposed to *P. aeruginosa* by CZOI testing for three days. There was no significant different between the log reduction values of the two dressings tested.

Table 2.2. Log Reductions of silver/gold dressings against *P. aeruginosa* after three days of CZOI testing. Shown as log reduction number ± standard deviation.

	P. aeruginosa
Acticoat®	4.23 ± 0.23
Ag50	4.45 ± 0.19

Table 2.3 displays the log reduction observed for a 30 minute exposure of 0.5% gold oxide or silver nitrate to log phase *P. aeruginosa*. The differences in kill between gold and silver trials is not statistically significant.

Table 2.3. Log Reductions by 0.5% solutions of $AgNO_3$ and Au_2O_3.

	P. aeruginosa
Gold Oxide	2.36 ± 0.34
Silver Nitrate	2.07 ± 0.45

Corrected Zone of Inhibition:

CZOIs for seven days are shown in Figure 2.3. While no significant differences were observed in the zone sizes on day 1, by day 7 Acticoat and Ag_{100} produced significantly larger inhibitory zones than the other dressings studied ($p<0.001$). Dressings with no gold also showed an increase in zone size from day 1 to day 3 ($p<0.01$) while those with higher gold content displayed a stagnant zone size. The zone size appeared to correlate with the amount of silver in the dressing.

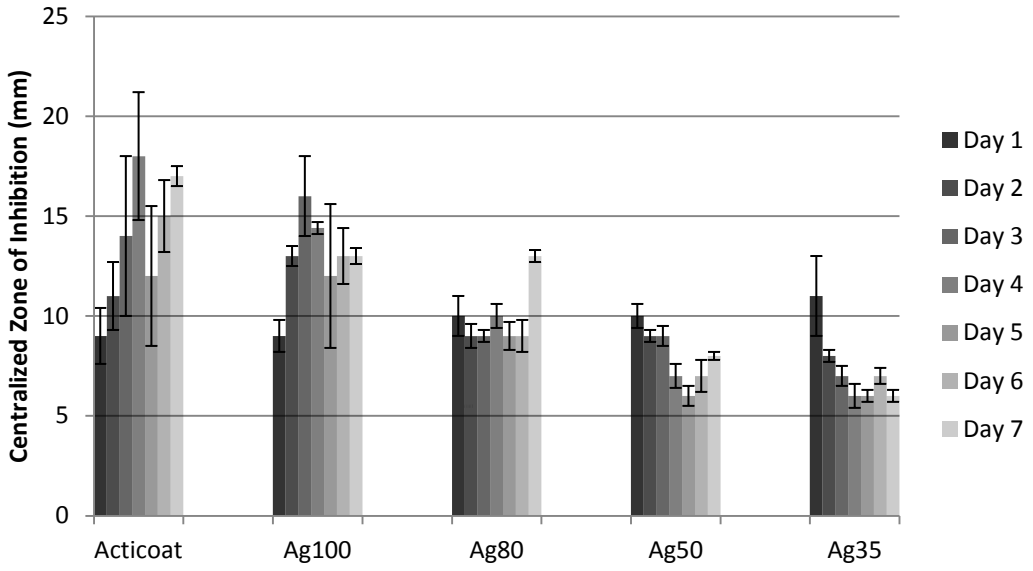

Figure 2.3. 7 day CZOI for silver/gold dressings against *P. aeruginosa*. Shown as corrected zone ± standard deviation.

AFM/SEM:

Roughness calculations from AFM images are shown in Table 2.4 and sample SEM images are shown in Figure 2.4. Overall, it can be seen that the structure gets less rough as the gold concentration increases. A notable statistically significant difference was that all dressings were smoother than Acticoat®($p<0.05$); however, no significant difference was observed between all other samples. This observation is supported by the SEM images obtained for the dressings. Note that images for Ag_{50} and Ag_{35} were obtained on a smaller scale and thus appear coarser. The sharp columnar structure of Ag_{100} smoothes out until the nanostructure lacks a significant column structures (seen in the Ag_{35} sample).

Table 2.4. Summary of roughness determined by AFM. Values are standard deviation of surface ± standard deviation.

Acticoat	Ag100	Ag80	Ag50	Ag35
45.1 ± 8.5	26.0 ± 6.1	30.1 ± 5.52	15.3 ± 3.2	21.6 ± 1.4

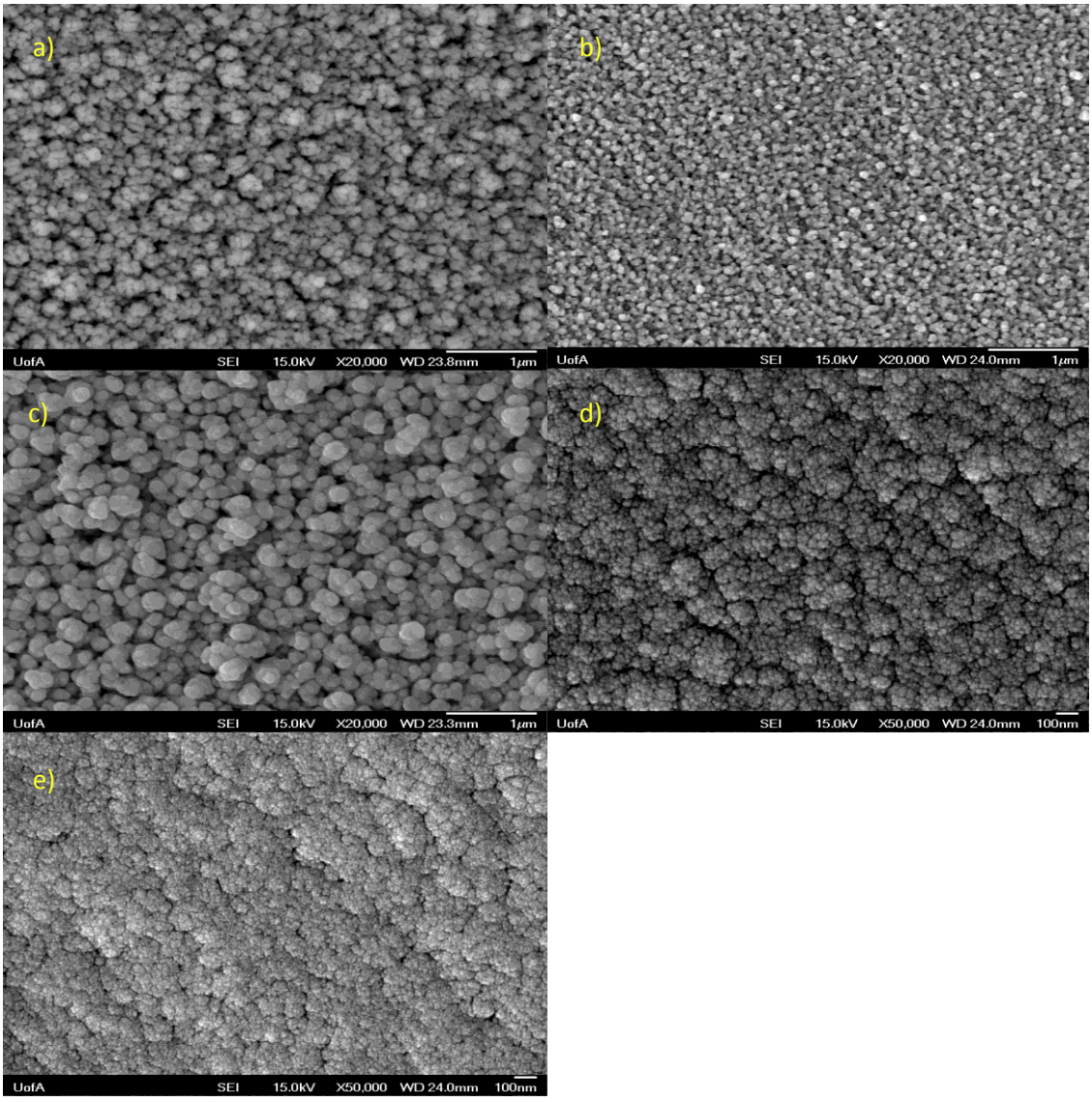

Figure 2.4. Representative SEM images of a) Acticoat®, b) Ag_{100}, c) Ag_{80}, d) Ag_{50} and e) Ag_{35}.

EDS:

Table 2.5 displays the dressing compositions determined by EDS. All concentrations are given in atm%. The ratio of oxygen to silver to gold (other elements excluded) is given in column 7. Carbon impurities were found in all samples and Mg impurities were found in all but Ag_{50} and Ag_{35}. Generally, the carbon impurities increased as more gold was added to the sample. The O/Ag/Au column normalized the atm% when disregarding both carbon and magnesium, the last column normalized the silver and gold signals while also disregarding the oxygen. The oxygen to silver ratio in Acticoat® and Ag_{100} is similar, as is the atomic percent oxygen in the Ag_{80}, Ag_{50} and Ag_{35} dressings. Overall, when gold is added to the target the atm% oxygen decreases around 15 atm%.

Table 2.5. Atomic concentrations of elements on gold/silver dressings by EDS.

1	2	3	4	5	6	7	8
	C	O	Mg	Ag	Au	O/Ag/Au	Ag/Au
Acticoat®	11.57	33.18	0.66	54.60	-	37.8/62.2/-	-
Ag_{100}	4.86	33.26	1.05	60.83	-	35.3/64.7/-	-
Ag_{80}	9.93	18.51	0.54	59.49	11.53	20.7/66.4/12.9	83.7/16.3
Ag_{50}	17.68	16.42	0.00	36.74	29.16	19.9/44.6/35.4	55.8/44.2
Ag_{35}	25.68	15.67	0.00	24.60	34.05	21.1/33.1/45.8	41.9/58.1

Table 2.6 shows the atomic concentrations of the targets used to sputter the dressings whose composition is shown in Table 2.5. Since Acticoat® was not produced in-house, the target used to produce this dressing could not be obtained for analysis. The weight percents provided by the target manufacturer were within 2.8% of those recorded experimentally. Significant carbon deposition was noticed on both the Ag_{50} and Ag_{35} targets and magnesium impurities were found on both the Ag_{100} and Ag_{80} targets. The atm% of the targets can be compared to those of the dressings shown in Table 2.5.

From this it can be observed that gold was preferentially sputtered at a ratio of 1.29, 1.17, 1.11 for Ag_{80}, Ag_{50} and Ag_{35}, respectively.

Table 2.6. Atomic concentrations of elements on gold/silver targets by EDS.

	C	O	Mg	Ag	Au	Ag/Au (atm%)	Ag/Au (wt%)
Acticoat®	-	-	-	-	-	-	-
Ag_{100}	4.66	0.00	1.36	93.98	-	-	-
Ag_{80}	6.50	0.00	0.95	80.86	11.69	87.37/12.63	79.12/20.88
Ag_{50}	31.62	0.00	0.00	42.39	25.99	62.10/37.90	47.29/52.71
Ag_{35}	26.46	4.20	0.00	32.88	36.45	47.61/52.39	33.23/66.77

XRD:

Figure 2.5 shows the XPS spectra obtained for the silver and gold dressings. The peak labels are also shown on this Figure for the Ag_{80} sample. The metallic peaks at 44, 64.5 and 77 $^{o}2\theta$ are observed to broaden when more gold was included in the dressings. The Ag_20 peak at 35 $^{o}2\theta$ was found to disappear with increasing gold content. Furthermore, the intensity of the $Ag/Ag_20/Au$ peak decreased and broadened with a higher gold content in the dressings. Minimum crystallite sizes determined by the Scherrer method are given in Table 2.7. It can be seen that the minimum crystallite size consistently decreases as more gold is added to the dressings. Furthermore, the minimum crystallite size of Acticoat® is significantly greater than that of Ag100. Other reports have found the crystallite size of Acticoat® to be 14 ± 2nm. [14]

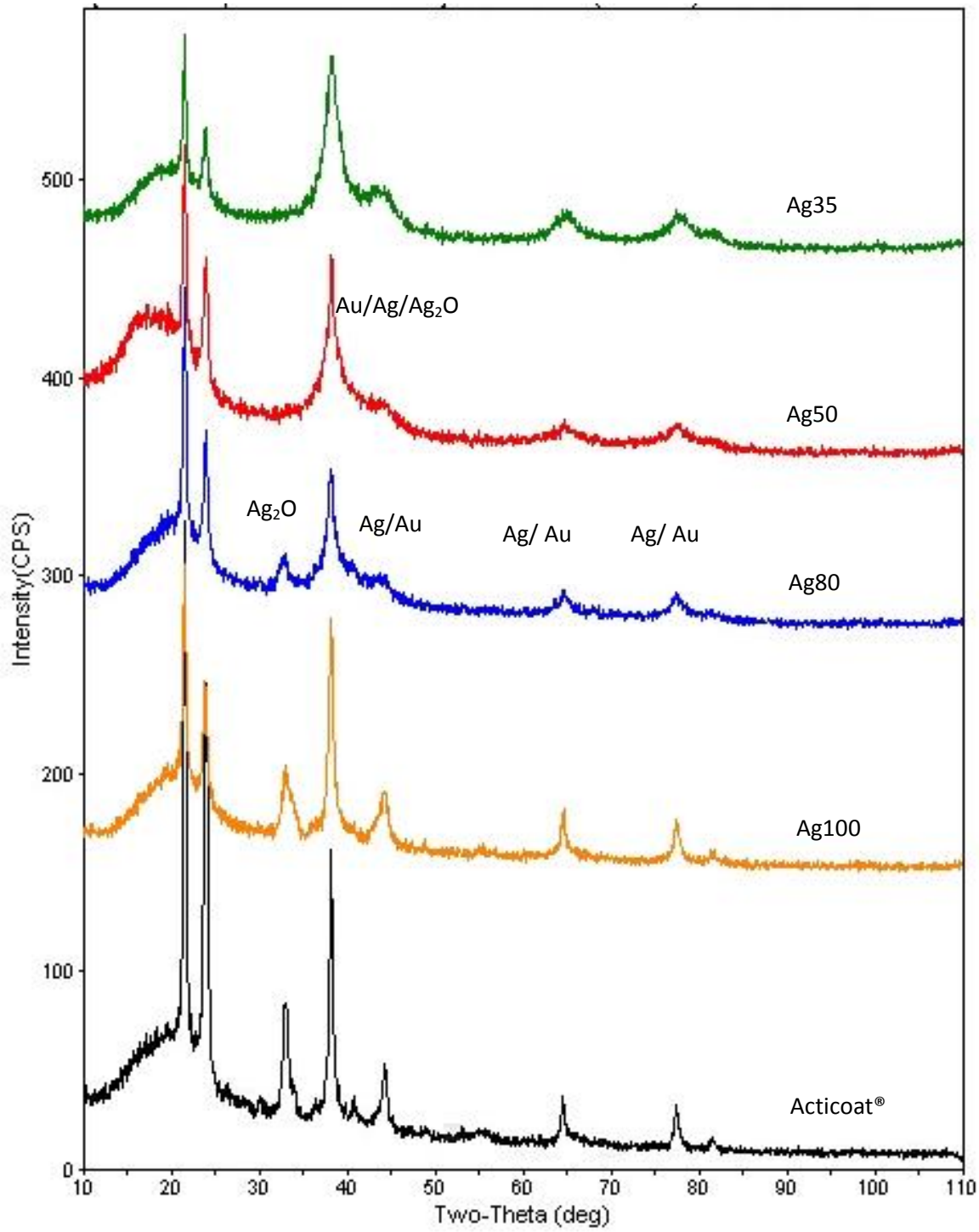

Figure 2.5. XRD spectra of gold/silver dressings.

Table 2.7. Minimum crystallite sizes determined from the XRD spectra (in nm).

Acticoat	Ag100	Ag80	Ag50	Ag35
17.87	13.151	10.36	8.247	4.89

XPS:

XPS spectra for gold/silver dressings are given in Figures 2.6-2.8 and sample de-convolutions of Ag_{80} and Ag_{100} are shown in Figure 2.9 and 2.10, respectively. The O1s spectra of the dressings showed smaller oxygen peaks for dressings sputtered with higher gold contents. This was supported by the smaller oxygen peak integrals for dressings with more gold. Specifically, the Ag-O peak at 529eV is observed to decrease as gold is introduced. The Ag_3d spectra confirmed that less silver is deposited as alloys with higher weight percent gold are used. The Au_4f XPS spectra showed significantly more gold being deposited from targets with higher gold content. Au_4f deconvolution showed a significant Au_2O_3 signal appearing at 85.4eV. This peak consisted of about 30% of the total gold deposited for all gold-containing samples. De-convolution of the Ag_3d peaks show almost equal ratios of silver and silver oxide for Acticoat® and Ag100 samples, but de-convolution of the Ag_3d peaks for the gold/silver alloys yielded arbitrary results and were thus not included.

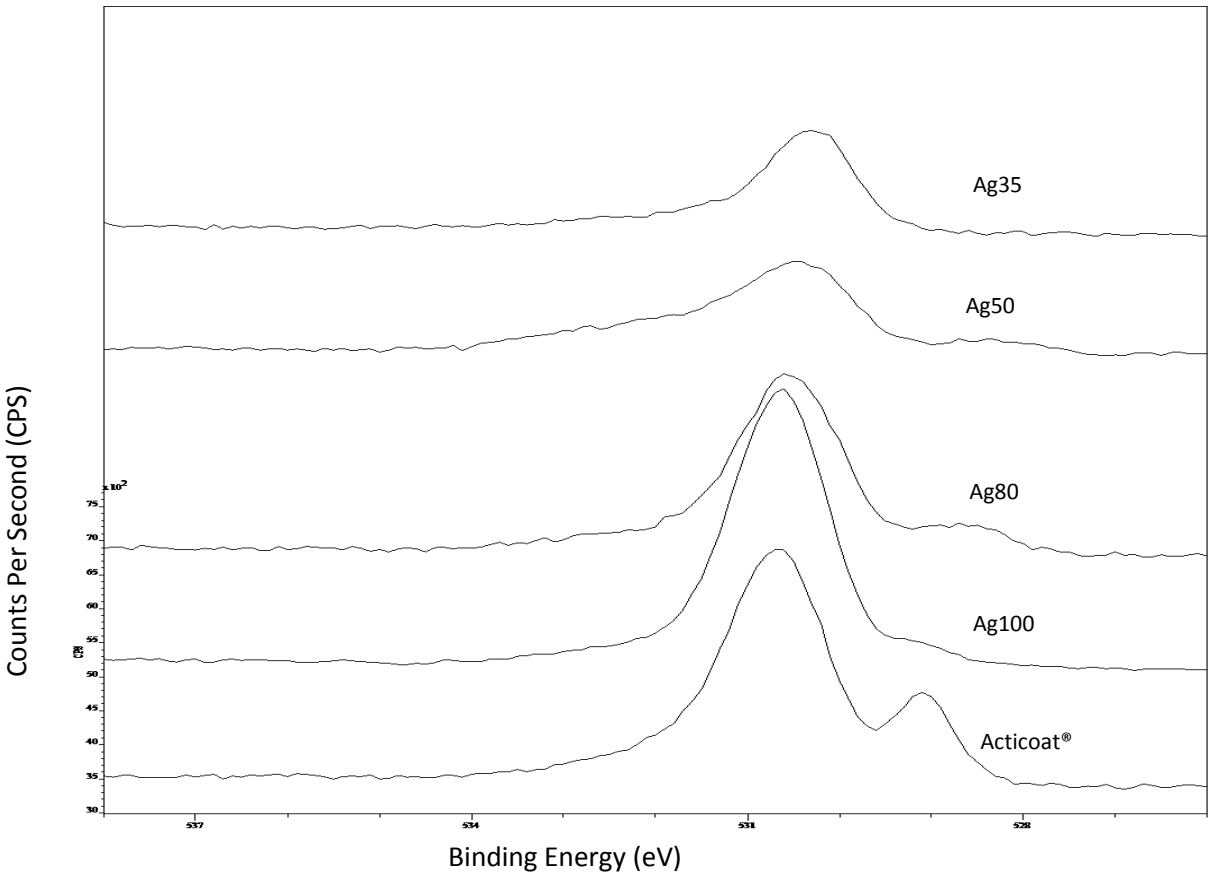

Figure 2.6. XPS spectra of O1s peaks for different alloy dressings.

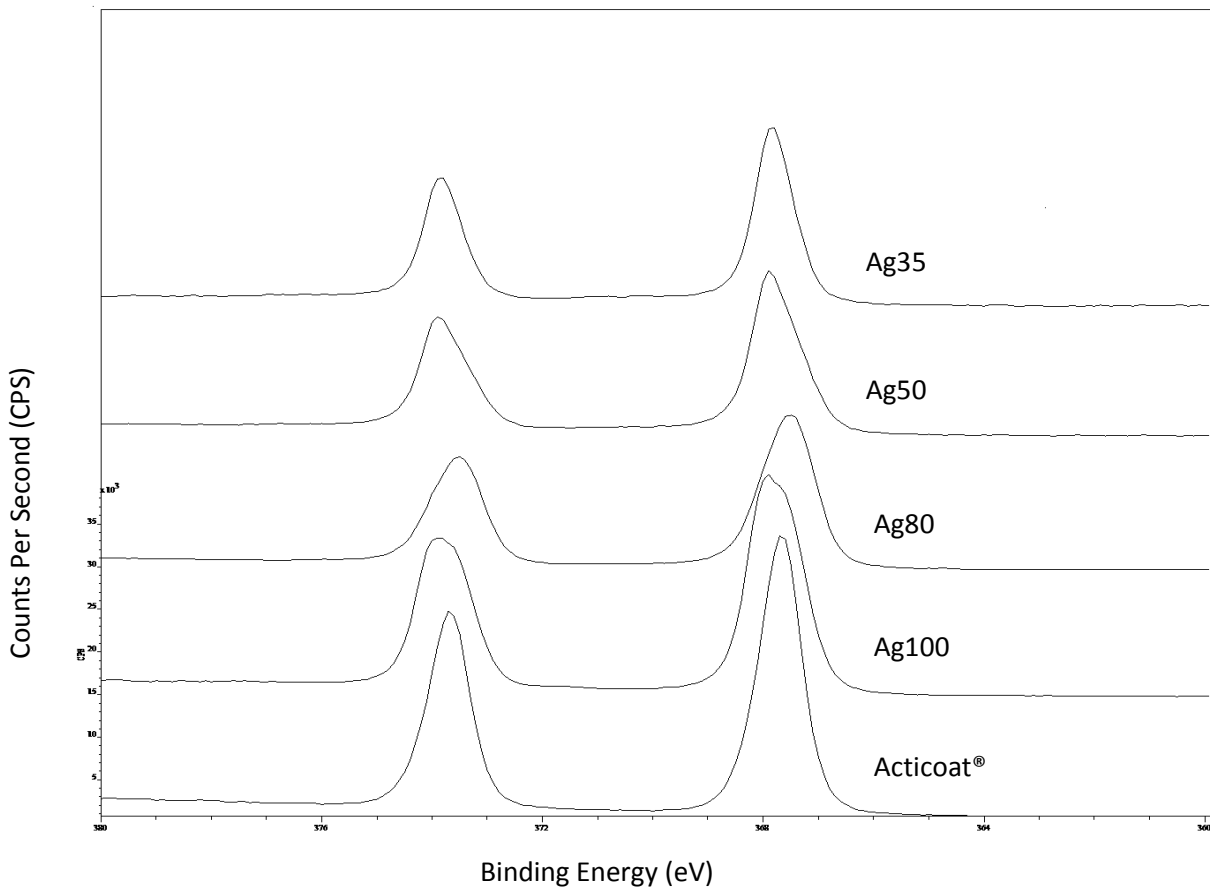

Figure 2.7. XPS spectra of Ag_3d peaks for different alloy dressings.

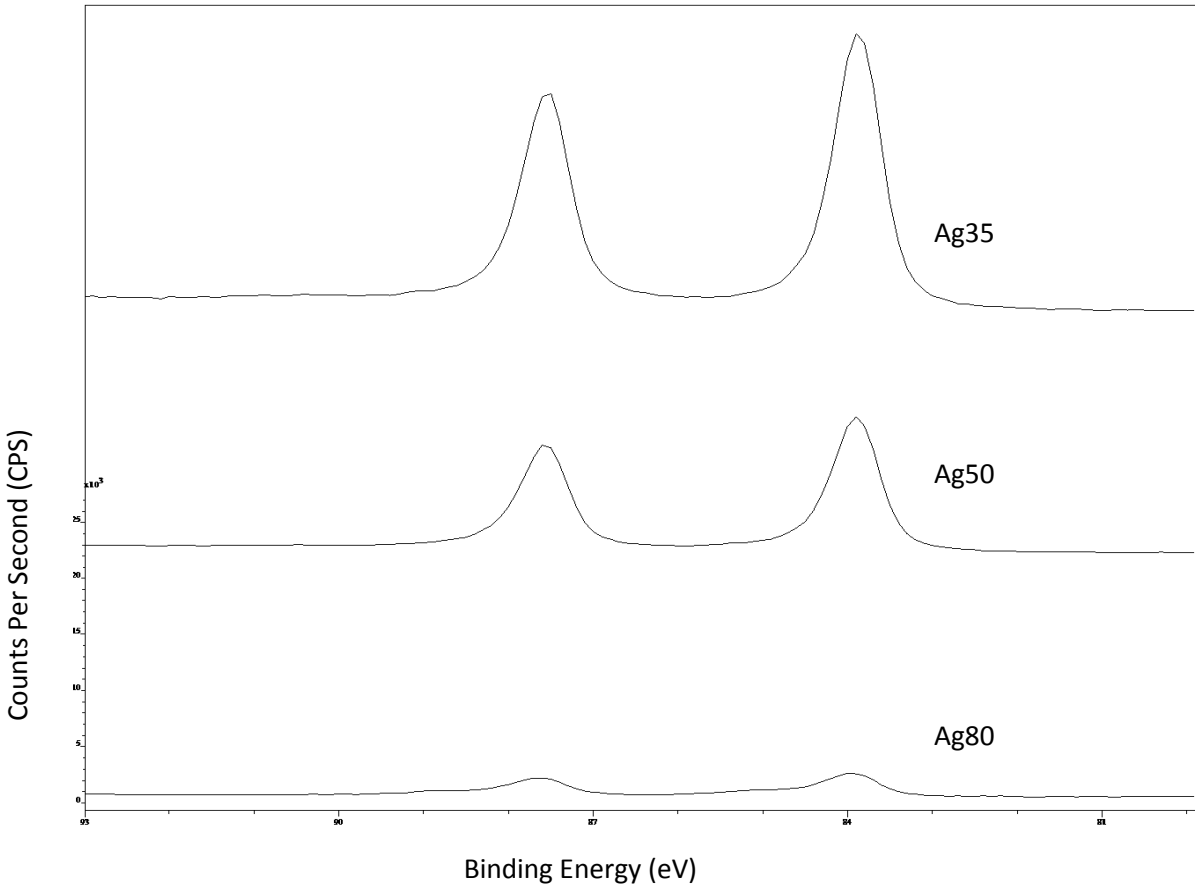

Figure 2.8. XPS spectra of Au_4f peaks for different alloy dressings with gold.

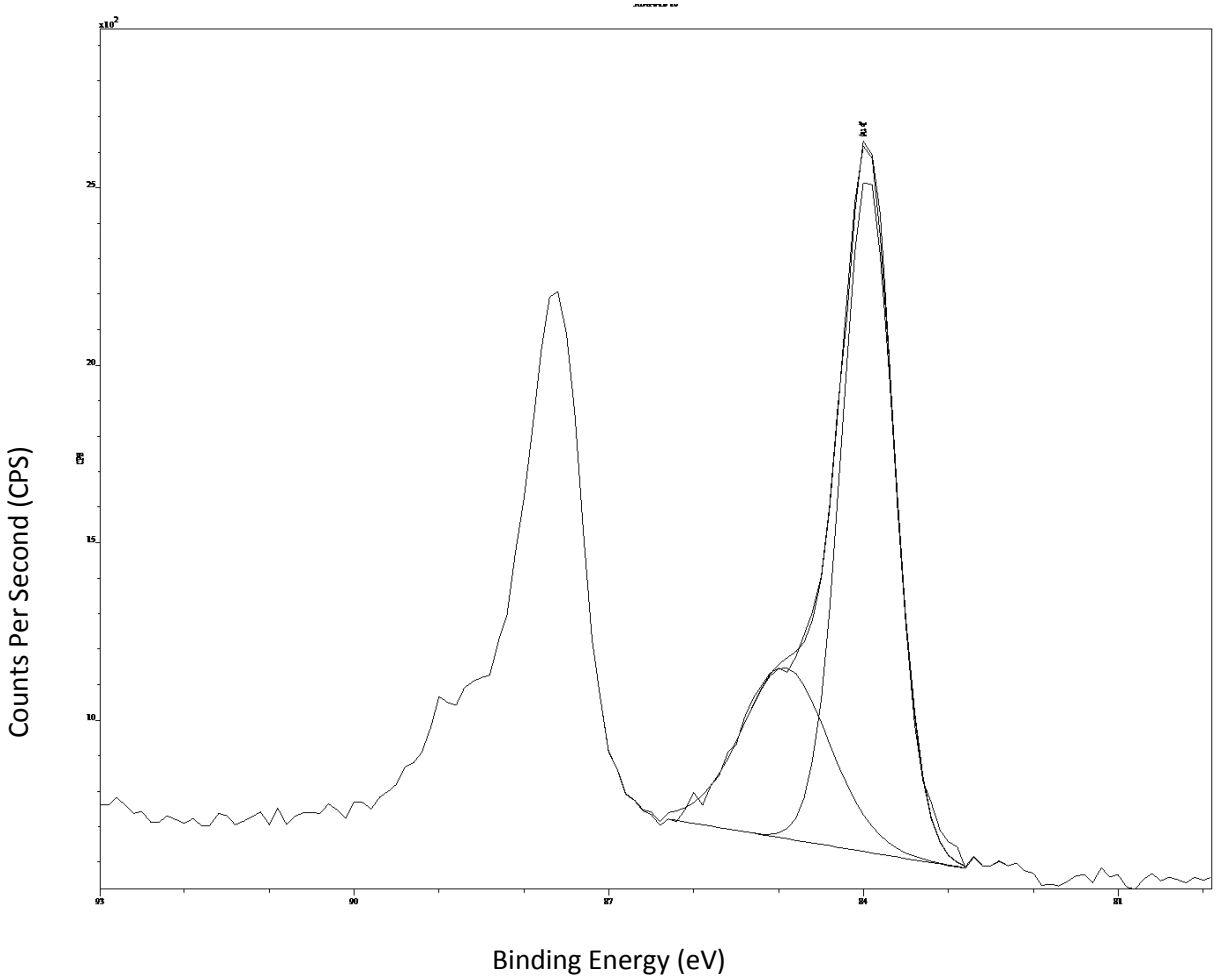

Figure 2.9. Sample deconvolution of the Au_4f XPS peak for Ag_{35}.

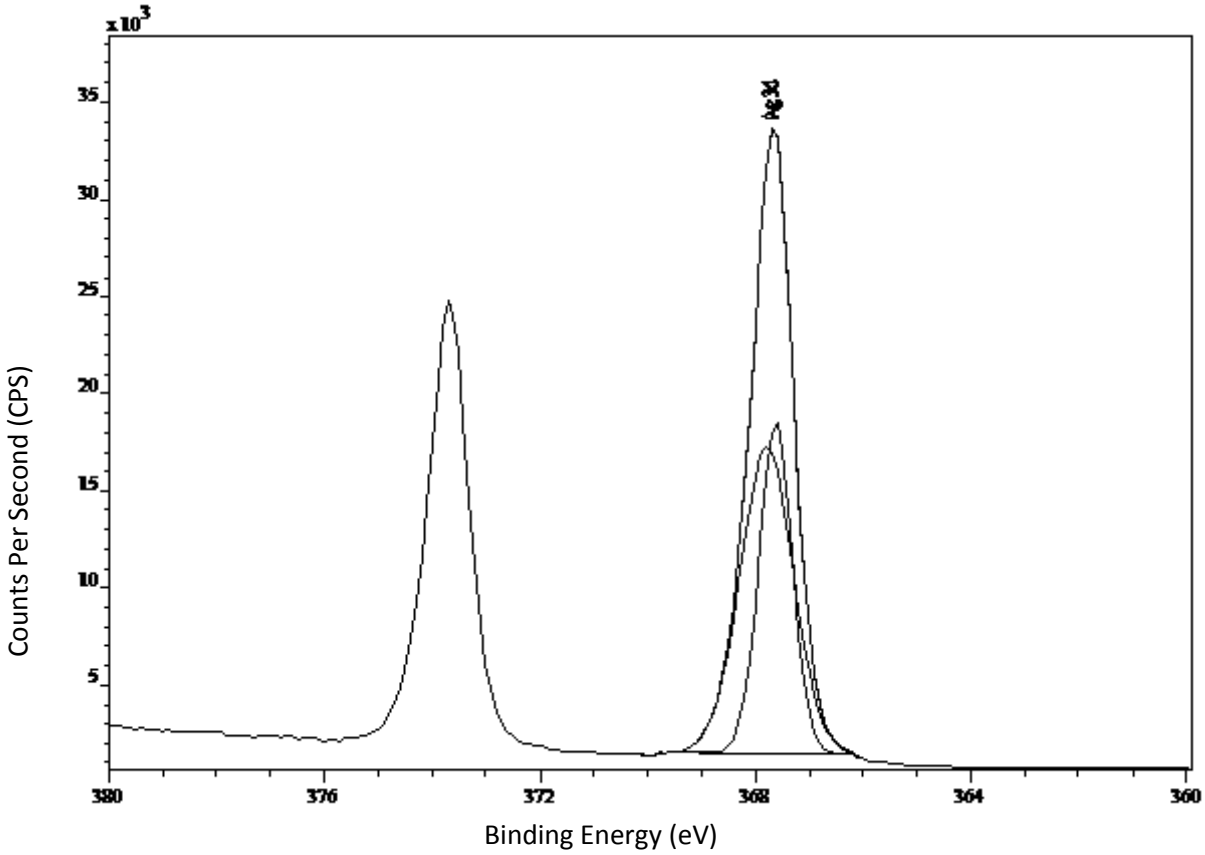

Figure 2.10. Sample de-convolution of the Ag_3d XPS peak for Ag_{100}.

AAS/ ICP-MS:

Table 2.8 shows the results from the AAS and ICP assays for one inch squared of sample in 10 mL of dH_2O. The numbers presented in the tables have already taken the dilution factor into account but have not been corrected for the amount of water used and the amount of acid added after dissolution. Concerning silver dissolutions in de-ionized water, Acticoat® was found to release less silver than both Ag_{100} and Ag_{80} ($p<0.05$) and both Ag_{100} and Ag_{80} released more silver than Ag_{35} ($p<0.05$). Previous studies have shown that Acitcoat® can release enough silver into 5 mL of distilled water over 24 hours to create a 15 ppm solution of Ag^+. [15] For the gold dissolutions in de-ionized water, about 100-1000x less gold than silver was released into the same volume of water over the same time interval. Both Ag_{80} and Ag_{50} released significantly less gold than Ag_{35} ($p<0.05$) but differences between Ag_{80} and Ag_{50} are not statistically significant.

Table 2.8. The concentration of silver or gold in 10 mL of de-ionized water after 24 hours of sample immersion ($1in^2$). Samples for silver and gold analysis were acidified with nitric acid and aqua regia, respectively.

	[Ag] ppm by AAS	[Au] ppm by ICP-MS
Acticoat	3.37 ± 0.87	n/a
Ag100	6.47 ± 3.31	n/a
Ag80	6.42 ± 0.96	0.0052 ± 0.00043
Ag50	4.21 ± 0.57	0.0074 ± 0.0014
Ag35	3.17 ± 0.61	0.0142 ± 0.0033

Table 2.9 gives the amount of silver released into 10 mL of 20.0 g/L of ammonium hydroxide over 3 minutes. While there is a clear trend of decreasing ammonium soluble silver release as the gold content increases, the only statistically significant differences are that Acticoat® and Ag_{100} release more silver than both Ag_{50} and Ag_{35} ($p<0.05$).

Table 2.9. The concentration of silver in 10 mL of 20.0 g/L ammonium hydroxide after 3 minutes of immersion ($1in^2$). Samples were acidified with nitric and tartaric acid.

	Ag ppm by AAS
Acticoat	66.70 ± 4.39
Ag100	73.70 ± 4.51
Ag80	61.02 ± 7.53
Ag50	50.08 ± 6.61
Ag35	46.54 ± 3.01

Table 2.10 shows the total gold released by 1 inch squared of dressing in aqua regia for 20 minutes. The dressings were observed to return to their original HDPE light white color after 3 minutes of submersion in aqua regia. Dressings with higher gold content released significantly more gold than dressings with lower gold content ($p<0.001$). The far right column displays the back-calculation results for the number of mg of gold on 1 in^2 of dressing. For Acticoat® about 3.25 mg of silver are contained in 1 in^2 of dressing.

Table 2.10. Concentration of gold in 20mL of aqua regia over 20 of submersion ($1in^2$) and the backcalculation of the total amount of gold on those dressings.

	Au ppm by AAS	Au (mg) on 1 in^2 of dressing
Ag80	57.4 ± 8.7	1.15 ± 0.17
Ag50	171.1 ± 13	3.42 ± 0.26
Ag35	294.4 ± 24.4	5.89 ± 0.49

Discussion

Biological Data:

Preliminary data showed that gold/silver nanostructures could be obtained and that they were stable under room temperature conditions. Log reduction assays showed that gold based nanostructures are effective antimicrobials against *P. aeruginosa* and *S. aureus*; however, while Acticoat® and Ag100 were bactericidal against *P. mirabilis*, dressings with higher gold content were not. *P. mirabilis* was chosen because certain strains are known to be somewhat resistant to silver because of their developed efflux pumps [16] and because the organism is often found in pressure sores in a clinical setting. [17] This not only made *P. mirabilis* a relevant organism to study, but it also gave us a good metric with which to compare the new gold/silver dressings to the existing structures. An initial screen of 5 different *Proteus* strains revealed that ATCC 25933 was both resistant to nobel metals and could grow at high enough concentration for log reduction testing; therefore, it was selected for log reduction testing.

The CZOI data noted a number of interesting trends. Firstly, it showed that after 7 days all dressings were still able to inhibit bacterial growth. Also, while all dressings produced zones that were of similar size on day 1, the pure silver dressing significantly outperformed the gold/silver dressings on day 7. On day 3 the zones produced by Acticoat® and Ag_{100} were significantly larger than those produced on day 1 by those same dressings. In fact, they were the only dressings to record a significant increase in CZOI over the first three days. This phenomenon is similar to what has been observed in literature

before [3], and is probably as a result of an unknown ligand produced by *P.aeruginosa* that increases silver mobility. [Personal communication, Dr. Rob Burrell] It was interesting that the gold dressings did not produce the same effect. However, it may be that the ligand is not produced by the organism in the presence of the gold containing dressings or it may be produced and the gold may be transported by this ligand but gold has less bactericidal efficacy than silver (as evidenced by the weaker log reduction).

Log reductions completed after the dressing had been challenged for three days of CZOI testing showed that the Ag_{50} dressing was as effective as Acticoat®. This demonstrates that while starting with a lower antimicrobial potency, the gold dressings may have a higher bactericidal longevity than pure silver nanostructured dressings.

The silver nitrate and gold oxide controls were completed to compare the antimicrobial action of nanostructured silver and gold to that of their pure ions. A solution of 0.5% silver nitrate or gold oxide was chosen because this concentration is popular in literature. Using 300μL of this solution, we obtain about 3 times more silver ions than what is released over a 1-day exposure of Acticoat®. This test is therefore an overestimation and serves as an excellent comparison between the antimicrobial activity on nanostructured dressings compared to their individual ions. Since the kill created by the 0.5% silver and gold solutions was significantly less than that of the nanostructured dressings it can be concluded that nanostructured silver and gold/silver dressings are significantly better antimicrobials than simply dissolved gold or silver ions.

Taken together, these findings suggests that silver is the primary antimicrobial agent in the gold/silver dressings. This would explain the trend of decreased zone size and reduced antimicrobial activity in the CZOI and log reduction assays, respectively. Furthermore, the fact that the zones of the pure silver dressings were significantly larger during the first three days of CZOI exposure suggest that fewer silver-oxygen coordination compounds are formed on the gold dressings than on the pure silver

dressings. It is known that a large zone is strongly correlated to the mobility of the silver compound on the agar plate and not necessarily to the antimicrobial capacity of the compound. [2] Silver in an $Ag(OH)_4^-$ compound is much more mobile since it does not react as readily with chloride in the agar media and precipitate out of solution to yield a biologically inert $AgCl_{(s)}$ compound. Furthermore, high concentrations of these silver-oxygen compounds have been speculated to cause a strong silver discharge over a short period of time. [15] Therefore, if more silver-oxygen complexes are present in the pure silver dressings than in the gold/silver dressings it would explain the larger zones seen in the CZOI testing.

The reduction of antimicrobial capacity after three days of CZOI treatment can be explained by a similar phenomenon. Acticoat® is known to produce high oxidation states of silver compounds like Ag^{+++}. [15] These compounds are relatively soluble and can react to form soluble silver-chloride complexes. It is possible that after three days of CZOI testing, these compounds are depleted and the residual antimicrobial capacity is only based on Ag^+ ions. Not only would this explain the reduced kill in the pure silver dressings, but it would also explain why both the silver and gold dressings had equal antimicrobial capacity after a few days of CZOI testing.

Physical Data:

Observations made from the EDS scans of the dressings helped elucidate the composition of the dressings and how the overall elemental profiles changed with the addition of gold. Carbon and magnesium impurities were an issue and were not affected by cleaning the sputtering machine. It was suggested that the gas cylinder could have been tainted with CO_2 but bubbling the argon and oxygen gasses through water for 5 minutes did not result in a decrease in the pH of the water and therefore the gas bottles were probably not the source of the carbon contamination. Interestingly, the compositions of the targets seem to correlate with the contaminations on the dressings. For example, both Ag_{100} and

Ag_{80} were observed to have magnesium impurities on their surface and this was reflected in the dressing chemistry. Dressings with high gold content also had more carbon deposited on their surface which was represented in the overall dressing chemistry as well. This suggests that the source of the contamination is the targets. A thorough revision of the protocol for changing sputtering targets and cleaning the machine should be re-examined to source potential contaminants that arise on the targets. These protocols are given in Appendix 2C.

Compositional data from EDS showed that dressings with higher gold content had a higher metal:oxygen ratio. Using normalized data (excluding impurities), for pure silver dressings around 63 atm% of the dressing was metal and for gold/silver dressings around 80 atm% of the dressing was metal. This shows that pure silver is more efficient at capturing oxygen from the sputtering environment than a mixture of gold and silver. The amount of gold in the system seemed to have relatively little effect on the amount of oxygen that was contained in the dressings. What was most interesting to observe from this data was that gold was preferentially sputtered from the gold/silver targets. According to sputtering yield literature at 300eV (the ion energy of our system) silver should out sputter gold by ratio of roughly 1.38:1. Instead, we found that gold was sputtered preferentially at ratios between 1.29:1 and 1.11:1. This suggests that this alloy system does not deposit these noble metals directly in accordance with sputtering yields but some other interactions during the sputtering process (be they on the target or in the system) cause less silver to reach the substrate than gold considering their relative atomic concentrations on the target.

AFM roughness scans were found to vary between sample batch and testing method. For Acticoat® in particular, other trials have reported a roughness of closer to 27 [Personal Communications, Dr. Loredana Dorobantu] while the roughness reported here was 45.1. Two explanations for this discrepancy could be the location of sampling and the tip used. Samples from this report were taken at

the intersection of the branches on the hexagonal surface while scans from Dr. Dorobantu's samples were taken on the branches (both shown in Figure 2.11). Furthermore, an Olympus 160TS tip was used to complete these trials while an Olympus240 ACS tip was used to generate Dr. Dorobantu's data. Since the 160TS tip is wider and shorter than the 240 ACS tip it could be that more error is induced by interactions with the surrounding nanostructure or the problem could lie in the longer tip interacting less with the sample and thus resulting in a smaller deflection. In either case, the results are consistently higher with the 160TS tip casting doubt on the absolute value of these measurements. Fortunately, the results can still be compared internally as they were all measured using the same equipment and technique.

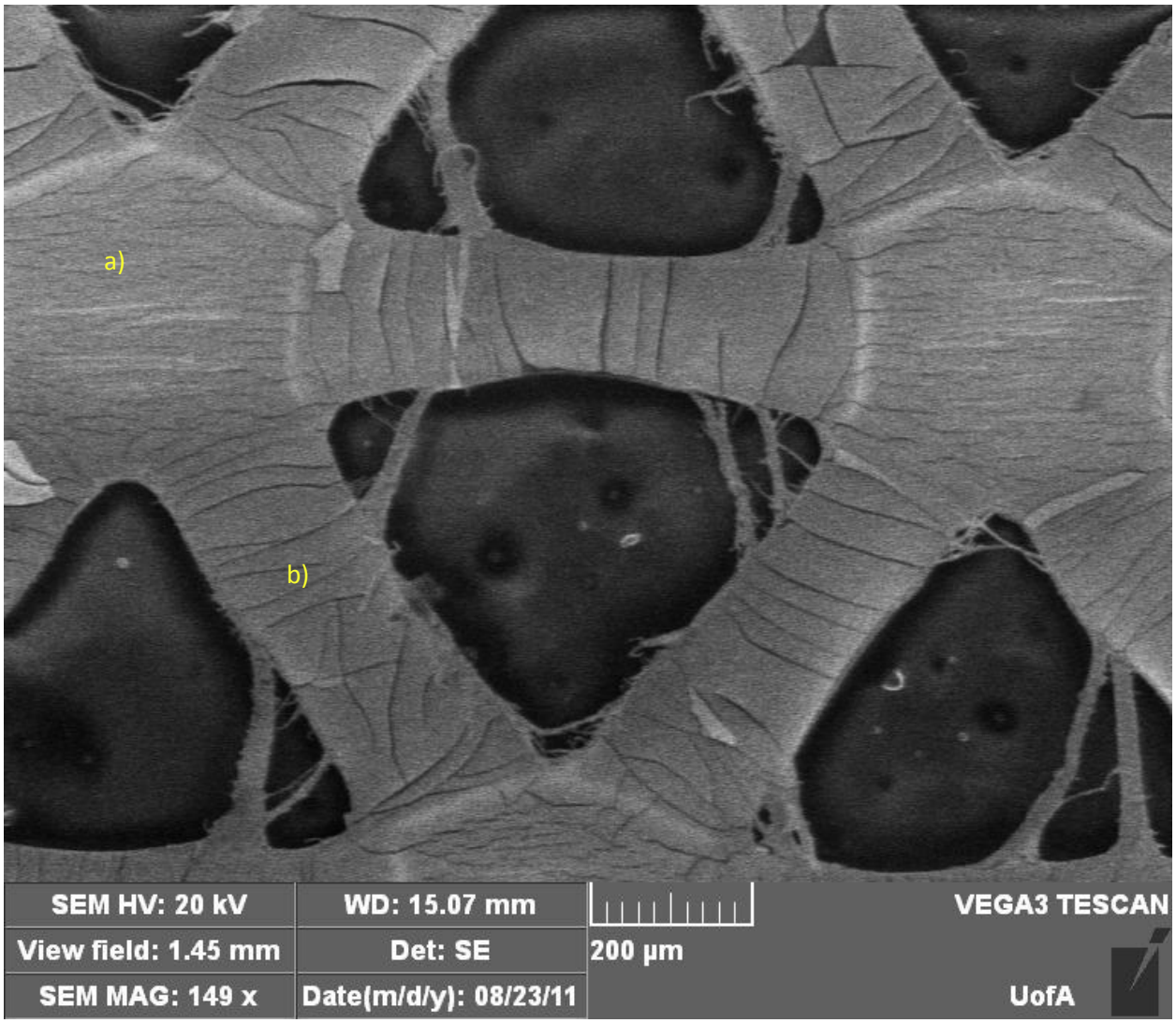

Figure 2.11. The branched structure of Acticoat and the locations tested by AFM. Location a) represents the location sampled in this report, location b) represents the location sampled by Dr. Dorobantu.

A comparison of SEM images b) (Ag_{100}) though e) (Ag_{35}) in Figure 2.4 shows a refinement in cluster size as more gold is added to the dressing alloy. This transformation is accompanied by a decrease in pore size and a more continuous structure being formed. Comparing image a) of Acticoat® and image b) of Ag_{100} it can be observed that there are significant differences between their respective nanostructures. This manifests itself in the dressing's biological properties where Acticoat® produced larger zones than Ag_{100} when challenged with *P. aeruginosa* but Ag100 was a better antimicrobial agent

when challenged with *P. mirabilis*. This is counterintuitive from the literature provided earlier which argued that high oxide concentrations are responsible for silver mobility since Acticoat® produced larger zones than Ag100 but has a larger crystallite size (a product of less silver-oxide pinning). Since the Ag_{100} nanostructure appears more highly pinned than that of Acticoat® this suggests that reducing the oxygen concentration below 4% in our sputtering process may result in a more appropriate control that is representative of the Acticoat® product.

A number of observations were made about the structure of the gold/silver dressing from analysis of the XRD pattern. Firstly, the broadening of the metallic peaks suggests that the crystallite size of the dressing is decreasing since peak width is inversely proportional to crystallite size in the Scherrer equation. The silver oxide peak at 33 $^{o}2\theta$ generally decreased as gold was added to the system. This supports the conclusion drawn from the log reduction data that silver oxide is reduced as the gold content of the dressing increases. Silver oxide is responsible for pinning the nanostructure and maintaining nanoclusters so its reduction with correspondingly smaller crystallite size was surprising. The peak at 37-38 $^{o}2\theta$ is a combination of silver, gold and silver oxide signals. The decrease in this peak suggests that either or both of the silver and silver oxide signals are decreasing as gold is added to the system; however, since the addition of gold is mitigating the peak reduction it is difficult to draw further conclusions from the observed decrease in this peak.

Taken together, AFM, SEM and XRD data all support the observation that the addition of gold to the microstructure contributed to creating a finer and smoother nanostructure. This is notable since more grain boundaries increase the surface area of the dressing and increase the number of grain boundary atoms that are present. Previous work hypothesized that it was these grain boundaries that were responsible for releasing the Ag^{0} compound and thus conferring the anti-inflammatory properties upon Acticoat®. [4] If this is true, the anti-inflammatory nature of gold and the increase in grain

boundary atoms from reduced crystallite size may contribute to an increase in anti-inflammatory properties. With a crystallite size of around 17nm (as was the minimum for the Acitcoat® samples) about 12% of the atoms in the crystal lattice are grain boundary atoms while for a crystallite size of 5nm (as was the minimum for the Ag_{35} samples) about 40% will be grain boundary atoms. [18] This significant increase in the number of grain boundary atoms present could have significant effects on the types and quantities of silver and gold atoms released from the nanostructure. This observation may also support previous work since prior theories thought that grain boundaries released Ag^0 clusters which were anti-inflammatory but not potent antimicrobials. The data collected for gold/silver dressings correlates the decrease in crystallite size with the reduction in antimicrobial potency thus supporting this hypothesis.

XPS data further supported the observations made about the changing nanostructure and offered insights into what is responsible for pinning the nanostructure in the presence of less silver oxide. The decrease in O1s signal with higher gold content showed that less oxygen was incorporated into the nanostructure when more gold was present. Also, the disappearance of the Ag-O peak at 529eV for Ag_{80}, Ag_{50}, and Ag_{35} dressings further supports the conclusion that very little oxygen is found in the Ag-O bond arrangement as was observed by the decrease in the silver oxide peak in the previous XRD data. However, the presence of an oxygen O1s signal in the gold/silver dressings does indicate that oxygen is being complexed in the dressing in some other form. Spectra results from the Ag_3d pass energies showed a slight reduction in the total amount of silver deposited as more gold was added to the dressings. This makes sense as the more gold replaces silver in the crystal lattice in these dressings. The Au_4f spectra showed inverse results as more gold was added as the silver content in the dressings decreased. Furthermore, the morphology of the gold spectra remained relatively consistent for the Ag_{80}, Ag_{50} and Ag_{35} dressings as more gold was added.

Deconvolution of the Ag_3d peaks for Acticoat® and Ag_{100} showed that the ratio of silver to silver oxide was almost 1:1. Unfortunately when this method was applied to the deconvoluton of the Ag_3d peak for Ag_{80}, Ag_{50} and Ag_{35} it was realized that small peak shifts could allow either one or two peaks to fit the spectra reasonably well. Since the literature values for the peak location of silver oxide and silver are very close to each other and tend to overlap it makes the deconvolution possible but tricky to interpret. For example, Ag_2O is found at the Ag 3d5/2 spectral line between 367.8 and 368.2eV while $Ag_{(s)}$ is found at the Ag 3d5/2 spectral line between 367.9 and 368.4 eV. [19-22, respectively]. This overlap is not serious when the sample chemistry is relatively well known but without that knowledge it makes interpretation of these peaks little more than an educated guess. With that in mind, it would appear more appropriate that these Ag_3d XPS signals were read such that a single peak described the curve well and that the amount of Ag-O in the sample is minimal.

Deconvolution of the Au4f peaks was significantly more straightforward and leads to much more interesting results. These peaks could be easily matched to gold(III) oxide (Au_2O_3) and $Au_{(s)}$ peaks for all the gold containing dressings. Au_2O_3 comprised around 30% of the total gold in the Ag_{80}, Ag_{50}, and Ag_{35} samples. The observance of gold oxide being preferentially created is supported by its higher reduction potential (1.5V for gold and 0.8V for silver). [23] Since we know that silver oxide is formed when sputtering silver under these condition, it would make sense that gold oxide should also form. What is more difficult to rationalize is the stable fraction of gold oxide in the gold dressings. One possible explanation for this behaviour is that gold is reacting quickly and to completion with the oxygen in the sputtering chamber. If this were the case, oxygen would be the limiting reagent in the reaction and this would explain the low levels of silver oxide in the sample and the consistent fraction of gold oxide in the dressing. While the number of moles in the sputtering chamber is much greater than those incorporated in the dressing, a local oxygen shortage could be possible if the physical set-up of the sputtering system is considered.

Figure 2.12 is a picture of the sputtering machine with the sliding cap removed showing the potential flow lines of inlet gas through the sputtering chamber. Lines labelled a) are the desired gas path through the machine and lines labelled b) represent the potential short-circuiting route. Small pipes are present beside the target to deliver fresh inlet gas directly to the plasma but they have observed to become blocked by sputtered silver from the plasma because of the diffusive nature of the sputtering parameters. Furthermore, the swagelock connections on the inlet gas port could be responsible for an oxygen "short-circuit" in the sputtering machine where the fresh inlet gas bypasses the sample and is directly pumped out of the chamber. When these fittings were water tested even tap pressure cause water to leak through the fittings. It can easily be imagined that incoming gas escapes instead of being released close to the target. This could augment the local shortage of oxygen around the target and account for a certain maximum oxygen uptake possible by the sample.

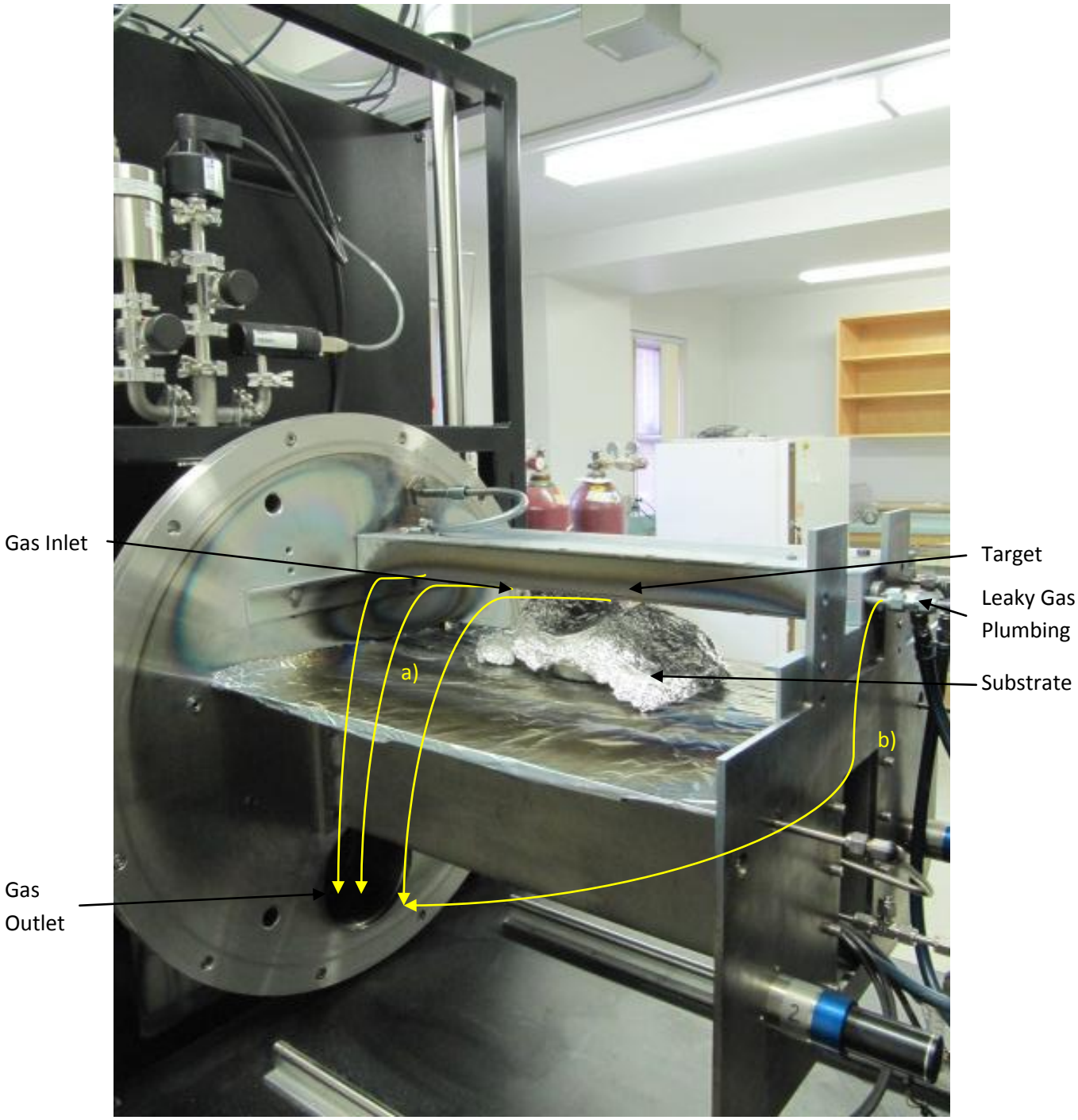

Figure 2.12. Locations of the gas inlet and vacuum outlet ports on the extreme sputtering machine. Lines labelled a) are the desired gas path and line b) is the short circuiting path.

Chemical Data:

AAS and ICP results were used to evaluate the release properties of the different alloyed dressings. The silver release in distilled water was proportional to the amount of silver on the dressing sample. The Acticoat® samples were not significantly different when compared to literature values. Ag_{100} dressing was observed to release more silver than Acticoat® which supports the hypothesis made earlier that silver is the sole antimicrobial compound because in all samples the amount of silver silver released tended to correlate with antimicrobial efficacy. The amount of gold released from these dressings was significantly less than the amount of silver released. This property probably contributes to the poor antimicrobial properties observed by the nanogold dressings. Controls of gold oxide and silver nitrate showed that the gold and silver ions are equally as potent antimicrobials (by weight) but less effective than sputtered materials. This suggests that if these dressings could be amended to release more gold it may contribute to their antimicrobial characteristics.

The amount of bioactive (dissolvable in ammonium hydroxide) silver available on the dressings decreased as a higher gold content was included in the dressing. This decrease, however, was not proportional to the amount of silver on the dressings. For example, Ag_{80} (83 atm% silver) released 61 ppm of bioactive silver while Ag_{35} (41 atm% silver) released 47 ppm. While dissolution tests are known to have saturation values that are only slightly dependent on the amount of silver exposed to the system, this phenomenon could also be explained by the presence of gold oxide and smaller crystallite size of the gold-based dressings which served to increase the proportion of bioactive silver on the gold/silver dressings. A time based study of the release of bioactive silver from gold/silver dressings exposed to ammonium hydroxide would be useful to know whether a saturation effect is responsible for this data or whether it can be attributed to an increase of bioactive silver on the gold dressings. Unfortunately, as was observed with the log reduction and AAS experiments this bioactive silver in the

gold dressings is not being sufficiently released into the dressing's surroundings to sufficiently aid in the antimicrobial properties of the gold/silver dressings.

Experiments by ICP concerning the total amount of gold on the dressings yielded interesting results. While Acticoat only contains about 3mg of silver per inch squared, EDS and ICP data in conjunction can be used to show that Ag_{35} contains roughly 5.9 mg of gold and 2.2mg of silver per inch squared of dressing. This was verified by showing that the weight of metal deposited on the dressing is 8 $\pm$ 0.35 mg. Furthermore this means that although Ag35 and Acticoat® have relatively similar amounts of silver, the silver in the Ag35 dressing is either not bioavailable or not in a bioactive form for the Ag35 dressing to produce suitable antimicrobial properties.

One unanticipated benefit that this observation lends itself to is the effect of including small amounts of gold on production time. Over 30 minutes, 3.25 mg of silver or 8.1 mg of a silver-gold alloy can be sputtered. Therefore, the incorporation of small fractions of gold in nanocrystalline silver dressings may not require a substantially longer time to produce.

Conclusions

The gold/silver dressings were created using DC magnetron sputtering and they were stable at room temperature. Biological assays show that gold based nanostructures can still be antimicrobial and can retain this activity for at least a week; however, the efficacy of these dressings is significantly reduced compared to those with pure silver. Physical characterization data supported the conclusion that the addition of gold to the microstructure contributed to creating a finer and smoother nanostructure. This was notable since more grain boundaries increase the surface area of the dressing and increase the number of grain boundary atoms that are present which, in turn, could result in a dressing with significantly better anti-inflammatory properties. Both physical and chemical data contributed to the conclusion that the incorporation of gold in the dressings decreases the proportion of

silver oxide and allows for the creation of a significant amount of gold oxide. These observations were consistent with the data from the biological assays. It is recommended that in-vivo tests be conducted to determine whether the anti-inflammatory nature of nanosilver dressings could be increased by adding gold to the dressings

References

1. Cavanagh MH, Burrell RE, Nadworny PL. **Evaluating antimicrobial efficacy of new commercially available silver dressings.** Int wound J. 2010;7(5):394-405.

2. Gallant-Behm CL, Yin HQ, Liu SJ, Heggers JP, Langford RE, Olson ME, Hart DA, Burrell RE. **Comparison of in vitro disc diffusion and time kill-kinetic assays for the evaluation of antimicrobial wound dressing efficacy**. *Wound Repair and Regeneration.* 2005;13:412-21.

3. Taylor PL, Ussher AL, Burrell RE. **Impact of heat on nanocrystalline silver dressings Part I: Chemical and biological properties.** *Biomaterials*. 2005;26:7221-29.

4. Taylor PL, Omotoso O, Wiskel JB, Mitlin D, Burrell RE. **Impact of heat on nanocrystalline silver dressings Part II: Physical properties.** *Biomaterials*. 2005;26:7230-40.

5. Mizushima Y, Okumura H, Kasukawa R. **Effects of gold and platinum on necrotizing factor, skin sensitizing antibody, and complement**. *Jpn J Pharmacol.* 1965;15:131-34.

6. Suzuki S, Okubo M, Kaise S, Ohara M, Kasukawa R. **Gold sodium thiomalate selectivity inhibits interleukin-5-mediated eosinophil survival**. *J Allergy Clin Immunol.* 1995;96:251-56.

7. Abraham G, Himmel PB. **Management of Rheumatoid Arthritis: Rationale for the Use of Colloidal Metallic Gold.** *Journal of Nutritional and Environmental Medicine.* 1997;7:295-305.

8. Mishra A, Tripathy SK, Yun SI. **Bio-synthesis of gold and silver nanoparticles from Candida guilliermondii and their antimicrobial effect against pathogenic bacteria.** *J Nanosi Nanotechnol*. 2011;11(1):243-8.

9. Zhang Y, Peng H, Huang W, Zhou Y, Yan D. **Facile preparation and characterization of highly antimicrobial colloid Ag or Au nanoparticles.** *J. Colloid Interface Sci.* 2008;325(2):371-376.

10. Fan F, Bard AJ. **Chemical, Electrochemical, Gravimetric, and Microscopic Studies on Antimicrobial Silver Films**. *Journal of Physical Chemistry B.* 2002;106:279-287.

11. Moyer CA, Brentano L, Gravens DL, Margraf HW, Monafo WW. **Treatment of large human burns with 0.5% silver nitrate solution.** *Arch Surg.*1965;90:812–67.

12. Wright JB, Hansen DL, Burrell RE. **The comparative efficacy of two antimicrobial barrier dressings: in vitro examination of two controlled release silver dressings.** *Wounds*. 1998;10:179–88.

13. Langford JI, Wilson AJC. **Scherrer after Sixty Years: A Survey and Some New Results in the Determination of Crystallite Size.** *J. Appl. Cryst.* 1987;11:102-113.

14.Landry BK, Nadworny PL, Omotoso OE, Maham Y, Burrell JC, Burrell RE. **The kinetics of thermal instability in nanocrystalline silver and the effect of head treatment on the antibacterial activity of nanocrystalline silver dressings.** *Biomaterials.* 2009;30:6929-39.

15. Nadworny P. **Biological Activity of Nanostructured Silver** [PhD Thesis]. Edmonton, AB: University of Alberta; 2010 [cited December 8 2011]. Available from: http://hdl.handle.net/10048/910.

16. Poole K. **Efflux-mediated multiresistance in Gram-negative bacteria.** *Clin Microbiol Infect.* 2004;10:12-26.

17.Livesley NJ, Chow AW. **Infected Pressure Ulcers in Elderly Individuals.** C*lin Infect Dis.*2002;35(11):1390-96.

18. Tjong SC, Chen H. **Nanocrystalline materials and coatings.** *Materials Science and Engineering* 2004, 45:1-88.

19. Gaarenstroom SW, Winograd N. **Initial and final state effects in the ESCA spectra of cadmium and silver oxides.** *J. Chem. Phys.* 1977;67:3500-06

20. Gerenser LJ. **Photoemission investigation of silver/poly(ethylene terephthalate) interfacial chemistry: The effect of oxygen-plasma treatment.** *J. Vac. Sci. Technol. A.* 1990;8:3682.

21.Fuggle JC, Kallne E, Watson LM, Fabian DJ. **Electronic structure of aluminum and aluminum-noble-metal alloys studied by soft-x-ray and x-ray photoelectron spectroscopies.** ***Phys. Rev. B.*** **1977;16:750-761.**

22.Romand R, Roubin M, Deloume JP. **X-ray photoelectron emission studies of mixed selenides $AgGaSe_2$ and Ag_9GaSe_6.** *J. Solid State Chem.* 1978;25:59-64.

23. 17. W. M. Haynes, ed., CRC Handbook of Chemistry and Physics, 92nd Edition (Internet Version 2012), CRC Press/Taylor and Francis, Boca Raton, FL.

Appendix 2A: Sample calculations for the Silver nitrate and gold oxide controls.

A 0.5% silver nitrate solution was taken to be 5 grams of silver nitrate per 100 mL of water.

$V_{\text{total inoculums(Bacteria + Metal Solution)}}$ = 300 µL

V_{Bacteria} = 250 µL

$V_{\text{Metal Solution}}$ = 50 µL

$$5\frac{g}{L}x300\frac{\mu L}{inoculation}x\frac{L}{10^6\mu L}=1.5x10^{-3}\frac{g}{inoculation}=1.5\frac{mg}{inoculation}$$

$$1.5\frac{mg}{inoculation}x\frac{inoculation}{50\mu L}=30\frac{mg}{mL}$$

Therefore, if solutions are made at a concentration of 30 mg/mL then adding 50mL of this solution to the 250 mL inoculation volume will result in a final concentration of 0.5% silver nitrate of gold oxide.

Appendix 2B: Sample calculations verifying EDS data with fit parameters greater than 15.

The Ag_{35} dressing was used as a comparison as it had the most gold and the highest EDS fit index (14.5). Since the manufacturer had stated in the machine literature that data obtained from a fit index above 10 may be unreliable, this data was checked against ICP and mass data to ensure that EDS was returning reliable results.

For Ag_{35} the following results were obtained.

EDS: 67.6 wt% Au / 24.6 wt% Ag for a dressing sample

ICP: 5.89 $\pm$ 0.49 mg of Au on a 1 in^2 dressing sample

Mass: 8.13 ± 0.37 mg of metal was deposited on a 1 in^2 dressing sample

(Wt % Au)(total metal mass) = gold mass on the dressing

$0.676(8.13mg) = 5.50\ mg\ of\ gold$

This is within one standard deviation of the mass of gold on the dressing reported by ICP; therefore, ICP with a fit index up to 15 seems to yield reliable results and can be included in observed data.

Appendix 2C: Protocol for changing the target on the Extreme Sputtering Machine.

Remove Old Target from and old Backing Plate

1. Remove target and backing plate from sputtering machine.
2. Place the target on the wire grid in the countertop convection oven.
3. Set the temperature set point to 450^{o}F and turn the oven on.
4. In about 45 minutes the solder will be seen to flow as will be seen at the interface between the target and backing plate.
5. Using heat resistant gloves, open the oven and remove the target. Place the target on a second wire grid to prevent it from touching the table.
6. Slide the target relative to the backing plate and remove the target.

Bond New Target to Backing Plate

1. Locate a spare backing plate and, if required, clean the bonding surface with an orbital sander and isopropanol solution.
2. Spread a thin layer of 157PA Paint-On-Paste Solder/Flux, diluting the paste with a trace of water if needed to allow the solder paste to spread easily.
3. Lay the backing plate on a wire grid from the countertop convection oven.
4. Lay the target onto the backing plate, positioning it centrally.
5. Set up 10 "C" clamps to hold the target securely.
6. Line the base of the countertop convection oven with a piece of aluminum foil.
7. Place the target and backing plate assembly into the oven.
8. Set the temperature set point to 450^{o}F and turn the oven on.
9. In about 45 minutes the solder will be seen to flow as will be seen at the interface between the target and backing plate.
10. Turn off the oven and allow the contents to cool.
11. Remove the target assembly from the oven and take off the "C" clamps.
12. Clean off any surplus solder and/or flux from the edge of the target.
13. Remove soiled aluminum foil from the oven and clean the wire support grid.

Chapter 3 – The Effect of Altering Dressing Oxygen Concentration and Exposing the Dressings to Heat on the Structure and Chemistry of Nanogold/silver Dressings

Introduction

Changing a materials production or storage methods can often give valuable insight into important physical and chemical properties. This analysis has already been completed for Acticoat® and helped elucidate how the crystallite size and grain morphology can be altered by exposing this wound dressing to heat. [1] It is desired that this study be performed on gold/silver dressings to give insight into how material properties can be manipulated. Furthermore, oxygen concentration is one of the key variables in the sputtering process. As silver-oxygen compounds have been suggested as a source for the dressing's antimicrobial capabilities [2], a study of how oxygen changes affect the dressing properties could be of importance to suggest how the dressing could be manipulated to obtain desirable properties.

For a discussion of the biological, physical and chemical properties of nanocrystalline gold/silver dressings please read Chapter 2. While this chapter will discuss how both the heat treatment and the changes in oxygen concentration affect the chemical and physical nature of the dressing, this chapter will not focus on combinatorial studies (e.g. the heat treatment of dressings sputtered in a high oxygen environment).

Materials and Methods

All materials were bought from Fisher Scientific Inc. unless otherwise indicated.

Dressing Fabrication:

Acticoat® was purchased locally (Acticoat®, Smith and Nephew Inc., Largo, Fl). Since gold dressings are not available on the market, all other gold and silver dressings were produced by batch

sputtering in our in-house Extreme sputtering machine at the University of Alberta. A base pressure of $2x10^{-5}$ Torr and an aquatrap temperature of 200 K were obtained before the system was sealed from the pump and a leak test was preformed. A leak rate of less than 1 mTorr per minute was considered acceptable. The silver and gold/silver alloys were then sputtered onto high density polyethylene mesh. The targets had a variable weight percent silver with the balance gold. The five targets employed in the study were: all silver (Ag_{100}), 80wt% silver (Ag_{80}), 50wt% silver (Ag_{50}) and 35 wt% silver (Ag_{35}). The nomenclature Ag_{100}, Ag_{80}, Ag_{50} and Ag_{35} will hereafter be used to refer to the dressings created from these targets unless otherwise specified. For clarification, a dressing will be called Ag_{80} because it was sputtered with a target that had 80wt% silver, not because the dressings contains 80wt% silver. While targets with gold were treated as experimental groups, the Ag_{100} dressing was used as a control for Acticoat® to ensure the sputtering process was similar since both products are produced by sputtering 100% Ag. The working pressure of the sputtering machine was 40 mTorr. For the oxygen dependent studies, the dressings were sputtering in atmospheres of high oxygen (8%), normal oxygen (4%) or low oxygen (2%). The balance of the sputtering gas environment was argon. For this Chapter, the oxygen permutation will be put in brackets behind the dressing type. For example, a dressings sputtered with a 50wt% silver dressing at 8% oxygen will be written $Ag_{50}(8)$. The dressings were sputtered using a constant current of 0.9 A. This resulted in an applied voltage of 300 ± 10 V between the target and substrate (ground). After each dressing was sputtered, the full mesh was removed from the sputtering machine and the sample directly under the middle of the target (a total of $10in^2$ per batch) was immediately cut from the HDPE mesh, placed in sterile bags and stored in the dark at 4^oC.

Heat Treatment:

Dressings prepared in house and Acticoat® were cut into 1 in^2 pieces and heat treated in a Fisher Scientific Isotemp oven at 50, 75, or 100^oC for 24 hours. Samples were placed in aluminum weight boats during the heat treatment and were exposed to ambient air with no humidity control. After heat

treatment, the dressings were placed in sterile plastic bags, wrapped in foil and stored at 4^{o}C for further processing.

Log Reduction:

To quantify the bactericidal properties of each of the dressings, log reduction analysis was performed in triplicate using the same method as Taylor et al 2005. [3] To obtain bacteria in the log-phase growth, first 2 to 3 isolated colonies of *Pseudomonas aeruginosa* (ATCC 27317), *Staphylococcus aureus* (ATCC 25923) or *Proteus mirabilis* (ATCC 25933) were used to inoculate a flask containing 100 mL of tryptic soy broth (TSB) and the flask was incubated overnight in a rotary shaker at 37°C and 120 rpm. The next morning, one milliliter of this culture was used to inoculate another 100 mL of TSB and incubated for 4 hours under identical conditions. Experimental groups were prepared as follows. An aseptically-cut 1 in^2 (6.45 cm^2) piece of dressing was placed coated-side up on a sheet of plastic (3 cm^2) in an inverted Petri dish lid and inoculated with 0.3 mL of the log phase bacteria. The inoculated dressing was covered with another layer of plastic followed by the upright Petri dish bottom to apply pressure. The inoculated dressings were incubated for 30 mins at 37°C. After incubation, the dressing was immediately placed in 2.7 mL of sodium polysorbate solution (SPS) containing 3.0g of NaCl, 0.050g of sodium thioglycolate, 0.50mL of Tween 20 and 0.050g of sodium thiosulphate in 50 mL of deionized water. This solution was used to inactivate the metal ions in the experimental groups and aid in bacterial recovery. By placing the dressing in the SPS, a 1 in 10 dilution was realized. The mixture was then vigorously mixed using a vortex in order to recover bacteria and inactivate noble metals. For control groups, 0.3 mL of the log-phase bacteria was used directly to inoculate 2.7 mL of SPS. The resulting experimental and control solutions were serially diluted to 10^{-6} and 10^{-8} respectively by transferring 0.1 mL to 0.9 mL of phosphate buffered saline (PBS) five times and mixing with a vortex between transfers. Three 20 μL drops of each dilution were pipetted onto tryptic soy agar (TSA), incubated at 37°C for 24 h and then individual colonies were counted. The CFUs from the control groups were used to determine

the $\log_{10}$ of bacteria in the original inoculum while the CFUs from the experimental groups were used to calculate the $\log_{10}$ of surviving bacteria. These two values were subtracted to yield the log reduction number. Controls of SPS were also completed to ensure the solution was not toxic to the microorganisms.

Centralized Zone of Inhibitions (CZOI):

The revised form of the Kirby-Bauer assay was used to assess the dressing longevity. [] *Pseudomonas aeruginosa* was grown to log phase as described for the log reductions. An aseptically-cut 1 in^2 piece of each dressing was placed coated-side down in the center of an inoculated plate and moistened to saturation with 0.3 mL of dH_2O. The plates were covered with their Petri dish lid and incubated overnight at 37°C. The dressings were transferred to a new log-phase bacteria lawn daily. If the dressings appeared dry, they were moistened with 0.1 mL of dH_2O. A total of six transfers were made over a period of seven days. Every day, the zones of bacterial inhibition were measured in two perpendicular directions. The dressing width was subtracted from the zone width for both directions and their results were averaged to yield the CZOI values. Tests were performed in triplicate.

A second set of log reductions was completed on dressings which had been subjected to three days of CZOI testing.

Scanning Electron Microscopy (SEM)/ Atomic Force Microscopy (AFM):

SEM and AFM analysis was used to image the surface microstructure and determine the roughness of the dressing samples, repectively. SEM testing was completed at the Alberta Centre for Surface Engineering and Sciences (ACSES). A JAMP 9500F auger microprobe was used to image subsections of a 1in^2 dressing sample by SEM. SEM images were taken between 10μm and 100nm scales. AFM images were taken to confirm SEM images and calculate the roughness of the dressings. For roughness calculations, a 25 nm^2 image was obtained at using an Olympus 160TS tip. MFD-3D from Asylum Research (Santa Barbara, CA), controlled by IGOR PRO software (Wavemetrics, Portland, OR),

calculated the roughness on three 1nm^2 subsections of the image located at (0.5nm,0.5nm), (2.5nm,2.5nm) and (4.5nm,4.5nm). These values were then averaged to give an average roughness for the dressing sample. The roughness was calculated by the RMS roughness given in Figure 3.1.

$$R_{rms} = \sqrt{\frac{\sum_{i=1}^{n}(z_i - z^-)^2}{n}}$$

Figure 3.1. RMS Roughness formula for calculating roughness using the AFM height retrace.

Energy-Dispersive X-ray Spectroscopy (EDS):

EDS was used to analyse the bulk dressing composition since the separation of the XRD peaks led to high error when deconvolution was attempted. EDS was completed on a 20mm^2 oxford x-max detector attached to a VEGA3 SEM at ACSES. A working distance of 10.0 mm was used and a dead time of 40% was acquired by increasing the beam intensity to between 15 and 17 nA before data acquisition began. A copper signal was omitted from the data as copper tape was used to adhere the sample to the target holder. When carbon tape was used instead of copper tape it was noted that the copper signal disappeared and the carbon signal increased. Peak significance was ensured by verifying that the fit index for the peak was less than 10. For gold peaks a fit index of up to 15 was accepted as dissolution data showed that the data was still reliable. This check is shown in Appendix 2B.

X-ray Diffraction (XRD):

Gold and silver dressings were analysed by XRD using a RIGAKU rotating anode XRD system in the Chemical and Materials Engineering Department at the University of Alberta. The dressings were scanned from 10 to 110 $^{o}2\theta$ in continuous mode using a step size of 0.05$^{o}2\theta$. A copper anode was used at a voltage of 40 KV and current of 110mamps. Minimum crystallite sizes were determined by the Scherrer method. [13] The values for minimum crystallite size were obtained by averaging the minimum crystallite size calculated from peaks at 44 and 64.5 $^{o}2\theta$. The Scherrer equation in Figure 3.2 was used for this calculation. In this equation, τ is the crystallite size, K is the shape factor and was assumed to be

0.9, λ was 1.54nm with a Cu anode, β is the full width at half maximum in $^{o}2\theta$ and θ is the width the peak spans in $^{o}2\theta$.

$$\tau = \frac{K\lambda}{\beta \cos\theta}$$

Figure 3.2. The Scherrer Equation for determining minimum crystallite size.

X-ray Photoelectric Spectroscopy (XPS):

Dressings were analysed by XPS at the ACSES facility. To obtain the spectra, an Axis 165 spectrometer (Kratos Analytical) with a monochromatic Al Ka source was used at a power of 210W. The samples were analysed at 3 x 10^{-10} Torr and a normal take off angle. The pass energy of 160eV was used for the survey spectra and a pass energy of 20 eV was used for the high-resolution spectra. Spectra were analysed using linear background corrections and Gauss/Lorentz approximations in CasaXPS software (Version 2.3.15© 1999-2009 Neal Fairley). The peaks were calibrated to a C1s signal at 284.8eV. The deconvolution of XPS peaks was considered acceptable when the Chi squared value was less than 50 without the RMS fitting option. No constraints were placed on the peaks when fitting them with the CasaXPS software.

Atomic Absorption Spectroscopy (AAS):

The release of silver into dH_2O and ammonium hydroxide (NH_4OH) were studied with AAS at the University of Alberta using methods similar to those of Wright et *al.* [4] For de-ionized water samples, one in^2 of dressing was placed in 10mL of de-ionized water for 24 hours at room temperature. After 24 hours, the dressing was removed with forceps and allowed to drip back into the vial for 10 s. The 10mL of water and dissolved silver was then acidified with 10 mL of nitric acid acidification solution (18% nitric acid/1.8% tartaric acid). The acidification prevented silver precipitation before analysis. No filtration was required as no visible particulate silver was present in the solutions. For the NH_4 samples, 1 in^2 of

dressing was placed in 10mL of 20.0g/L ammonium hydroxide for 3 minutes. The samples were also acidified with 10 mL of acidification solution. Both water and NH_4OH samples were submitted for total silver analysis on a Varian 220 FS double beam Atomic Absorption Spectrophotometer. A lean air-acetylene flame and a silver hollow cathode lamp (λ = 328.1 nm) were used with this spectrophotometer. Samples were diluted if the silver concentration was greater than the upper limit of the calibration plot (5.0ppm). The results were then corrected for the applied dilution factor.

Inductively Coupled Plasma- Mass Spectroscopy (ICP-MS):

Gold release was too small to be measured by AAS, so ICP was used as it can provide a much more accurate measurement. dH_2O dissolutions were made by submersing 1 in^2 of dressing in 10mL of de-ionized water for 24 hours at room temperature. After 24 hours, the dressing was removed with forceps and allowed to drip back into the vial for 10 s. The 10mL of water and gold was then acidified with 10 mL of aqua regia. The aqua regia is known to dissolve gold and precipitate silver. Furthermore, dissolution of 1 in^2 of dressing into 20 mL of aqua regia was used to determine the total amount of gold in the dressing samples. Both the dH_2O dissolution and the total gold digest were measured in the University of Alberta's Radiogenic Isotope Facility using a Perkin Elmer Elan6000 quadrupole ICP-MS. A calibration plot up to 300 ppm was created using a gold standard stock solution of 1000ppm. dH_2O samples were diluted by a factor of 10 and aqua regia dissolution samples were diluted by a factor of 1000 before measurement. The dilution factor was re-applied after analysis.

Statistics:

One way ANOVA with Tukey-Kramer Multiple Comparisons were performed using GraphPad Instat version 3.10. For log reductions, only trials with exact numbers (i.e. not greater than numbers) were statistically analysed. This method was also used to test for statistical significance in the CZOI, AFM and dissolution (AAS and ICP) data.

Results

Log Reduction/ CZOI:

Figures 3.3-3.5 show the log reduction with *P. aeruginosa* with low oxygen (2%), normal (4%) and high oxygen (8%) dressings, respectively. Dressings recorded a complete kill for *P. aeruginosa* at normal and high oxygen levels. However, at low oxygen levels Ag_{100}, Ag_{80} and Ag_{50} were bactericidal while Ag_{35} was not (defined as a log reduction greater than three).

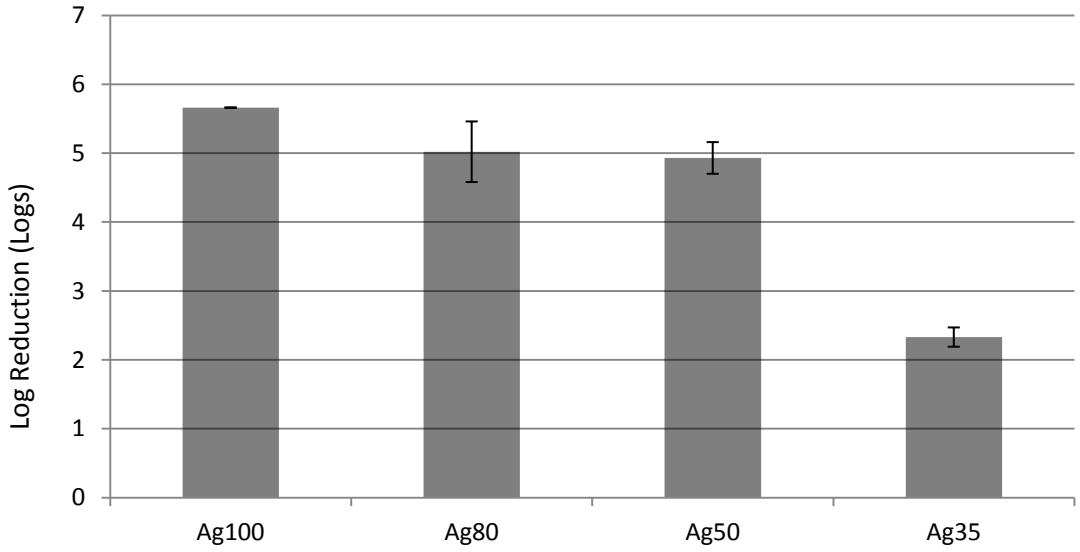

Figure 3.3. Log reduction of *P. aeruginosa* with dressings sputtered in a low O_2 (2%) environment.

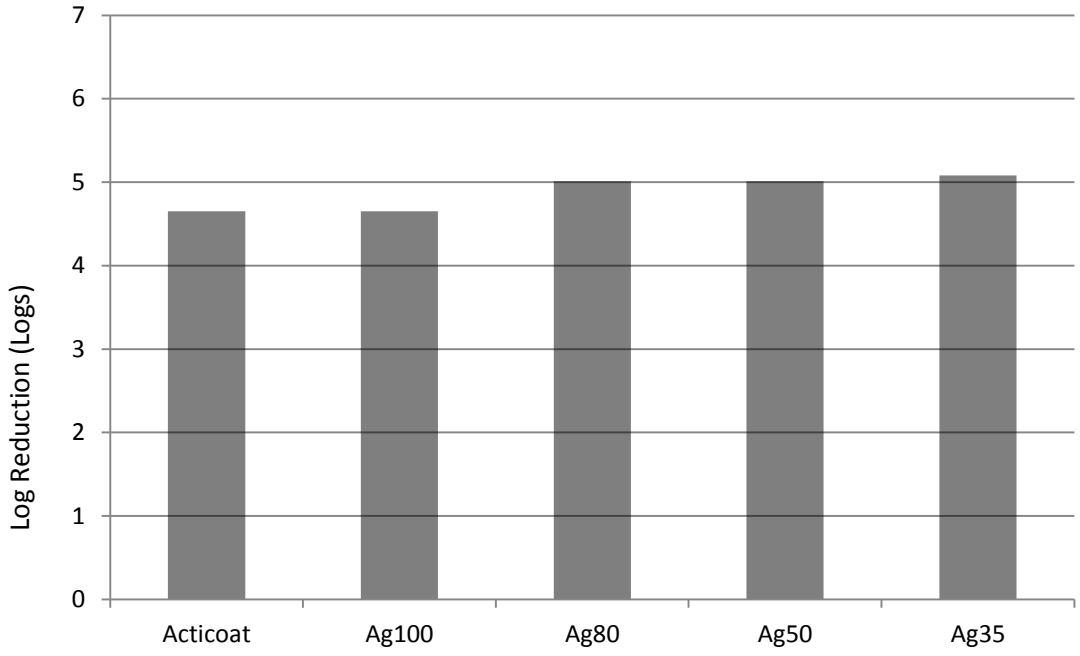

Figure 3.4. Log reduction of *P. aeruginosa* with dressings sputtered in a normal O_2 (4%) environment.

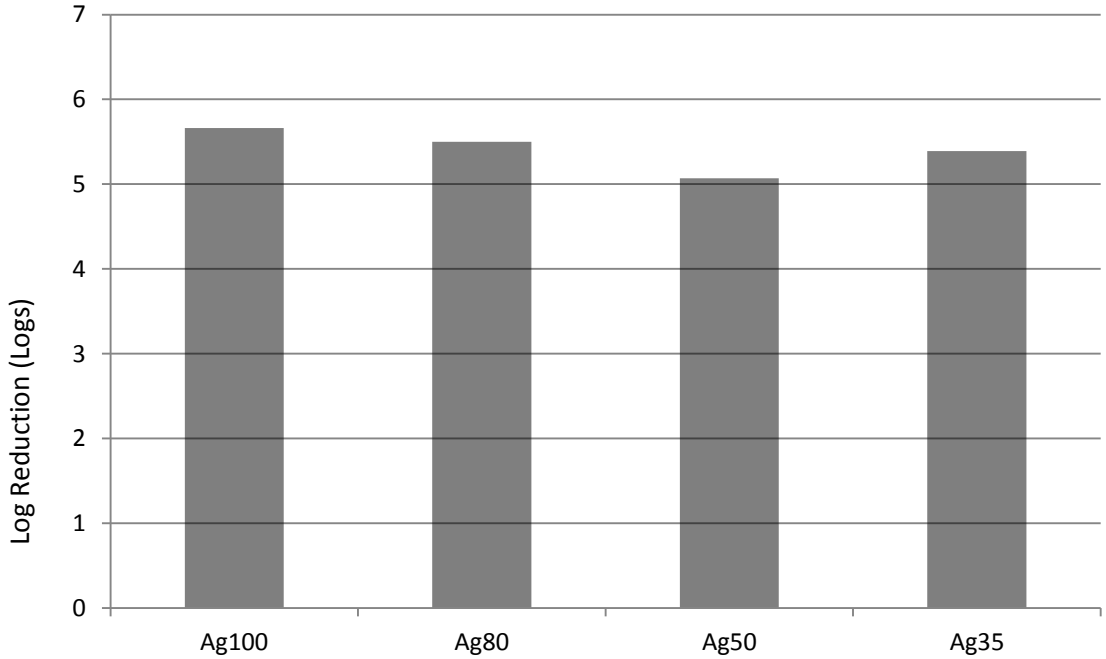

Figure 3.5. Log reduction of *P. aeruginosa* with dressings sputtered in a high O_2 (8%) environment.

Figures 3.6-3.8 show the log reduction with *S. aureus* with low oxygen (2%), normal (4%) and high oxygen (8%) dressings, respectively. Again, dressings recorded a complete kill for *S. aureus* at

normal and high oxygen levels. However, at low oxygen levels all dressings did not produce a log reduction greater than three.

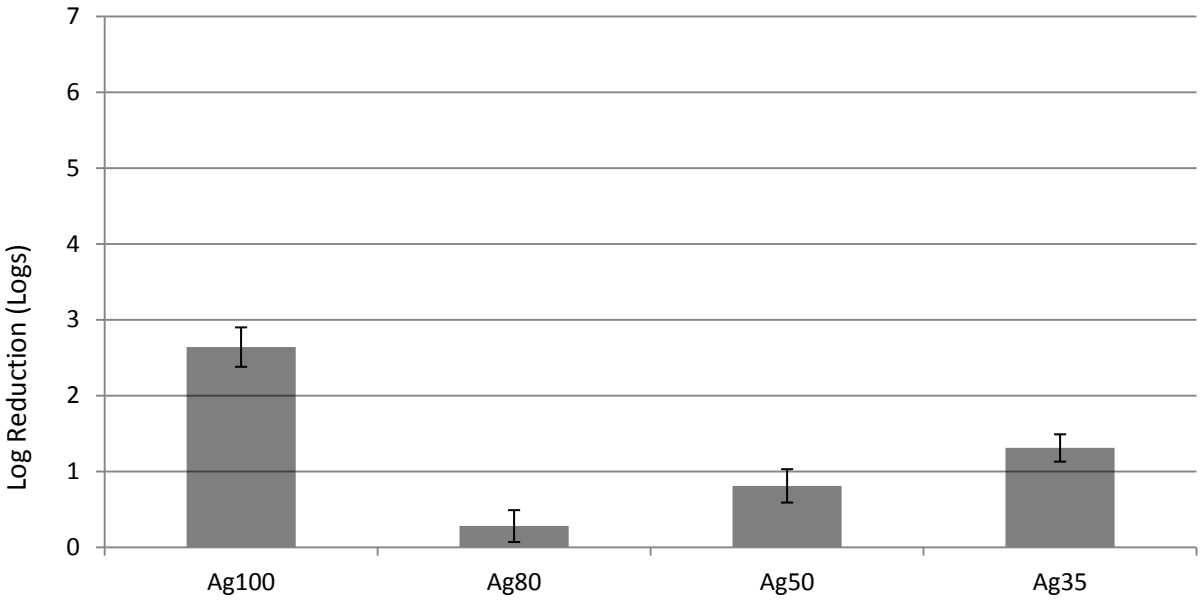

Figure 3.6. Log reduction of *S. aureus* with dressings sputtered in a low O_2 (2%) environment.

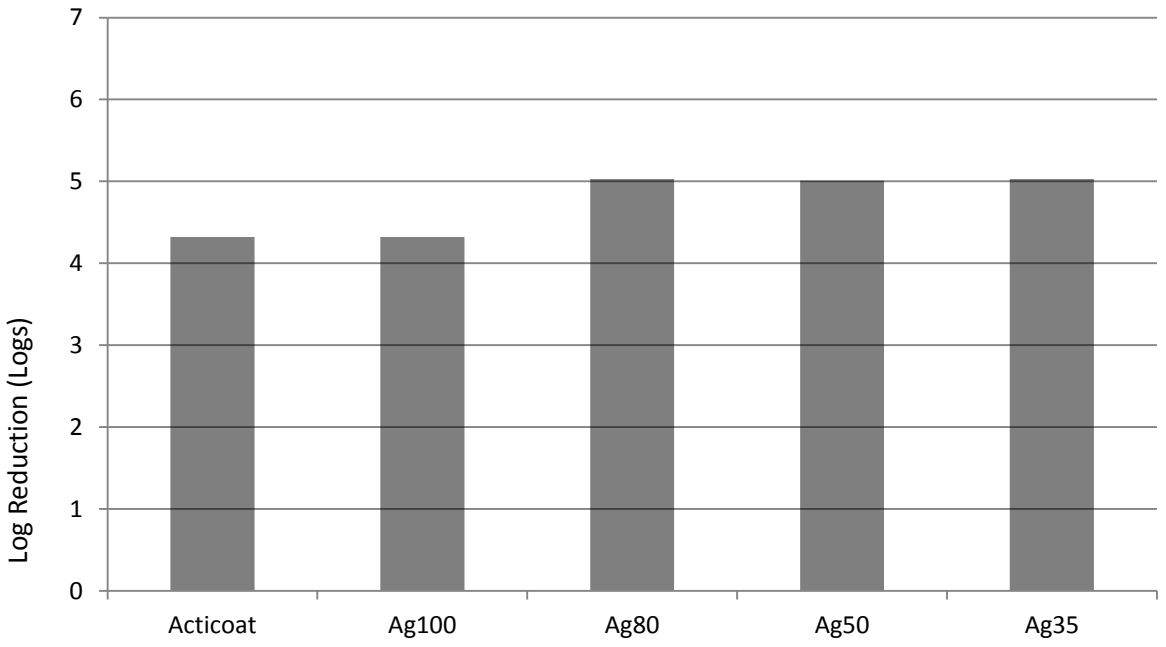

Figure 3.7. Log reduction of *S. aureus* with dressings sputtered in a normal O_2 (4%) environment.

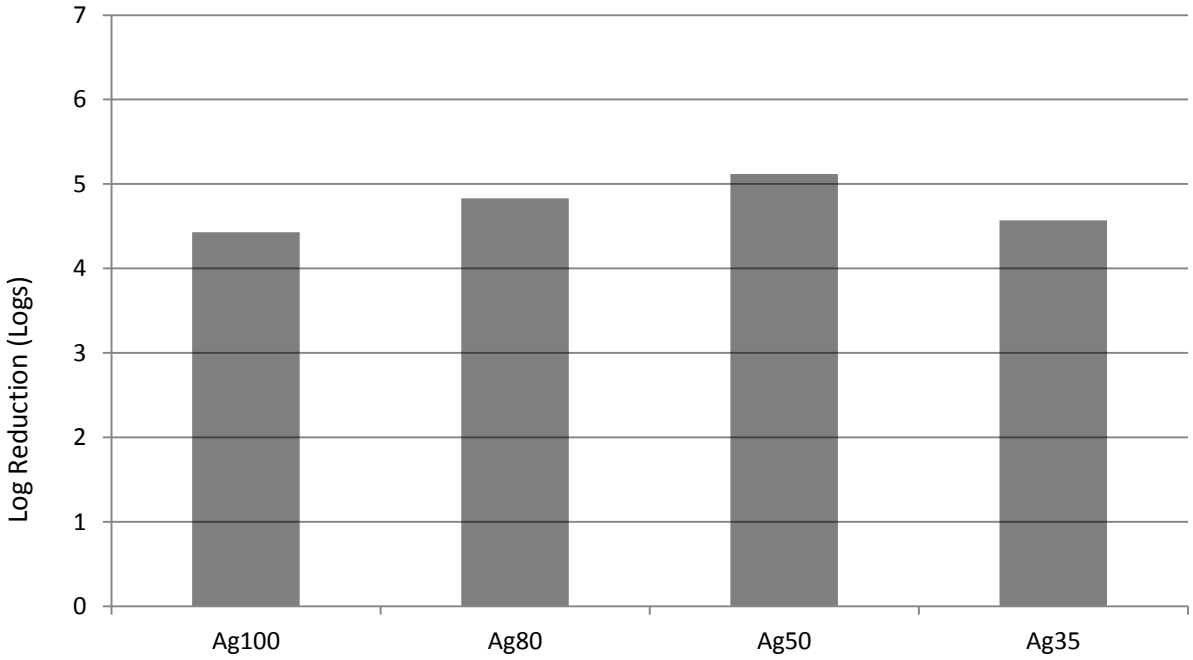

Figure 3.8. Log reduction of *S. aureus* with dressings sputtered in a high O_2 (8%) environment.

Figures 3.9-3.10 show the log reduction numbers for *P. aeruginosa* with dressings heat treated for 24 hours at 50, 75 and 100°C, respectively. All dressings heat treated at 50 and 75°C produced a complete kill while only Acticoat® was bacterioicidal after heat treatment at 100°C.

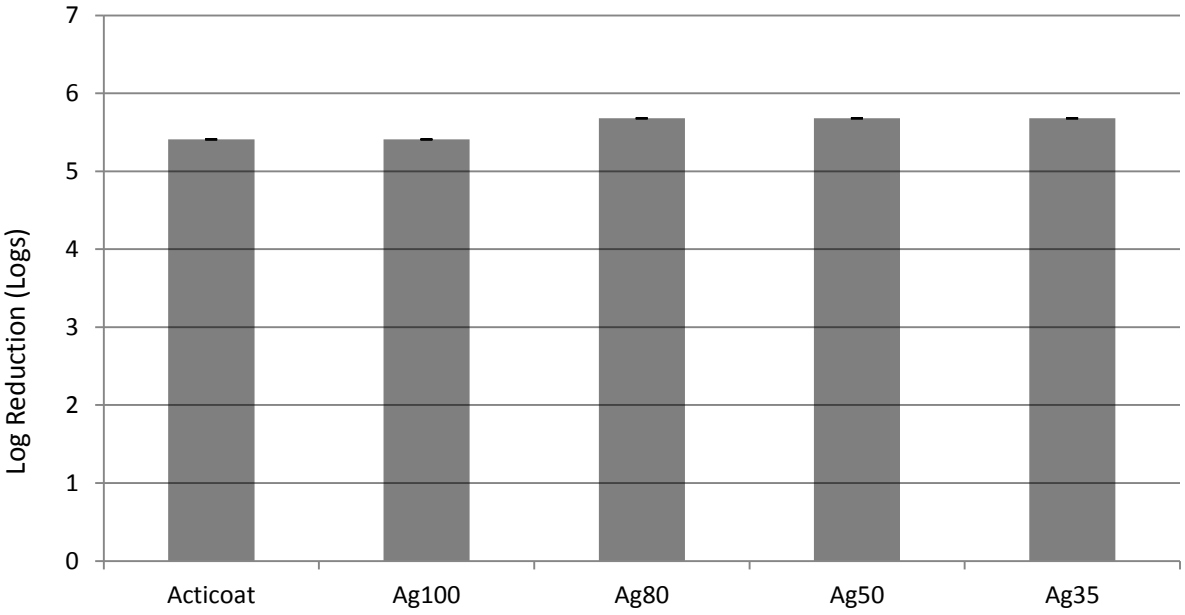

Figure 3.9. Log reduction of *P. aeruginosa* with dressings heat treated at 50°C.

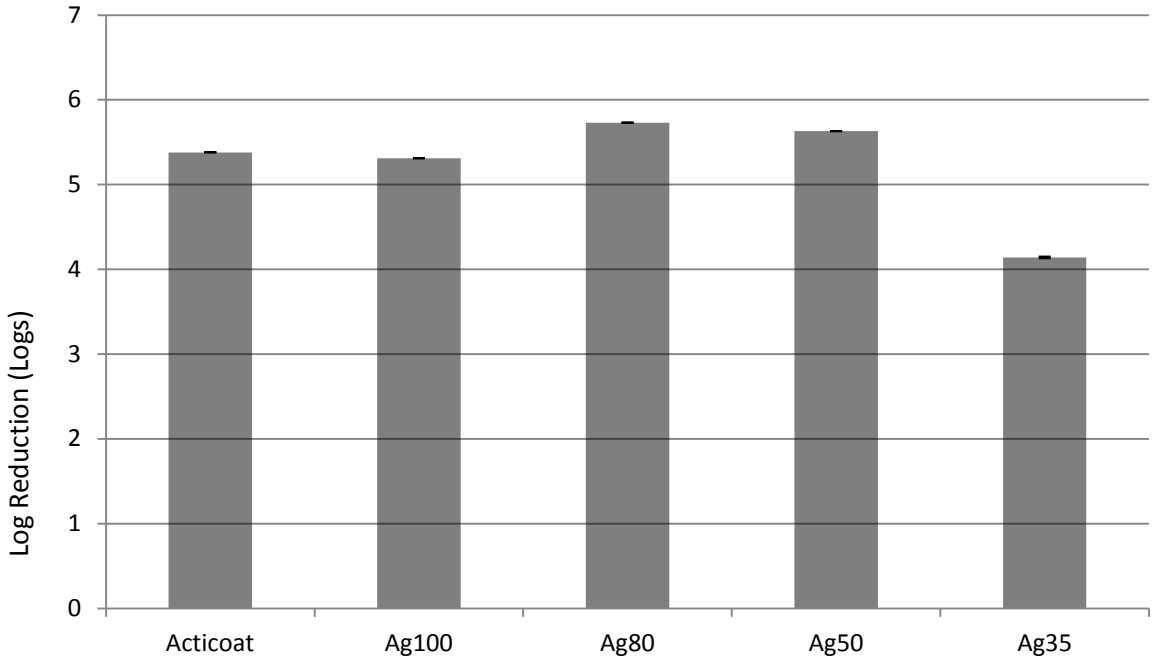

Figure 3.10. Log reduction of *P. aeruginosa* with dressings heat treated at 75°C.

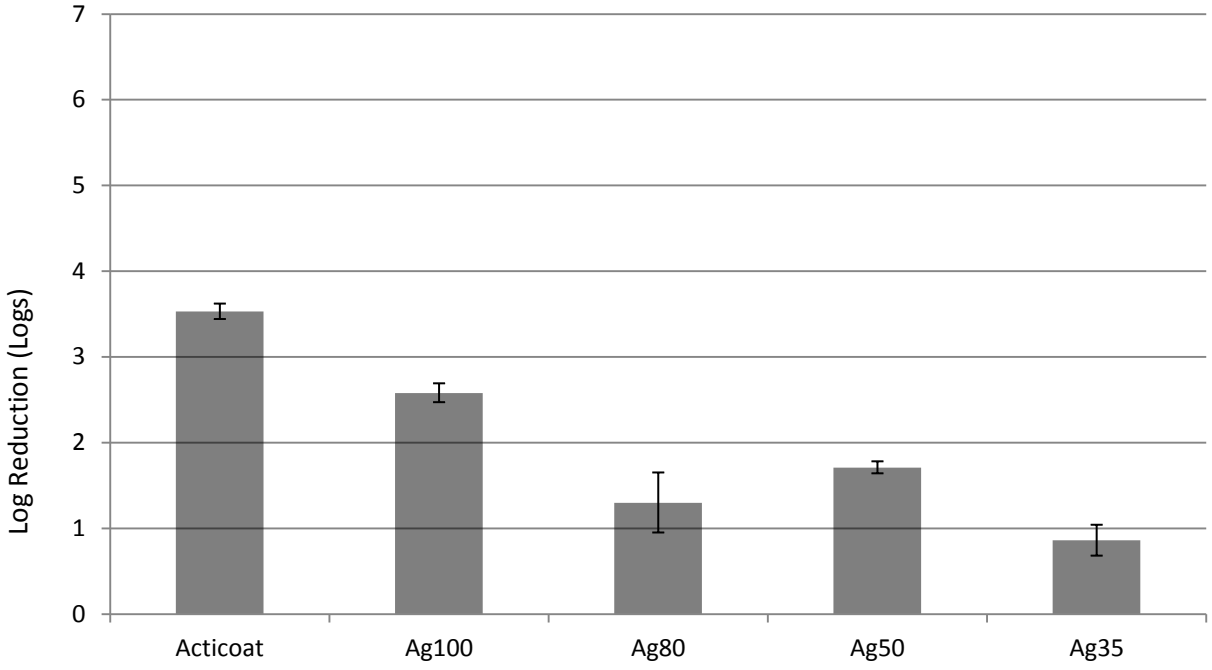

Figure 3.11. Log reduction of *P. aeruginosa* with dressings heat treated at 100°C.

Figures 3.12-3.14 show the log reduction results for *S. aureus* with dressings heat treated at 50, 75 and 100°C, respectively. After a 50°C temperature treatment only Ag35 had a log reduction less than three while at 75°C Ag_{50} and Ag_{35} both produced log reductions less than three. At 100°C the observed log reduction for all dressings was less than 2.5.

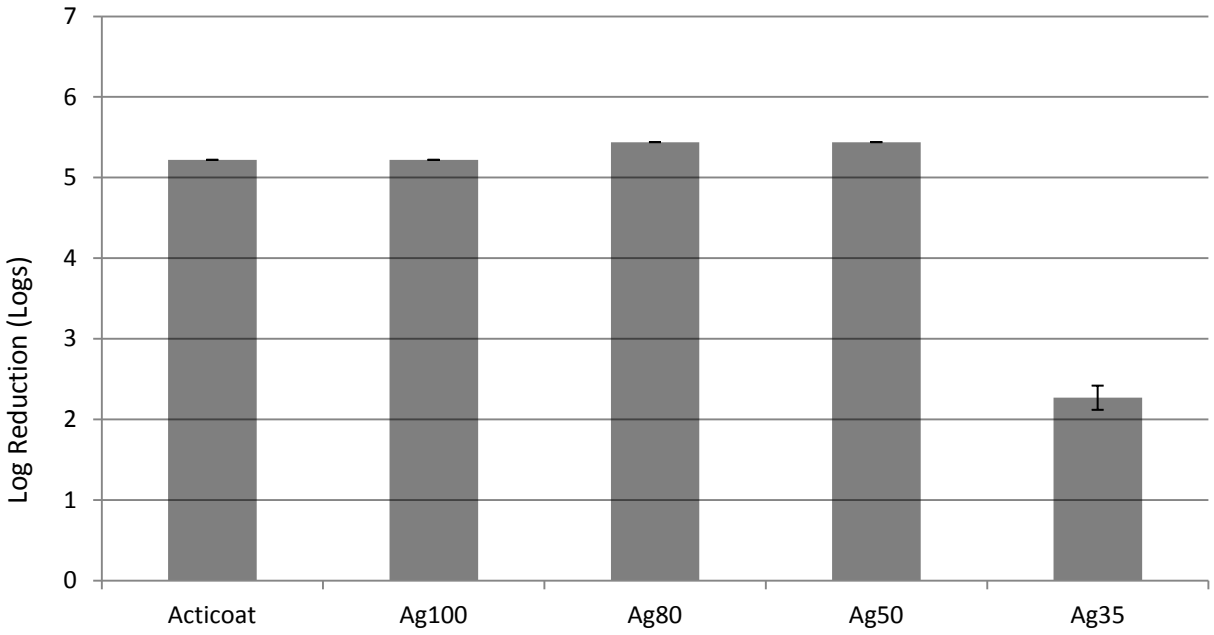

Figure 3.12. Log reduction of *S. aureus* with dressings heat treated at 50°C.

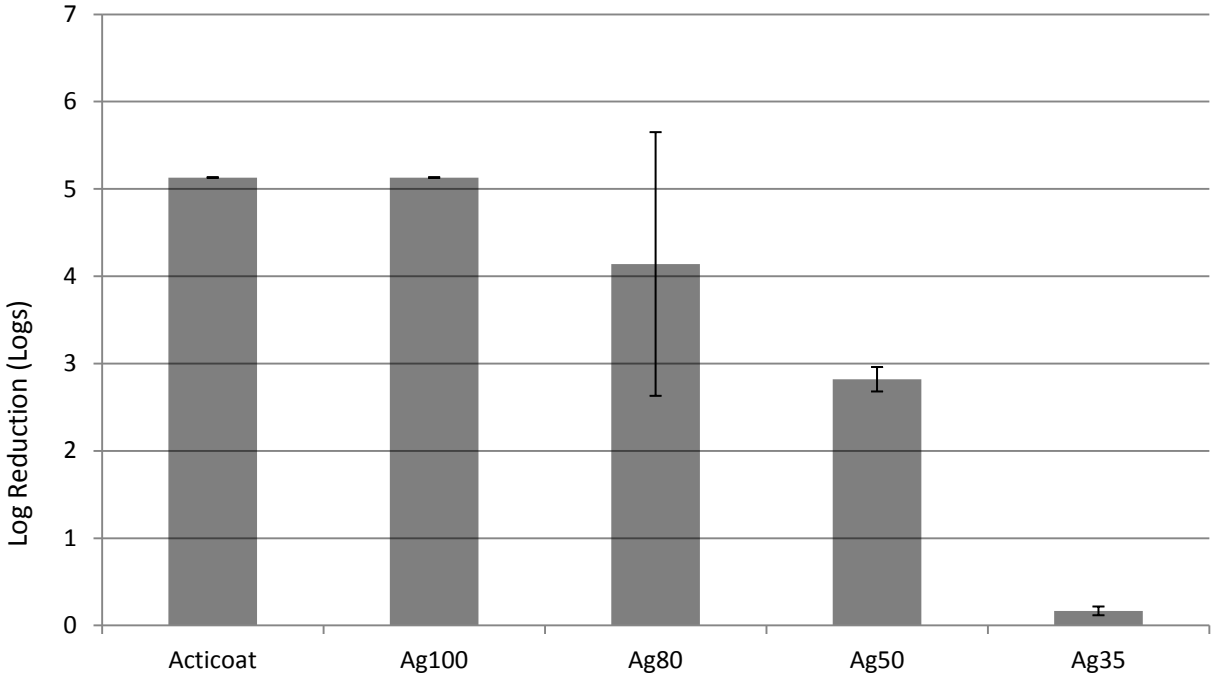

Figure 3.13. Log reduction of *S. aureus* with dressings heat treated at 75°C.

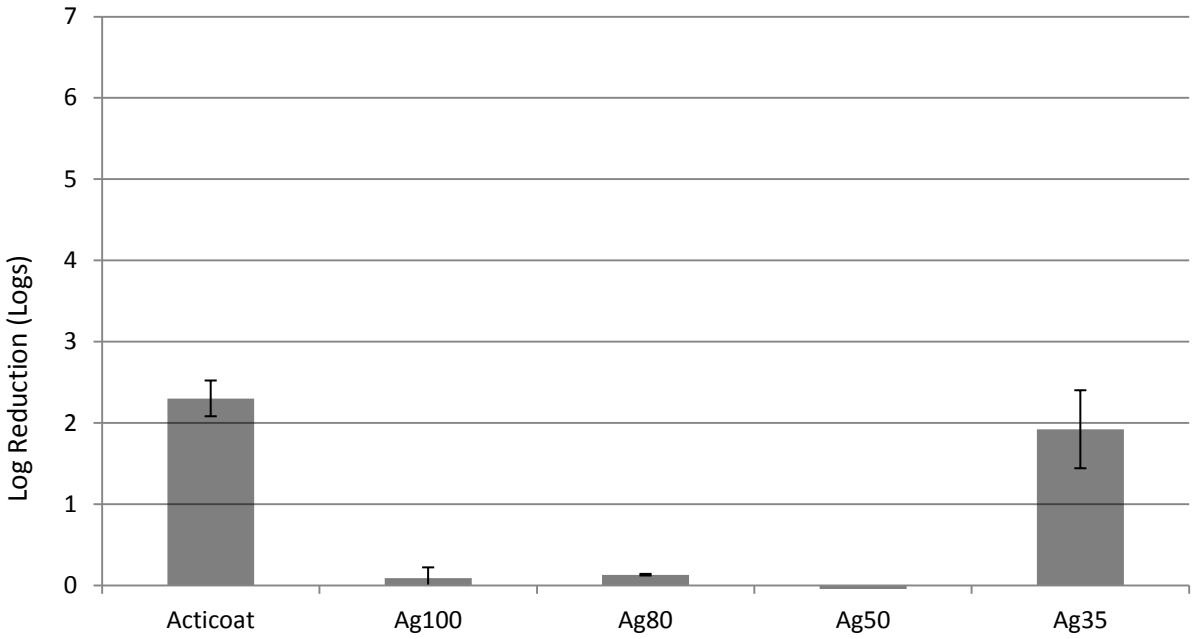

Figure 3.14. Log reduction of *S. aureus* with dressings heat treated at 100°C.

Figures 3.15-3.16 show the CZOIs for *P. aeruginosa* with dressings sputtered at low and high oxygen, respectively. The zones produced by dressings created in a low oxygen environment were significantly smaller than those created by the dressings created in a high oxygen environment except for the zones produced on Day 1 where the only significant difference was between $Ag_{35}(8)$ and $Ag_{35}(2)$ ($p<0.05$).

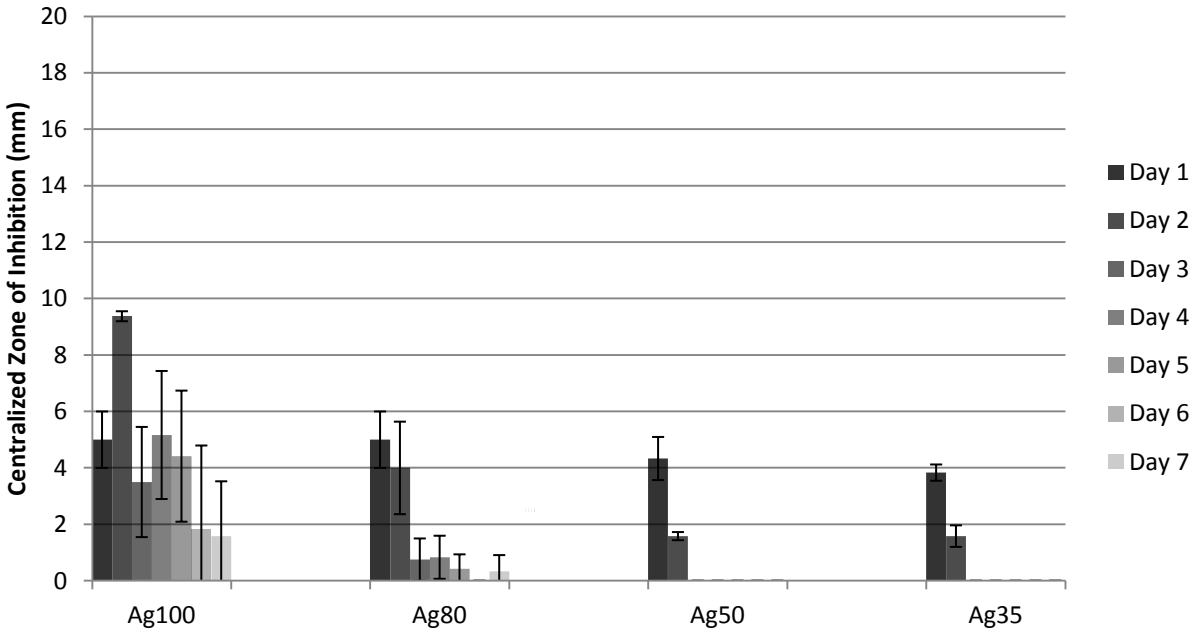

Figure 3.15. CZOI of *P. aeruginosa* for dressings created in a low O_2 (2%) environment.

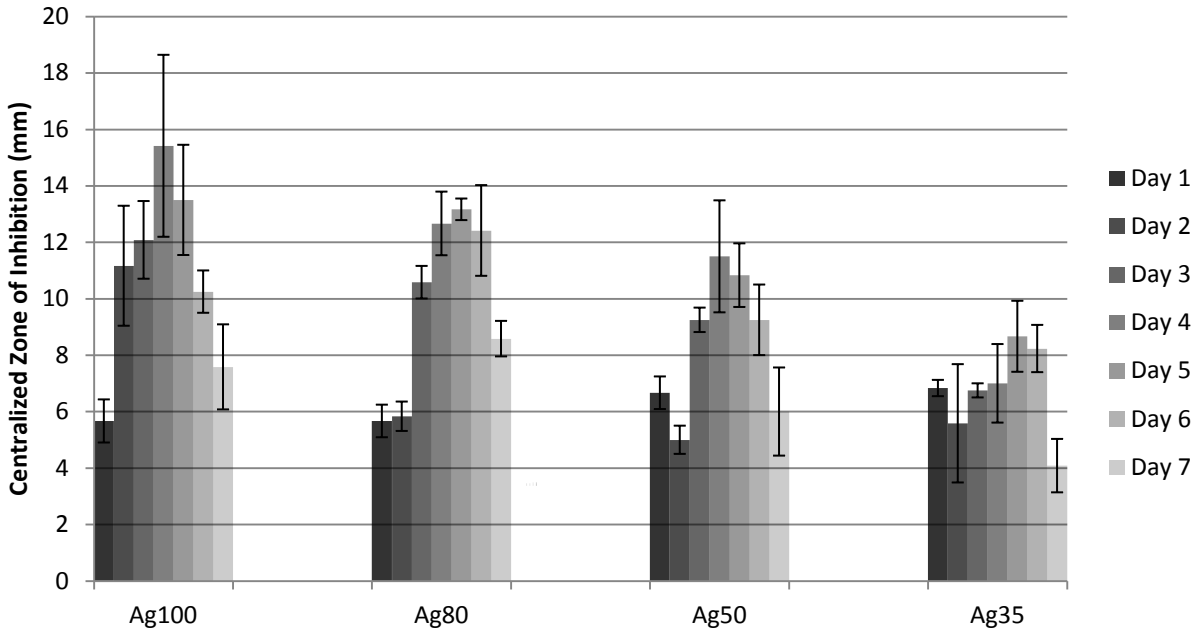

Figure 3.16. CZOI of *P. aeruginosa* for dressings created in a high O_2 (8%) environment.

Figures 3.17-3.19 show the CZOIs for *P. aeruginosa* with dressings heat treated at 50, 75 and 100^{o}C, respectively. In general, dressings treated at lower temperature created larger zones. Dressings with high gold content (Ag_{50} and Ag_{35}) heat treated at 75^{o}C could not create a zone after 3 trial days.

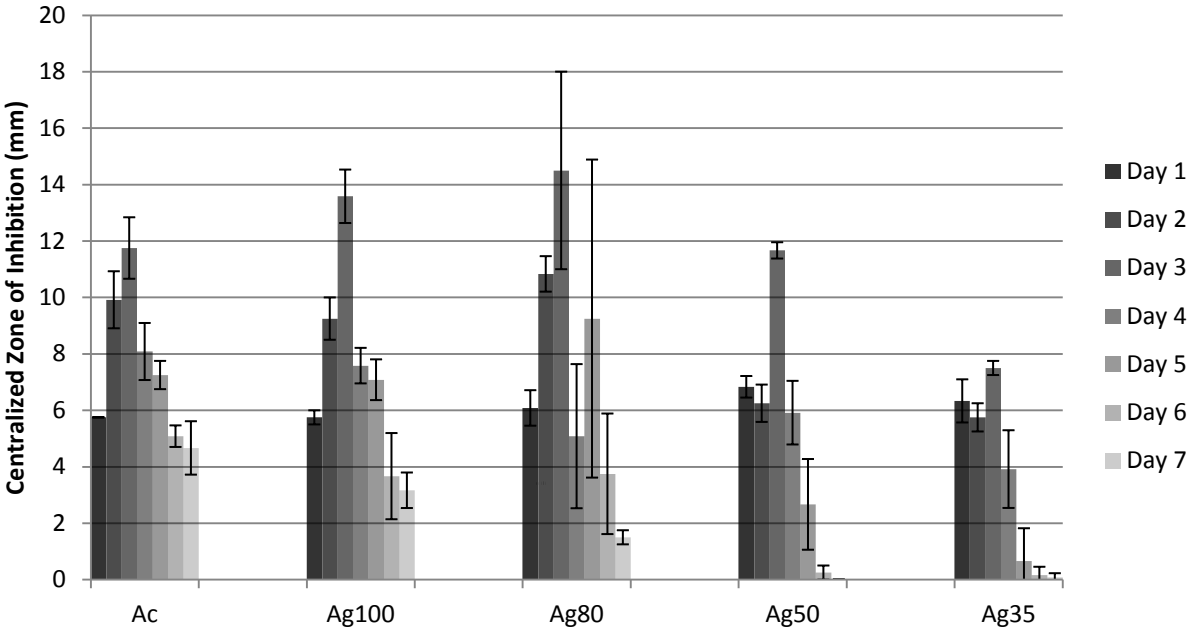

Figure 3.17. CZOI of *P. aeruginosa* for dressings heat treated at 50°C for 24 hours.

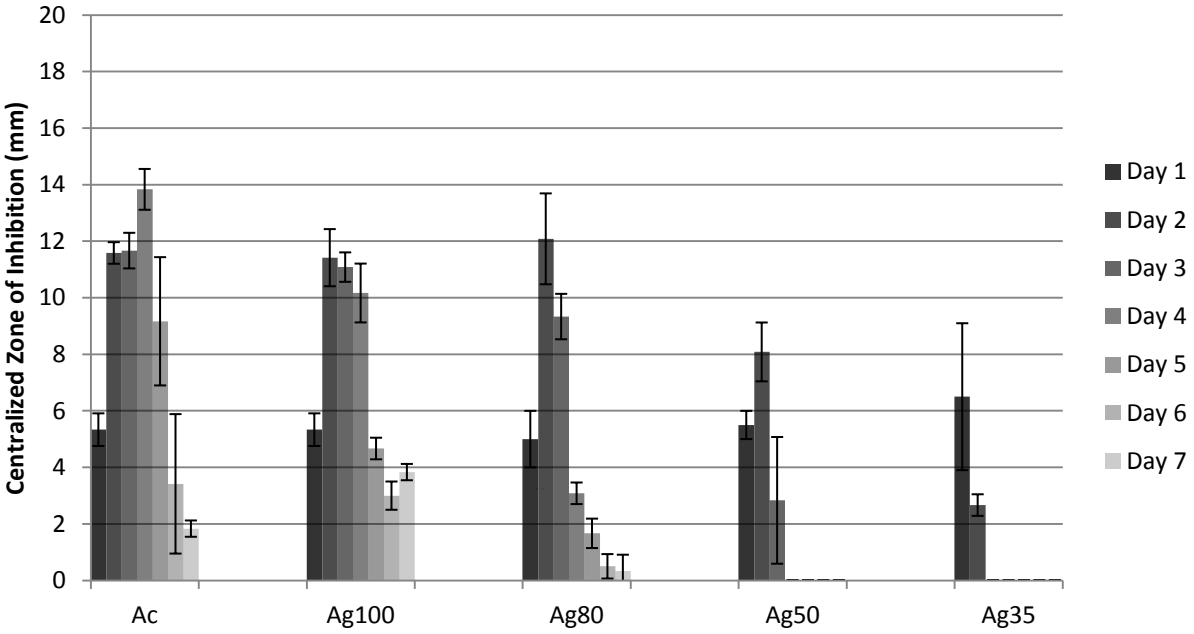

Figure 3.18. CZOI of *P. aeruginosa* for dressings heat treated at 75°C for 24 hours.

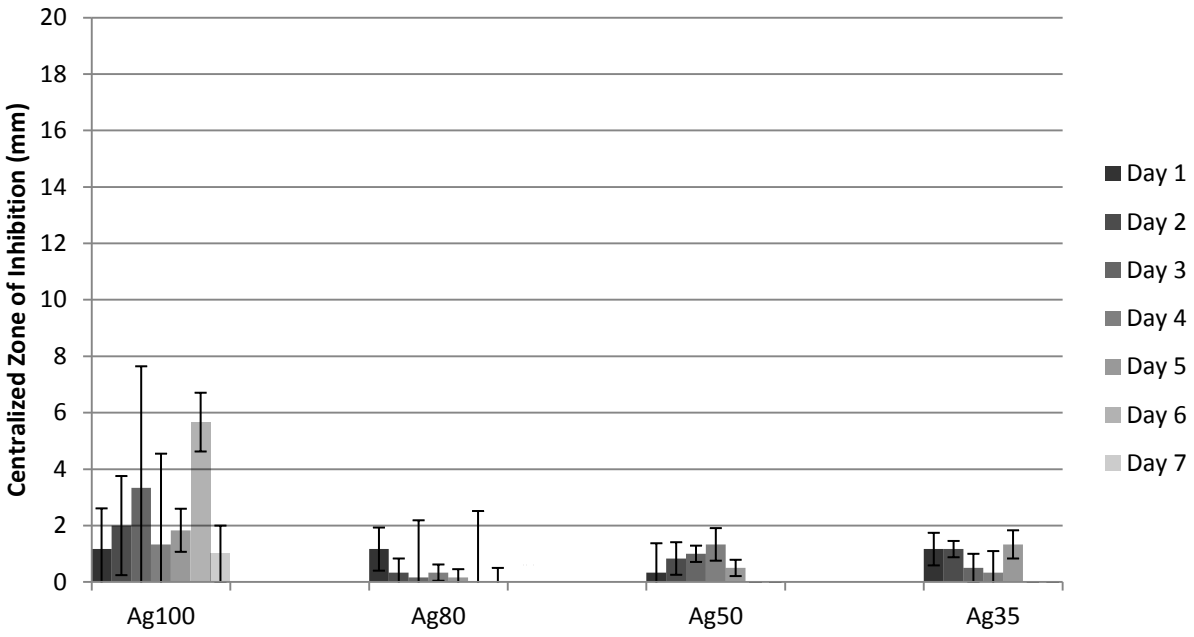

Figure 3.19. CZOI of *P. aeruginosa* for dressings heat treated at 100^{o}C for 24 hours.

SEM/AFM:

Table 3.1 shows the AFM roughness data for all dressings sputtered at different oxygen levels and heat treated at 50, 75 and 100^{o}C. The roughness of high oxygen dressings were greater than those created in a low oxygen environment except for Ag_{100}. As dressings were heat treated at higher temperature they became less rough except for changes between Ag_{50} (50^{o}C) and Ag_{50} (75^{o}C), and Ag_{100} (75^{o}C) and Ag_{100} (100^{o}C) where the changes were both non-significant ($p>0.05$).

Table 3.1. AFM roughness data for all dressings sputtered at different oxygen levels and heat treated at 50, 75 and 100°C. All results are roughness ± standard deviation.

	Acticoat®	Ag_{100}	Ag_{80}	Ag_{50}	Ag_{35}
Normal (4% O_2)	45.1 ± 8.5	26.0 ± 6.1	30.1 ± 5.5	15.3 ± 3.2	21.6 ± 1.4
High (8% O_2)	n/a	24.4 ± 2.9	53.5 ± 3.5	21.7 ± 6.3	36.2 ± 25.6
Low (2% O_2)	n/a	30.4 ± 1.8	22 ± 12.9	16.6 ± 4.8	15.9 ± 3.9
50°C	49.2 ± 9.9	55.7 ± 26.2	84.4 ± 5.0	12.2 ± 4.4	13.6 ± 2.1
75°c	41.8 ± 17.6	35.8 ± 7.2	77.9 ± 57.8	13.8 ± 8.9	13.9 ± 9.9
100°C	42.7 ± 11.5	46.9 ± 15.5	69.5 ± 17.6	7.17 ± 1.4	6.3 ± 0.03

Figures 3.20-3.22 show representative SEM images of Ag_{80} temperature treatment, Ag_{80} oxygen treatment and Ag_{35} oxygen treatment, respectively. Heat treatment of Ag_{80} in Figure 3.20 shows increasing grain size and smoothing of cluster edges as the dressing is treated at higher temperatures. Similarly, Figure 3.21 shows that sputtering in an atmosphere with a higher oxygen content creates a dressing with a finer nanostructure than dressings sputtered in a low oxygen environment. Figure 3.22 shows some of the cracking observed in some low oxygen samples along with the nanostructure differences compared to the same dressing sputtered in a high oxygen environment.

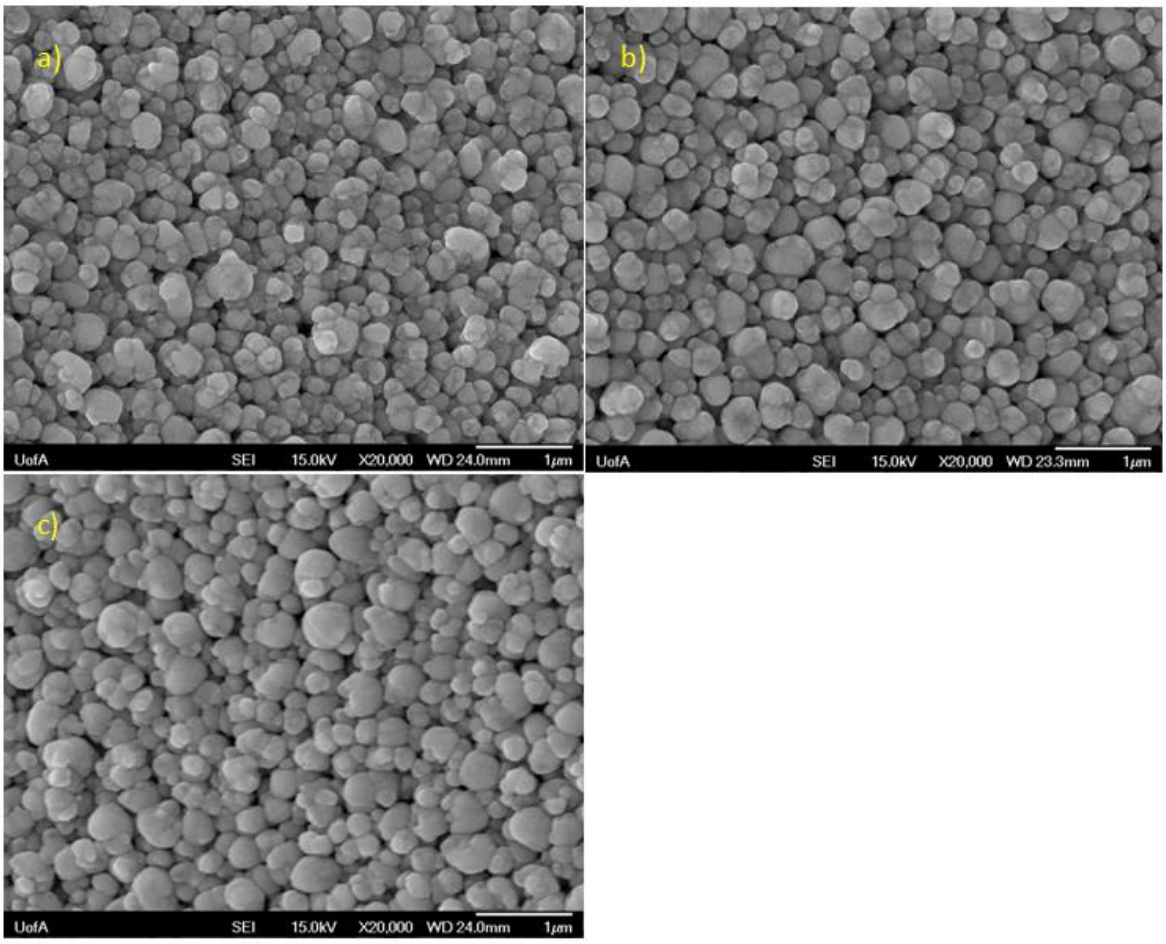

Figure 3.20. Sample images of Ag_{80} after heat treatment at: a) 50°C, b) 75°C and c) 100°C for 24 hours.

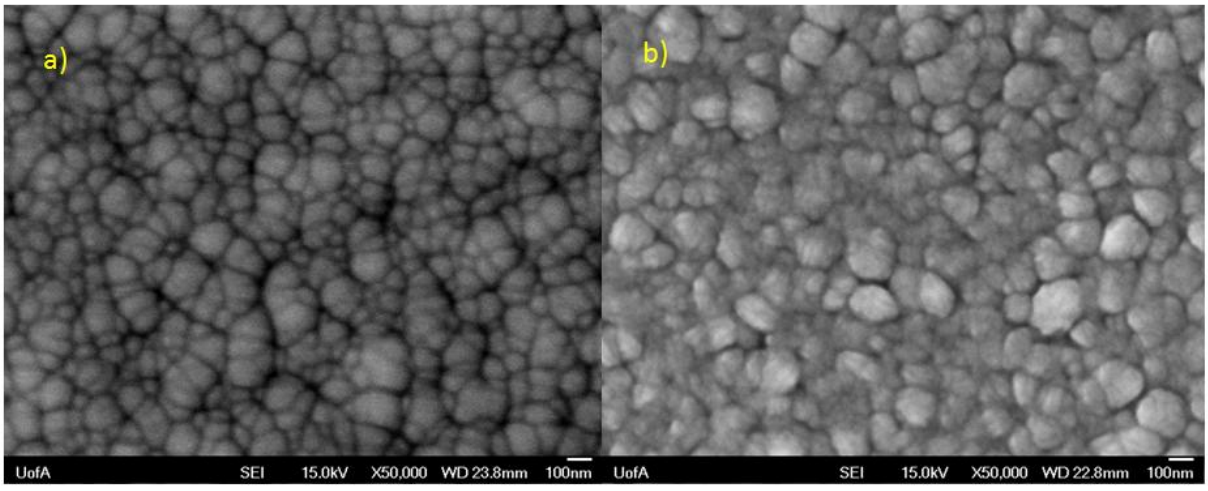

Figure 3.21. Sample images of Ag_{80} when sputtered with a) high (8%) and b) low (2%) oxygen.

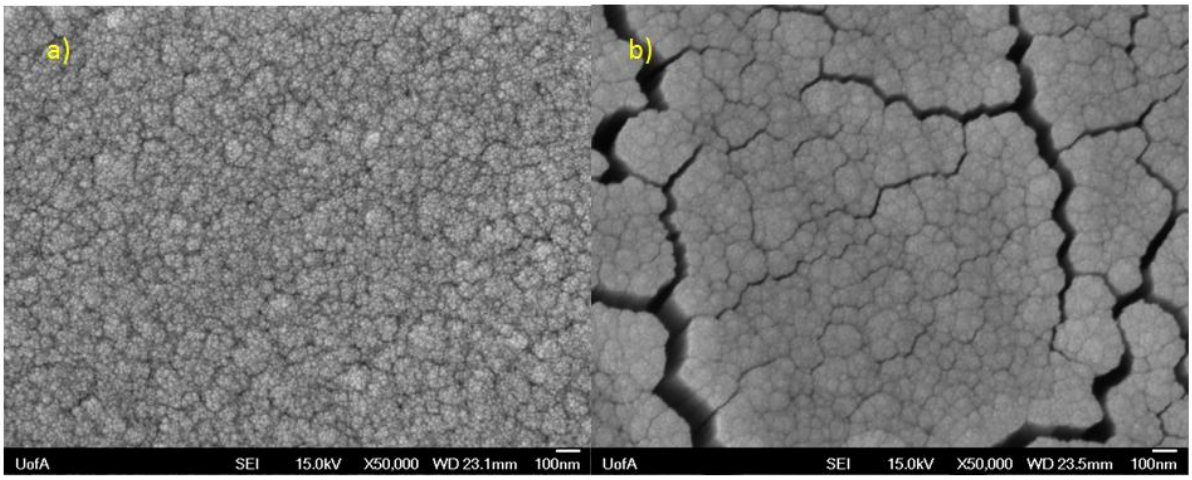

Figure 3.22. Sample images of Ag_{35} when sputtered with a) high (8%) and b) low (2%) oxygen.

EDS:

Tables 3.2-3.6 Show the results from the EDS characterization of the dressings. Dressings sputtered in a high oxygen environment incorporate at least double the atm% of oxygen in their nanostructures. A discussion of impurities is given in Chapter 2. The ratio of silver to gold on the dressings is affected by the environment as more silver relative to gold is sputtered in a low oxygen environment. Heat treatment at higher temperature served to decrease the oxygen content of the dressings and did not have any effect on the silver to gold ratio on the dressings.

Table 3.2 EDS characterization of samples sputtered with high oxygen (8%). Values are listed in atm%.

	C	O	Mg	Ag	Au	Ag/Au
Acticoat	-	-	-	-	-	-
Ag100	5.73	43.49	0.70	50.08	-	-
Ag80	10.80	25.46	0.44	52.43	10.87	82.86/17.14
Ag50	21.15	26.35	0.00	29.37	23.13	56.35/43.65
Ag35	23.22	26.64	0.00	21.11	29.02	42.65/57.35

Table 3.3. EDS characterization of samples sputtered with low oxygen (2%). Values are listed in atm%.

	C	O	Mg	Ag	Au	Ag/Au
Acticoat	-	-	-	-	-	-
Ag100	4.86	22.26	1.05	71.83	-	-
Ag80	9.96	5.31	0.00	71.41	13.32	84.28/15.72
Ag50	21.82	7.02	0.00	40.69	30.46	57.34/42.66
Ag35	37.69	5.05	0.00	25.20	32.06	44.32/55.68

Table 3.4. EDS characterization of samples heat treated at 50^{o}C. Values are listed in atm%.

	C	O	Mg	Ag	Au	Ag/Au
Acticoat	5.50	34.42	0.00	60.07	-	-
Ag100	5.20	22.75	0.97	71.08	-	-
Ag80	30.38	21.86	0.07	39.52	8.17	82.90/17.10
Ag50	36.67	11.28	0.00	29.30	22.75	56.63/43.37
Ag35	25.01	14.25	0.00	25.11	35.64	41.66/58.34

Table 3.5. EDS characterization of samples heat treated at 75^{o}C. Values are listed in atm%.

	C	O	Mg	Ag	Au	Ag/Au
Acticoat	4.71	20.28	1.14	73.87	-	-
Ag100	6.04	30.20	0.49	63.27	-	-
Ag80	46.31	13.43	0.34	33.23	6.69	83.23/16.77
Ag50	29.47	13.72	0.00	32.80	24.01	58.02/41.98
Ag35	26.88	5.51	0.00	28.55	39.06	42.45/57.55

Table 3.6. EDS characterization of samples heat treated at 100^{o}C. Values are listed in atm%.

	C	O	Mg	Ag	Au	Ag/Au
Acticoat	7.06	0.00	1.01	91.93	-	-
Ag100	5.83	0.00	1.55	92.62	-	-
Ag80	19.26	0.00	1.08	66.56	13.10	83.56/16.44
Ag50	32.80	5.64	0.00	35.15	26.41	57.31/42.69
Ag35	36.78	4.65	0.00	23.82	34.75	40.98/59.02

XRD:

Figures 3.23 and 3.24 show representative XRD spectra of Ag_{35} and Ag_{80} when sputtered with different oxygen levels. Figures 3.25 and 3.26 show Ag_{35} and Ag_{80} after various temperature treatments. When dressings are created with higher oxygen levels there is a broadening of the metallic peaks. While there is reduction of the Ag_20 peak at $44^o2\theta$, the broadening of the metallic peak at 38 $^o2\theta$ tends to smooth over it as well. Heat treated samples showed sharpening of all peaks even the silver oxide peak at $44^o2\theta$. Minimum crystallite calculations using the Scherrer formula showed that the minimum crystallite size of the high oxygen dressings was smaller than that of the low oxygen dressings. Also, the minimum crystallite size was observed to decrease as the dressings were heat treated at higher temperatures.

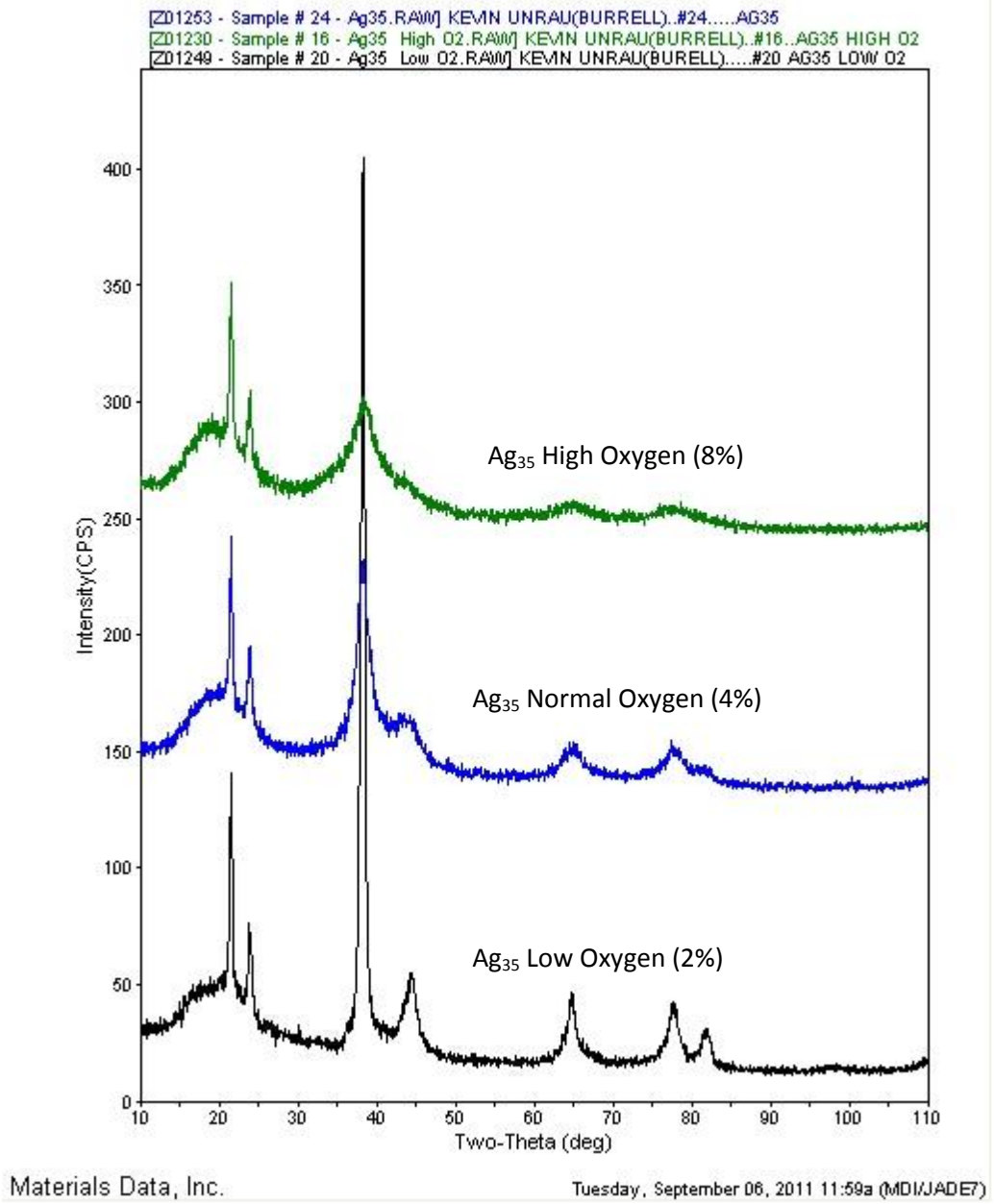

Figure 3.23. XRD spectra of Ag_{35} sputtered in low (2%), normal (4%) and high (8%) oxygen atmospheres.

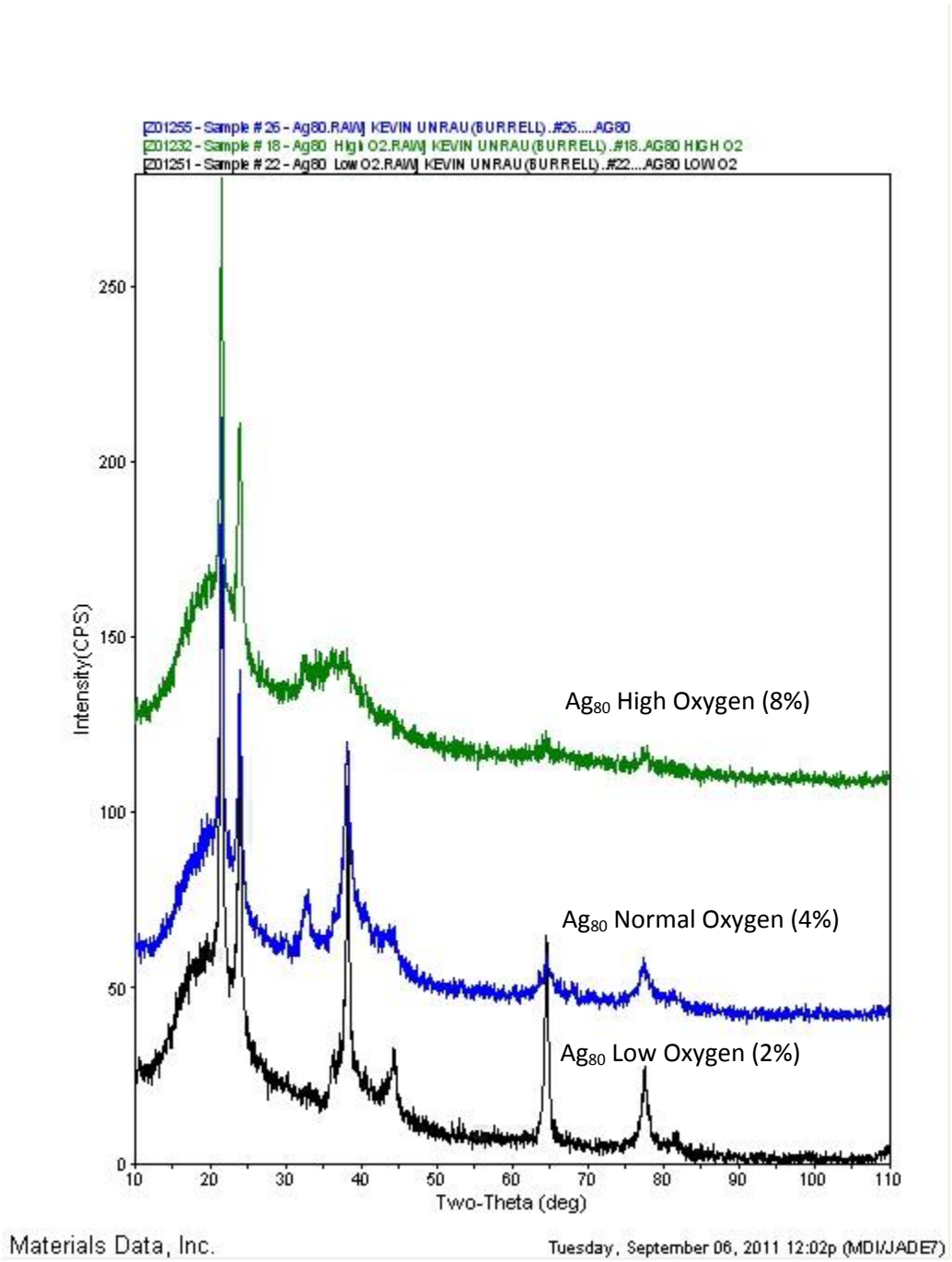

Figure 3.24. XRD spectra of Ag_{80} sputtered in low (2%), normal (4%) and high (8%) oxygen atmospheres.

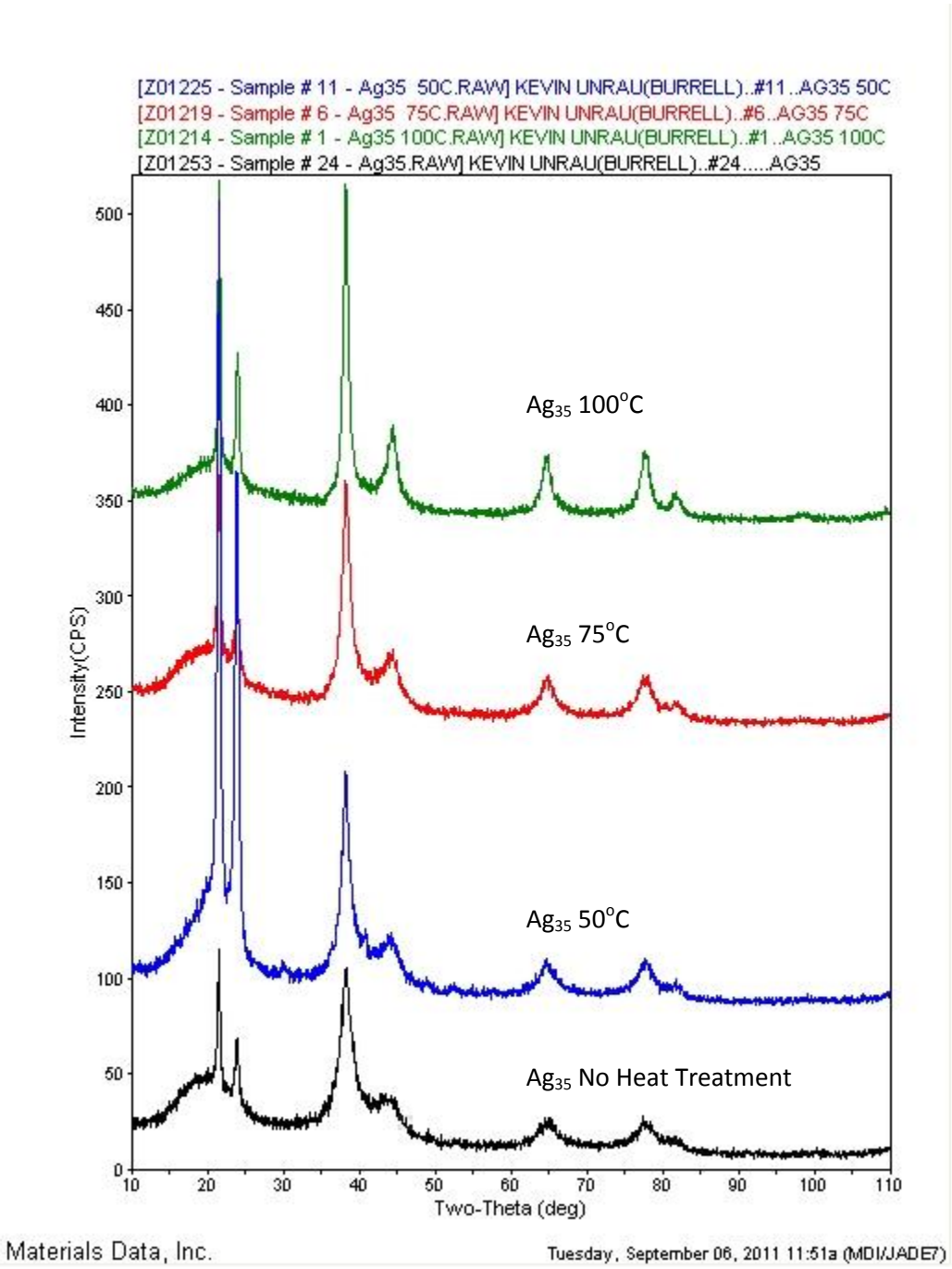

Figure 3.25. XRD spectra of Ag_{35} after 24 hour heat treatments at 50, 75 and 100°C.

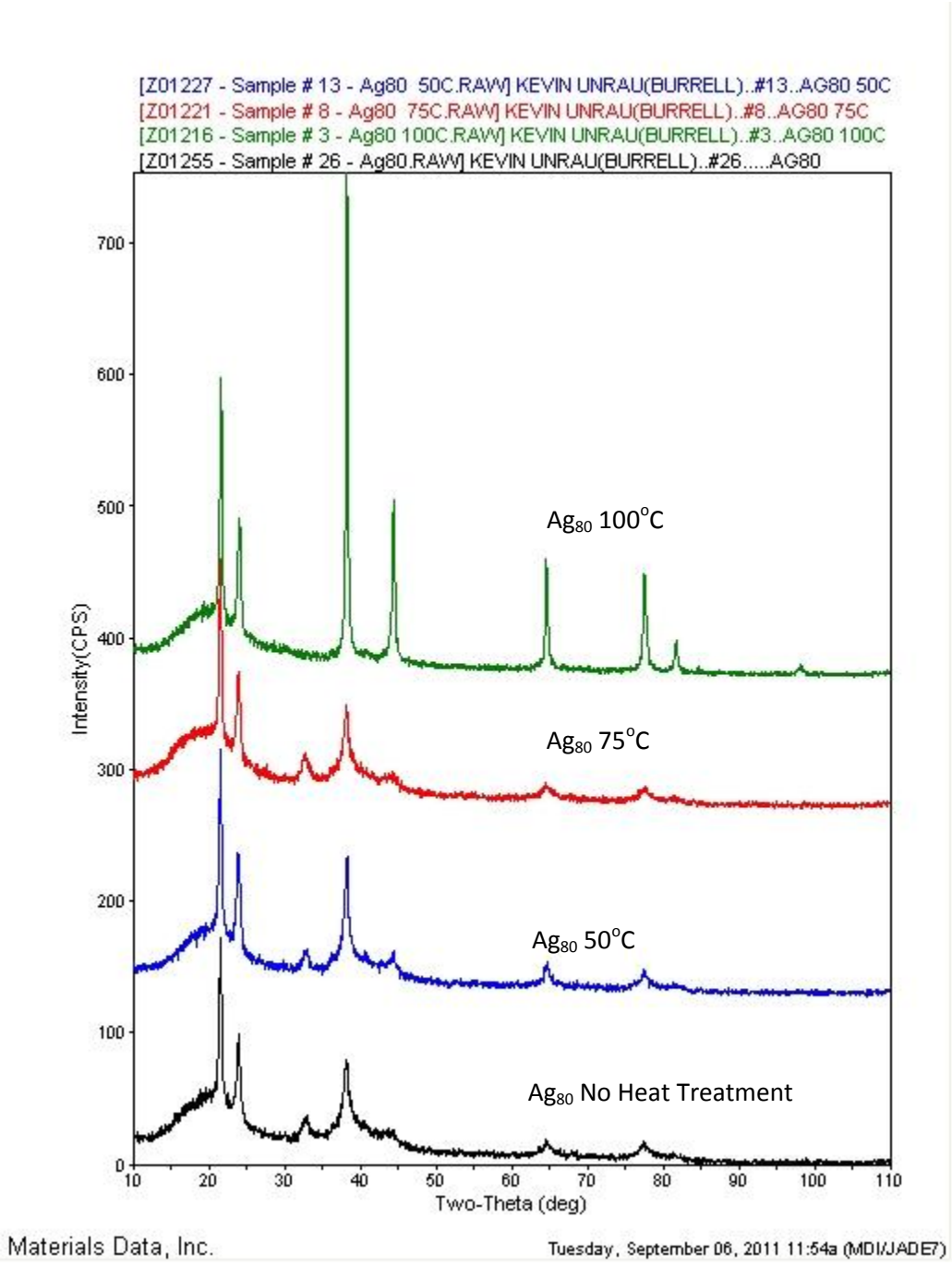

Figure 3.26. XRD spectra of Ag_{80} after 24 hour heat treatments at 50, 75 and 100°C.

Table 3.7. Minimum crystallite size for all dressings sputtered with different O_2 levels and heat treated at various temperatures for 24 hours.

Sample	Average Minimum Crystallite Size (nm)
A_{35} 100°C	6.520
Ag_{50} 100°C	8.576
Ag_{80} 100°C	25.071
Ag_{100} 100°C	31.274
Acticoat® 100°C	31.285
Ag_{35} 75°C	5.915
Ag_{50} 75°C	7.276
Ag_{80} 75°C	7.504
Ag_{100} 75°C	21.228
Acticoat® 75°C	19.50
Ag_{35} 50°C	7.065
Ag_{50} 50°C	7.019
Ag^{80} 50°C	15.074
Ag_{100} 50°C	16.390
Acticoat® 50°C	18.369
Ag_{35} HighOx	6.403
Ag_{50} High Ox	7.027
Ag_{80} High Ox	9.805
Ag_{100} High Ox	12.273
Ag_{35} Low Ox	8.434
Ag_{50} Low Ox	11.935
Ag_{80} Low Ox	16.329
Ag_{100} Low Ox	16.219
Ag_{35}	4.89
Ag_{50}	8.247
Ag_{80}	10.362
Ag_{100}	13.151
Acticoat®	17.874

XPS:

Figures 3.27 to 3.31 show representative images of XPS spectra from heat exposure and oxygen manipulation. O1s spectra of high and low oxygen samples show that Ag_{35} dressings sputtered in a low oxygen environment have the Ag-O/Au2O3 peak but lack the free oxygen peak. This trend is observed in Figure 3.30 as with increasing exposure to heat the free oxygen peak to the left becomes less distinct while the silver/gold oxide peak remains relatively the same. Figures 3.28 and 3.29 show that as less

oxygen is used while sputtering or the temperature of the heat exposure is increased a smaller gold oxide peak is observed between 84.5 and 85.0eV.

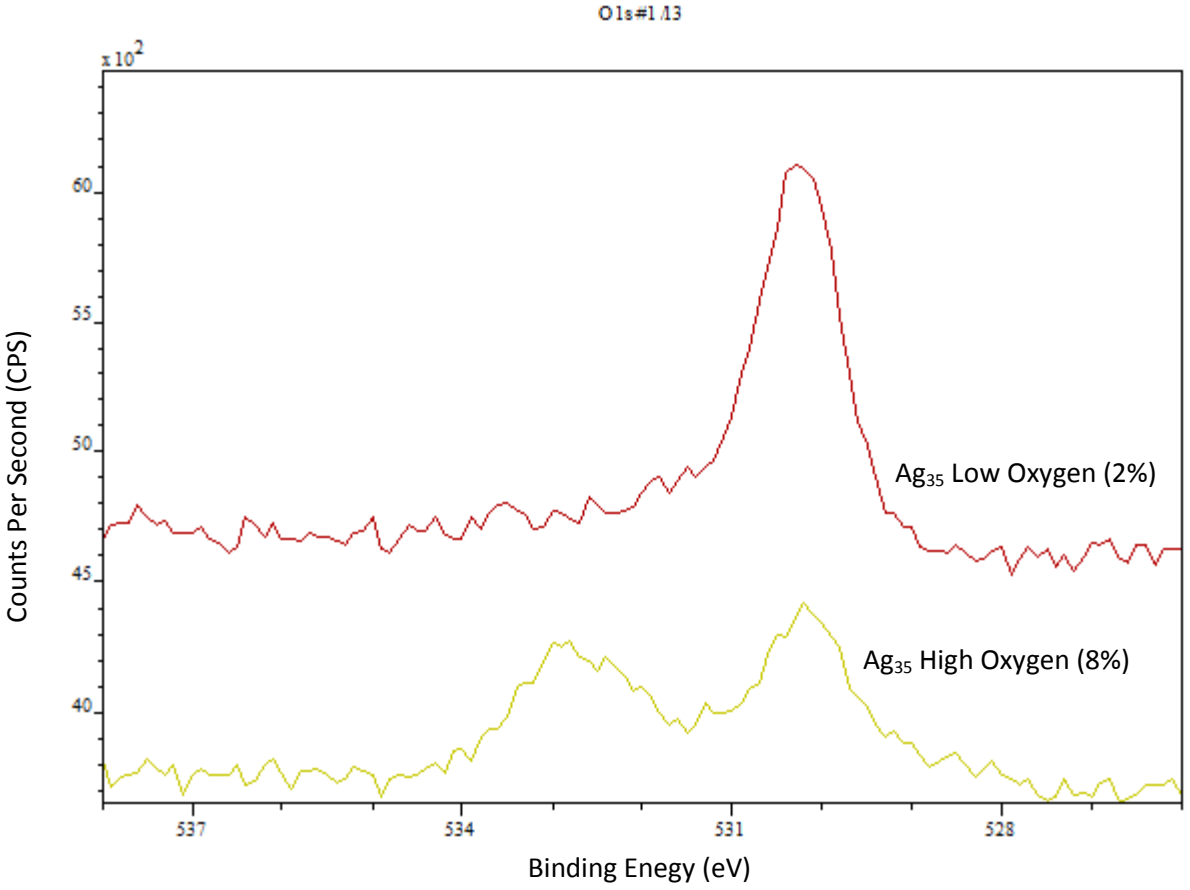

Figure 3.27. O1s XPS spectra of Ag_{35} sputtered in a high oxygen environment (8% O_2) [yellow] and low oxygen environment (2% O_2) [red].

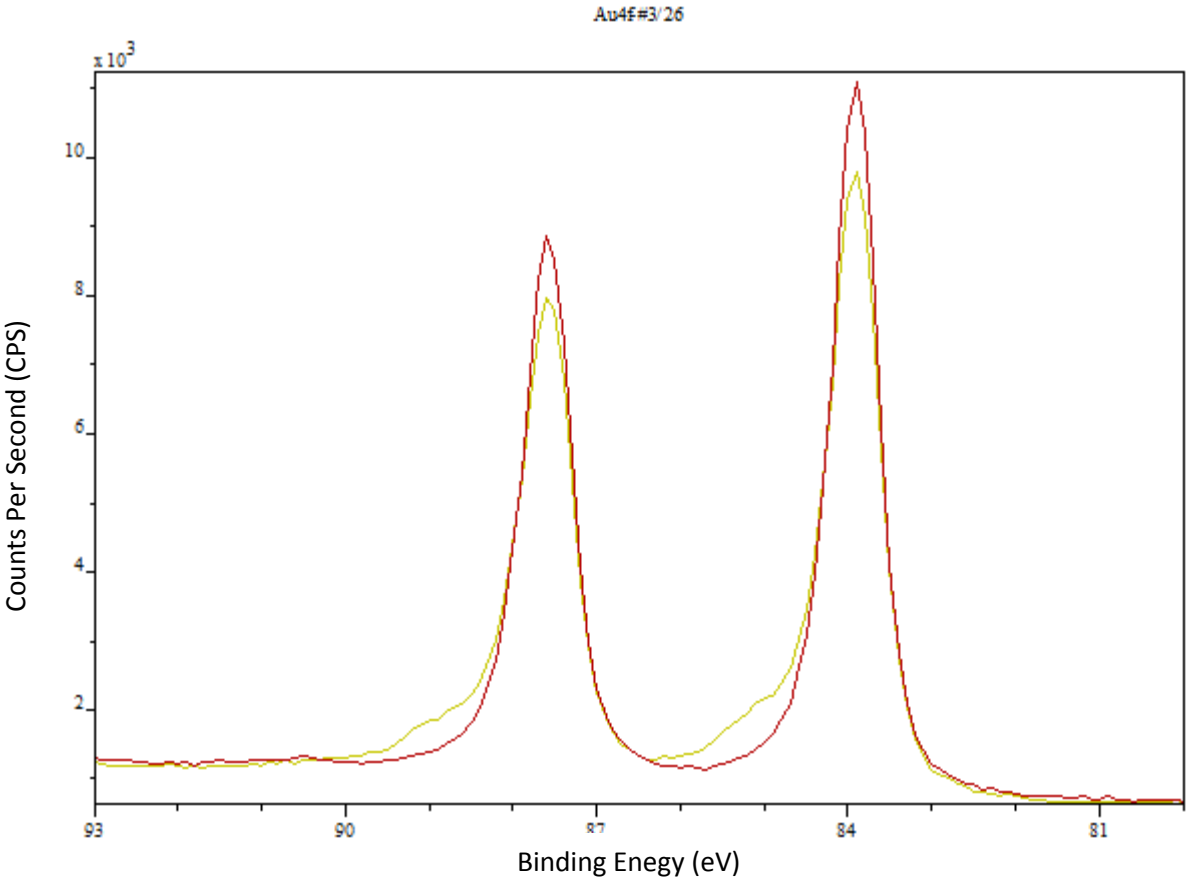

Figure 3.28. Au_4f XPS spectra of Ag_{50} sputtered in a high oxygen environment (8% O_2) [yellow] and low oxygen environment (2% O_2) [red].

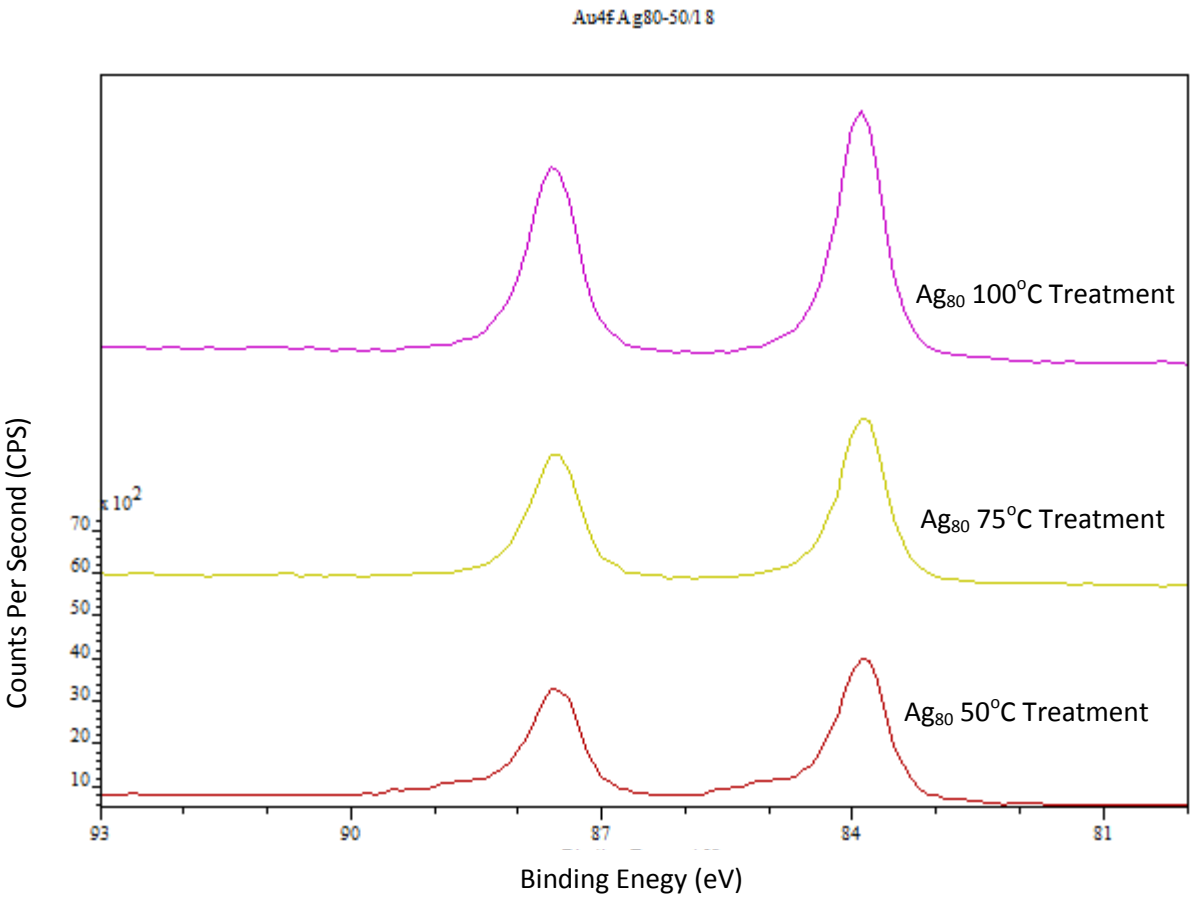

Figure 3.29. Au_4f XPS spectra of Ag_{80} heat treated at 50 (red), 75 (yellow) and 100°C (purple) for 24 hours.

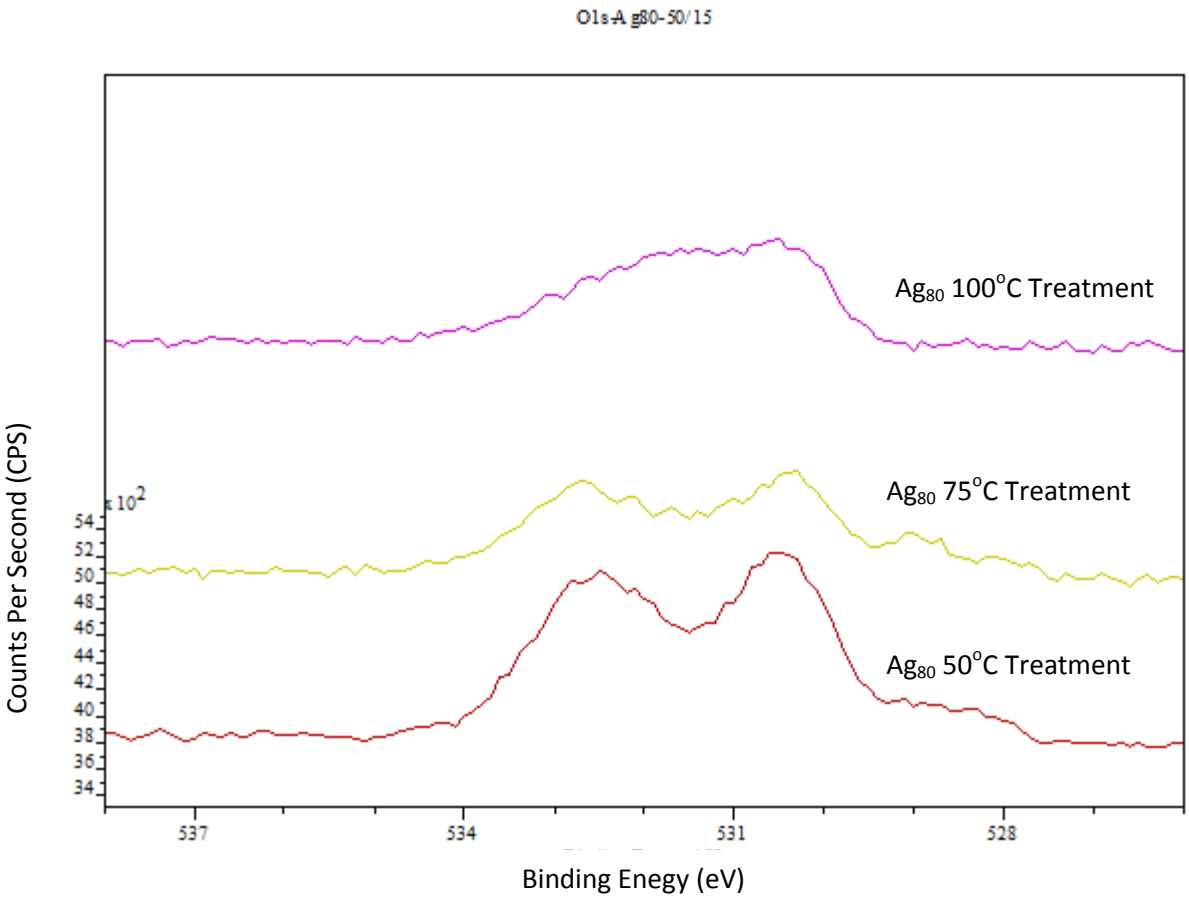

Figure 3.30. O1s XPS spectra of Ag_{80} heat treated at 50 (red), 75 (yellow) and 100°C (purple) for 24 hours.

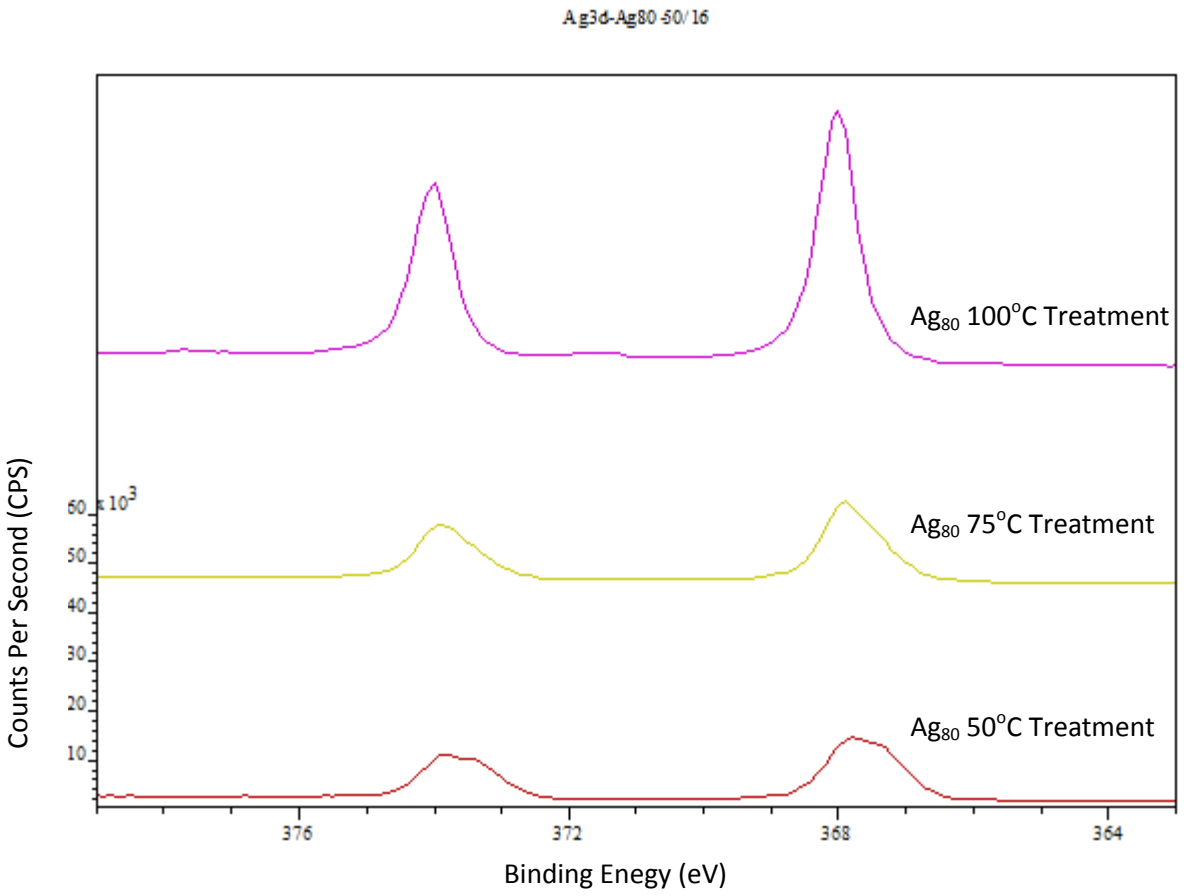

Figure 3.31. Ag_3d XPS spectra of Ag_{80} heat treated at 50 (red), 75 (yellow) and 100°C (purple) for 24 hours.

AAS:

Table 3.8 shows the values for silver released in de-ionized water over 24hours for both the heat treated and the variable oxygen samples. Between 50°C and 75°C treatments the amount of silver released for Acticoat®, Ag100 and Ag50, and decrease for Ag80 and Ag35. The amount of silver released after heat treatment at 100°C was significantly smaller than after treatment at the other temperatures ($p<0.01$). The only significant difference in the oxygen manipulated samples was that $Ag_{80}(8)$ released more silver than $Ag_{80}(2)$ ($p<0.05$). Table 3.9 displays the amount of silver released into a 20.0 g/L

ammonium hydroxide solution for 3 minutes for the sample sputtered at different oxygen levels. Samples with higher oxygen content released more ammonia soluble silver than those with less oxygen.

Table 3.8. Concentration of silver realized by submersing $1in^2$ of dressings into 10mL of deionized water for 24 hours. Values are given in ppm ± standard deviation.

	100°C (ppm)	75°C (ppm)	50°C (ppm)	High Oxygen (ppm)	Low Oxygen (ppm)
Acticoat®	0.68 ± 0.03	12.9 ± 3.5	8.14 ± 2.8	n/a	n/a
Ag_{100}	0.50 ± 0.1	27.3 ± 0.7	20.2 ± 5.8	n/a	n/a
Ag_{80}	0.44 ± 0.07	10.9 ± 1.3	14.3 ± 3.8	14.7 ± 0.6	10.2 ± 1.7
Ag_{50}	0.69 ± 0.02	7.63 ± 1.6	5.5 ± 1.2	5.9 ± 1.1	7.7 ± 0.42
Ag_{35}	0.45 ± 0.03	4.47 ± 1.3	7.07 ± 1.1	4.7 ± 0.6	4.7 ± 0.56

Table 3.9. Concentration of silver realized by submersing $1in^2$ of dressing into 10mL of ammonium hydroxide for 3 minutes. Values are given in ppm ± standard deviation.

	Normal (ppm)	High Oxygen (8%) (ppm)	Low Oxygen (2%) (ppm)
Acticoat®	66.7 ± 4.4	n/a	n/a
Ag_{100}	73.7 ± 4.5	120.9 ± 11.9	18.0 ± 3.7
Ag_{80}	61.0 ± 7.5	123.5 ± 9.9	11.9 ± 0.7
Ag_{50}	50.1 ± 6.6	70.5 ± 3.0	11.6 ± 0.6
Ag_{35}	46.5 ± 3.0	48.9 ± 4.9	4.27 ± 1.1

ICP:

Table 3.10 shows the amount of gold released into 10mL of de-ionized water over 24 hours at room temperature. While Ag50(8) released more gold than Ag50(2) (close to significance at p=0.067) all other differences between high and low oxygen levels were non-significant. Dressings with higher gold content released more gold than those with lower gold content.

Table 3.10. Concentration of gold realized by submersing 1in^2 of dressing into 10mL of distilled water for 24 hours followed by acidification with 10mL of aqua regia. Presented in ppm ± standard deviation.

	High Oxygen (8%) (ppm)	Low Oxygen (2%) (ppm)
Ag_{80}	0.0069 ± 0.0016	0.0070 ± 0.0050
Ag_{50}	0.0198 ± 0.0049	0.0061 ± 0.0015
Ag_{35}	0.0189 ± 0.0020	0.0154 ± 0.0032

Discussion

Biological Data:

Log reduction data showed that dressings sputtered in a low oxygen environment were less antimicrobial than those sputtered in a normal or high oxygen environment. This was supported by the incomplete kill observed with *Pseduomonas* log reductions and the log reductions less than three shown in trials against *S. aureus* for low-oxygen dressings. This data also attests to *S. aureus*'s increased silver resistance as it was better able to resist a kill from a less antimicrobial dressing.

Log reductions on gold/silver dressings completed after heat treatment showed what has already been demonstrated for Acticoat® in the literature. [1,5] Exposure to higher temperature reduced the antimicrobial action of the dressings and this reduction was especially noted with *S. aureus*. It appeared that the dressings with higher gold content were more susceptible to losing their antimicrobial capacities after temperature exposure than dressings with more silver. From what was shown in Chapter 2, this may be because the gold dressings are less antimicrobial to begin with than their counterparts with more silver.

CZOI data supported the previous conclusion that the amount of silver in the dressing was proportional to its biological activity and showed that creation in a low oxygen atmosphere or significant heat treatment served to decrease the dressing's longevity. The increase in longevity observed when the dressings were sputtered in an oxygen rich environment was remarkable and could be due to the creation of significantly more highly mobile silver such as $Ag(OH)_4^-$. This compound has been previously

speculated to occur on Acitcoat® and its creation in higher concentrations could account for increased longevity as it is less likely to be depleted after multiple days of CZOI testing.

Physical Data:

Since most trends observed in the SEM and AFM studies were explained by XPS, XRD and EDS the latter will be discussed first to give background to the images presented first.

XRD showed that sputtering in a higher O_2 environment created dressings with smaller minimum crystallite sizes. This agrees with the current model as silver oxide is thought to pin the dressing structure and more silver oxide should be found in this dressing. Heat treatment at increasing temperatures was found to monotonically increase the crystallite size of the dressings. This is due to more rapid grain growth at increased temperatures causing nanoclusters to coalesce. XRD also showed that heat treatment decreased the silver oxide peak at 33 $^{o}2\theta$ which indicates supports the idea that dressings lose silver oxide as they are heat treated. Interestingly, the 4% oxygen normally used in the process seems to be the minimum amount of oxygen required for the dressings to have a recordable silver oxide concentration by XRD. It was interesting to note that the crystallite size of these dressings is highly modifiable and can be tailored to be anywhere between 4.9 and 31.3 nm. This could impact the production of these wound dressings as a desired crystallite size (an integral property for determining both antimicrobial and anti-inflammatory behaviour) could be modified in a specific dressing by altering the oxygen content of the sputtering system. Coupling this data with the biological data it seems that dressings with higher concentrations of Ag-O bonds are more mobile.

XPS data shows that low oxygen environments reduces the O-O bonds in the dressing and results in a decrease in the amount of gold oxide in the dressings. This observation was supported by trends in the EDS characterizations. This data agrees with what was observed in the biological data gathered as more silver oxide and higher oxidation state silver compounds are known to increase silver mobility. The dressings that incorporated more oxygen compounds in the dressing created bigger

inhibition zones and were more antimicrobial *in vitro*. XPS was also useful for imaging the change in gold oxide concentration as dressings were produced in atmospheres with varying oxygen concentrations. It seems that a certain minimum concentration (around 4%) is required to form gold oxide in considerable quantities on the dressings.

EDS supports the idea that increasing oxygen concentration during the sputtering process; however, it is evident that chemisorbed water may contribute to an unknown fraction of this oxygen signal as heat treated dressings at 100^{o}C show minimal oxygen incorporation. Furthermore, XPS shows that this oxygen tends to be included in O-O bonds rather than in Ag-O bonds. While it is not completely clear which O-O bond is responsible for this extra O-O peak, however, it is thought to be some silver/oxygen coordination complex as O_2 is unlikely to be readily included in the dressings.

SEM and AFM data both supported the assertion that temperature treatment increased the grain size and made a smoother nanostructure. There was a significant reduction of surface area and grain boundaries when the samples were treated at temperatures of 75 and 100^{o}C. The effect of oxygen changes in the sputtering process had a similar result. High oxygen samples appeared more highly pinned and had more grain boundaries than samples with low oxygen. The concentration of silver oxide in the samples is thought to result in pinning the nanostructure and these two processes were observed to have the same net result (a reduction of oxygen in the nanostructure) causing similar trends to emerge. Furthermore, the Ag35(2) experience major cracking not observed in other samples. This could be because the sample is so continuous (smaller grain size) that it is less flexible and less resistant to stress than other samples leading to a cracked appearance upon minor deflection.

Chemical Data:

Dissolution data showed few significant trends; however, it is important to not that the amount of bioactive silver (ammonia-soluble silver) increased significantly with high oxygen sputtering compared to low oxygen sputtering. Furthermore, the amount of gold released was not affected by the oxygen

concentration of the sample. This supports the idea that gold does not behave like silver on these dressings and is not released in complex oxygen containing clusters. More probably, gold can be used as a modifier of surface properties but its actual ability to participate in the antimicrobial properties of the dressing is somewhat limited.

Conclusion

Heat treatment experiments showed that the silver/gold dressings were more susceptible to property change as a result of heating than pure silver dressings. The addition of more oxygen to the microstructure resulted in a more antimicrobial dressings with greater longevity. This 'extra' oxygen is thought to be included in O-O bonds rather than Ag-O bonds thus refuting the notion that the addition of more oxygen just increases the silver oxide concentration in the dressing. Adding extra oxygen increases bioactive silver but does not radically alter the already low amount of gold released; therefore, gold should be used as a property modifier for the dressing rather than a complex included to participate as an antimicrobial compound.

References

1. Landry BK, Nadworny PL, Omotoso OE, Maham Y, Burrell JC, Burrell RE. **The kinetics of thermal instability in nanocrystalline silver and the effect of head treatment on the antibacterial activity of nanocrystalline silver dressings.** *Biomaterials.* 2009;30:6929-39.

2. Demling R, Burrell RE. **The beneficial effects of nanocrystalline silver as a topical antimicrobial agent.** *Leadership Medica.* 2002;16:10 pages.

3. Taylor PL, Ussher AL, Burrell RE. **Impact of heat on nanocrystalline silver dressings Part I: Chemical and biological properties.** *Biomaterials*. 2005;26:7221-29.

4. Wright JB, Hansen DL, Burrell RE. **The Comparative Efficacy of Two Antimicrobial Barrier Dressings: In-vitro Examination of Two Controlled Release Silver Dressings.** *Wounds.* 1998;10:179-188.

5. Nadworny P. **Biological Activity of Nanostructured Silver** [PhD Thesis]. Edmonton, AB: University of Alberta; 2010 [cited December 8 2011]. Available from: http://hdl.handle.net/10048/910.

Chapter 4 – The Effect of Sterilization on the Biological Efficacy of Nanogold/silver Dressings

Introduction

The sterilization of wound dressings is an important concern if they are to be used in an *in vivo* setting. There are numerous concerns when sterilizing a product such as whether the material will cross link, store harmful chemical or suffer a great reduction of activity as a direct result of the sterilization. The characteristics of nanocrystalline silver and gold dressings have been covered in Chapter 2 and the effect of exposing these dressings to heat has been explored as part of Chapter 3. Keeping these characteristics in mind, the effect of different sterilization methods on nanocrystalline silver and gold/silver dressings is studied in this Chapter.

Sterilization options are numerous and can include steam treatment, or exposure to ethylene oxide (EO), radiation or fixatives. For the purposes of this report, steam treatment was not studied as data from Chapter 2 showed that the biological properties of the dressing were seriously reduced after exposure to $100^{o}C$, and fixatives were not studied as they require a long time to exposure and since the inner layers of the dressing are hydrophilic both log reduction and CZOI tests would be difficult to perform on a saturated dressing.

EO is one of the most common sterilization methods used for medical device sterilization. Gaseous EO is used because of its high diffusivity and permeability making packing of the medical product relatively easy and the total sterilization procedure is relatively cheap as large volumes can be sterilized simultaneously. Unfortunately, EO is known to leave toxic residues which can be reduced if the material is subjected to detoxifying scrubbers after sterilization. [1] Relevant process parameters of EO exposure systems include: relative humidity, temperature, dwell time and EO concentration. Preconditioning can increase spore susceptibility to dry heat and aeration helps reduce the amount of

EO residue left on the medical device after processing. [2] Ethylene oxide is a strong alkylating agent which causes the addition of alkyl groups to proteins and DNA by binding to (among other moieties) their amino and carboxyl groups, respectively. [3] This binding renders the cell nonviable.

Gamma irradiation and E-beam sterilization are two types of irradiation sterilization. The choice between these two sterilization methods comes down to a balance between penetration of the sterilization method and damage done to the material. Gamma rays are electromagnetic radiation having a wavelength less than 10 pm and were patented for sterilization in 1921. [4] While they allow materials to be sterilized in their final container since there is very little temperature change of the target, gamma radiation can cause a change in color and odour for the final product. A Sterility Assurance Level (SAL) of 10-6 can be achieved with a 25kGy dose according to Pharmacopoeia.

E-beam sterilization relies on bombarding the substrate with high energy electrons with energies usually in the MeV range. One of the biggest advantages of E-beam sterilization is that the dosing rate is much higher than gamma irradiation allowing for shorter sterilization times to be accomplished. [4] E-beam sterilization like gamma irradiation is an ionizing radiation and it sterilizes the product by inducing electron absorption which can break chemical and molecular bonds and destroy the DNA chain. The important characteristics of and E-beam sterilizer are its absorbed dose and accelerated energy. [4]

The choice of which sterilization method is the most appropriate is heavily dependent on the material that is desired to be sterilized. Material characteristics such as susceptibility to ionizing cleavage may make irradiation techniques undesirable while cracks in the material or organic deposits may extend the length of time needed for sterilization.

The characterization of sterilization methods was limited to biological properties of the dressing. Nanogold/silver dressings were exposed to EO, E-beam or gamma irradiation at conditions reasonable

with industrial standards. The materials were them tested for antimicrobial efficacy and bacteriostatic longevity using log reduction and CZOI testing, respectively.

Materials and Methods

All materials were bought from Fisher Scientific Inc. unless otherwise indicated.

Dressing Fabrication:

Acticoat® was purchased locally (Acticoat®, Smith and Nephew Inc., Largo, Fl). Since gold dressings are not available on the market, all other gold and silver dressings were produced by batch sputtering in our in-house extreme sputtering machine at the University of Alberta. A base pressure of $2x10^{-5}$ Torr and an aquatrap temperature of 200 K were obtained before the system was sealed from the pump and a leak test was preformed. A leak of less than 1 mTorr per minute was considered acceptable. The silver and gold/silver alloys were then sputtered onto high density polyethylene mesh. The targets had a variable weight percent silver with the balance gold. The five targets employed in the study were: all silver (Ag_{100}), 80wt% silver (Ag_{80}), 50wt% silver (Ag_{50}) and 35 wt% silver (Ag_{35}). The nomenclature Ag_{100}, Ag_{80}, Ag_{50} and Ag_{35} will hereafter be used to refer to the dressings created from these targets unless otherwise specified. For clarification, a dressing will be called Ag_{80} because it was sputtered with a target that had 80wt% silver, not because the dressings contains 80wt% silver. While targets with gold were treated as experimental groups, the Ag_{100} dressing was used as a control for Acticoat® to ensure the sputtering process was similar since both products are produced by sputtering 100% Ag. The working pressure of the sputtering machine was 40 mTorr (4% O_2 with the balance Ar). The dressings were sputtered using a constant current of 0.9 A. This resulted in an applied voltage of 300 ± 10 V between the target and substrate (ground). After each dressing was sputtered, the full mesh was removed from the sputtering machine and the sample directly under the middle of the target (a total of $10in^2$ per batch) was immediately cut from the HDPE mesh, placed in sterile bags and stored in the dark at 4^oC.

EO Sterilization:

Samples for EO sterilization were submitted to STERIS® Isomedix Services (Minneapolis, MN) for an EO Engineering Run. Engineering runs expose the product to a generic EO process and are not claimed to be sterile; however, it helps researchers understand how the material withstands the sterilization process. The samples were sealed in gas permeable sterilization pouches (McGaw Park, IL) before processing. Samples were subjected to 25.25 hours of preconditioning at above 50% relative humidity and between 32 and 42^{o}C. Samples were then processed for 8.83 hrs at 37^{o}C and 65% relative humidity at 8inHg of EO. After processing, the samples were then aerated for 8.08 hours at 37^{o}C. A certificate of processing is shown in Appendix 4A.

Gamma Sterilization:

Samples were submitted for gamma sterilization to STERIS® Isomedix Services (Libertyville, IL) for a Gamma Engineering Run. Although dosing could not be guaranteed with this run type, the dosing was noted by the operator to be 25 ± 2 kGy. For the sterilization treatment, the samples were sealed in sterilization pouches (McGaw Park, IL) and shipped in a small cardboard box that they were then sterilized in without removal.

E-beam Sterilization:

Samples were submitted to BeamOne LLC (San Diego, CA) for sterilization by E-beam exposure. samples were sealed in sterilization pouches (McGaw Park, IL) and shipped in a small cardboard box that they were then sterilized in without removal. Minimum and maximum dose specifications were given to be 25 kGy ± 10%. A dosimitry report is given in Appendix 4.B.

Log Reduction:

To quantify the bactericidal properties of each dressing after sterilization, log reduction analysis was performed in triplicate using the same method as Taylor et al 2005. [5] To obtain bacteria in the log-phase growth, first 2 to 3 isolated colonies of *Pseudomonas aeruginosa* (ATCC 27317), *Staphylococcus*

aureus (ATCC 25923) or *Proteus mirabilis* (ATCC 25933) were used to inoculate a flask containing 100 mL of tryptic soy broth (TSB) and the flask was incubated overnight in a rotary shaker at 37°C and 120 rpm. The next morning, one milliliter of this culture was used to inoculate another 100 mL of TSB and incubated for 4 hours under identical conditions. Experimental groups were prepared as follows. An aseptically-cut 1 in^2 (6.45 cm^2) piece of dressing was placed coated-side up on a sheet of plastic (3 cm^2) in an inverted Petri dish lid and inoculated with 0.3 mL of the log phase bacteria. The inoculated dressing was covered with another layer of plastic followed by the upright Petri dish bottom to apply pressure. The inoculated dressings were incubated for 30 mins at 37°C. After incubation, the dressing was immediately placed in 2.7 mL of sodium polysorbate solution (SPS) containing 3.0g of NaCl, 0.050g of sodium thioglycolate, 0.50mL of tween 20 and 0.050h of sodium thiosulphate in 50 mL of deionized water. This solution was used to inactivate the metal ions in the experimental groups and aid in bacterial recovery. By placing the dressing in the SPS, a 1 in 10 dilution was realized. The mixture was then vigorously mixed with a vortex in order to recover bacteria and inactivate noble metals. For control groups, 0.3 mL of the log-phase bacteria was used directly to inoculate 2.7 mL of SPS. The resulting experimental and control solutions were serially diluted to 10^{-6} and 10^{-8} respectively by transferring 0.1 mL to 0.9 mL of phosphate buffered saline (PBS) five times and mixing with a vortex between transfers. Three 20 μL drops of each dilution were pipetted onto tryptic soy agar (TSA), incubated at 37°C for 24 h and then individual colonies were counted. The CFUs from the control groups were used to determine the $\log_{10}$ of bacteria in the original inoculum while the CFUs from the experimental groups were used to calculate the $\log_{10}$ of surviving bacteria. These two values were subtracted to yield the log reduction number. Controls of SPS were also completed to ensure the solution was not toxic to the microorganisms.

CZOI:

The revised form of the Kirby-Bauer assay was used to assess the dressing longevity. [6] *Pseudomonas aeruginosa* was grown to log phase as described for the log reductions. An aseptically-cut 1 in^2 piece of each dressing was placed coated-side down in the center of an inoculated plate and moistened to saturation with 0.3 mL of dH_2O. The plates were covered with their Petri dish lid and incubated overnight at 37°C. The dressings were transferred to a new log-phase bacteria lawn daily. If the dressings appeared dry, they were moistened with 0.1 mL of dH_2O. A total of six transfers were made over a period of seven days. Every day, the zones of bacterial inhibition were measured in two perpendicular directions. The dressing width was subtracted from the zone width for both directions and their results were averaged to yield the CZOI values. Tests were performed in triplicate.

Statistics:

One way ANOVA with Tukey-Kramer Multiple Comparisons were performed using GraphPad Instat version 3.10. For log reductions, only trials with exact numbers (i.e. not greater than numbers) were statistically analysed. This method was also used to test for statistical significance in the CZOI data.

Results and Discussion

Figures 4.1-4.3 show the log reduction of *S. aureus* by sterilized dressings and Figure 4.4 shows the control of the unsterilized dressings. Figures 4.5-4.7 show the log reduction of *P. aeurginosa* for all sterilized gold/silver dressing types and Figure 4.8 displays the log reduction by the unsterilized control. Log reductions with *P. aeurginosa* yielded a maximum kill and therefore were not able to be compared statistically. From this data it can be concluded that all the sterilized dressings are strong antimicrobials when challenged with *P. aeurginosa*. When dressings were sterilized with EO and then challenged with *S. aureus* there was a significant reduction in the observed kill compared to non-sterilized dressings shown in Chapter 2. This is thought to be a result of the dressing's exposure to heat and humidity during the EO sterilization process; however, this was surprising since the materials were only exposed to 40°C temperature. In Chapter 3, dressings were found to retain antimicrobial capacity even up to a 24 hour

treatment at 75^{o}C. This means that either the ethylene oxide or the humidity of the chamber resulted in the reduction of observed properties.

Comparison of the log reductions after sterilization by gamma irradiation and E-beam reduce the observed log reduction compared to those of the same dressings without sterilization. While Ag_{80} and Ag_{50} can seen to have a significant reduction in antimicrobial capability, only Acticoat® could be shown statistically to have a reduce log reduction when sterilized with gamma irradiation compared to E-beam ($p<0.05$). The repressed log reduction with gamma sterilization is thought to result from the different characteristics of the ionizing radiation. While the same dose was delivered with both systems, the electrons used by E-beam sterilization have a much smaller penetration depth than gamma irradiation; therefore, the surface layer of the silver could be affected by the electron beam sterilization but not the bulk silver underneath while the entire dressings could be affected by gamma sterilization. The ionizing radiation could cause silver to oxidize to Ag^{+} thus creating a wound dressing that behaves more like silver nitrate or gold oxide than nanosilver or nanogold. The log reductions shown agree with the data presented for these control compounds in chapter 2 and this is likely what is happening in the system. Additionally, this result could occur as a result of the sterilization process. For example, ionizing radiation could interact with the cardboard or plastic sterilization pouches to release components that may inactivate the silver. If required, further material studies such as XPS would help reveal how the physical nature of the dressing changes when sterilized.

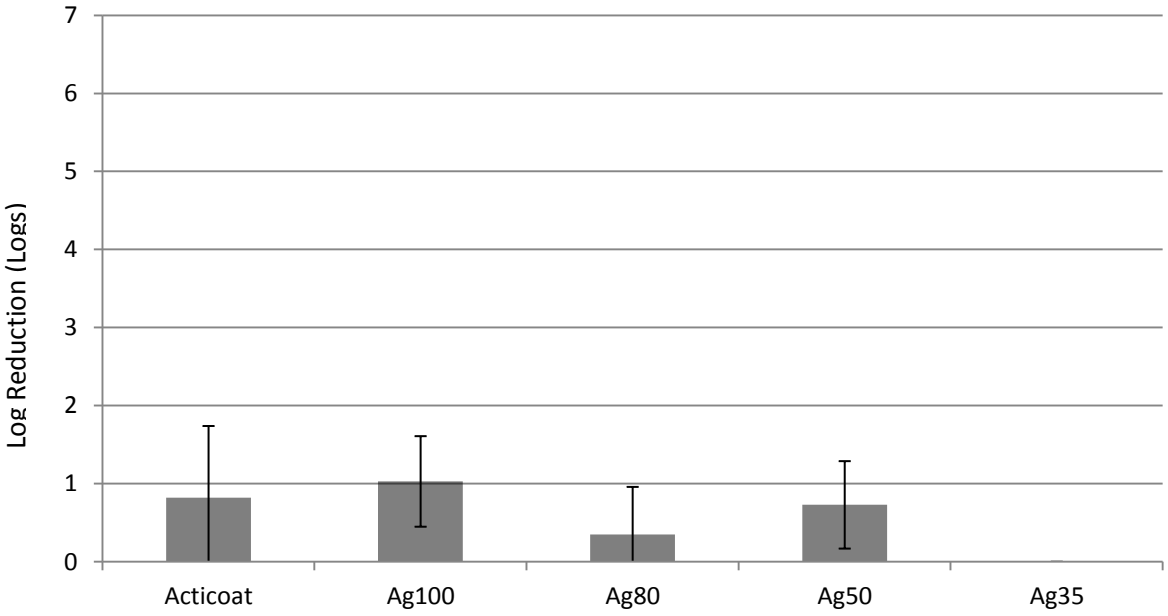

Figure 4.1. Log Reduction of S. aureus after EO sterilization of the dressings.

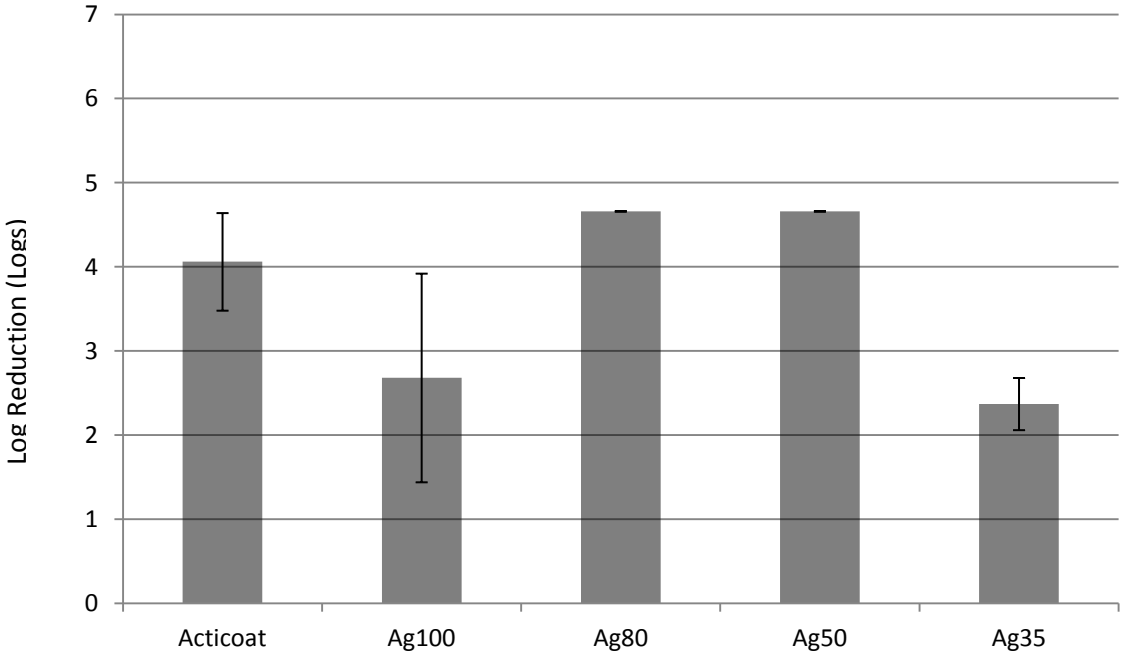

Figure 4.2. Log Reduction of S. aureus after E-beam sterilization of the dressings.

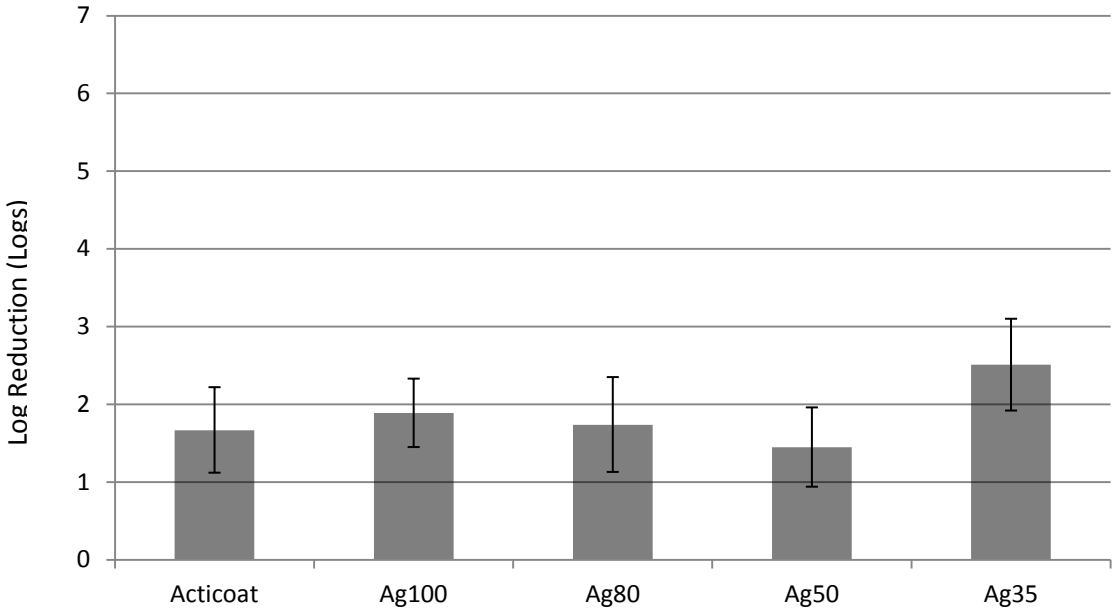

Figure 4.3. Log Reduction of S. aureus after gamma sterilization of the dressings.

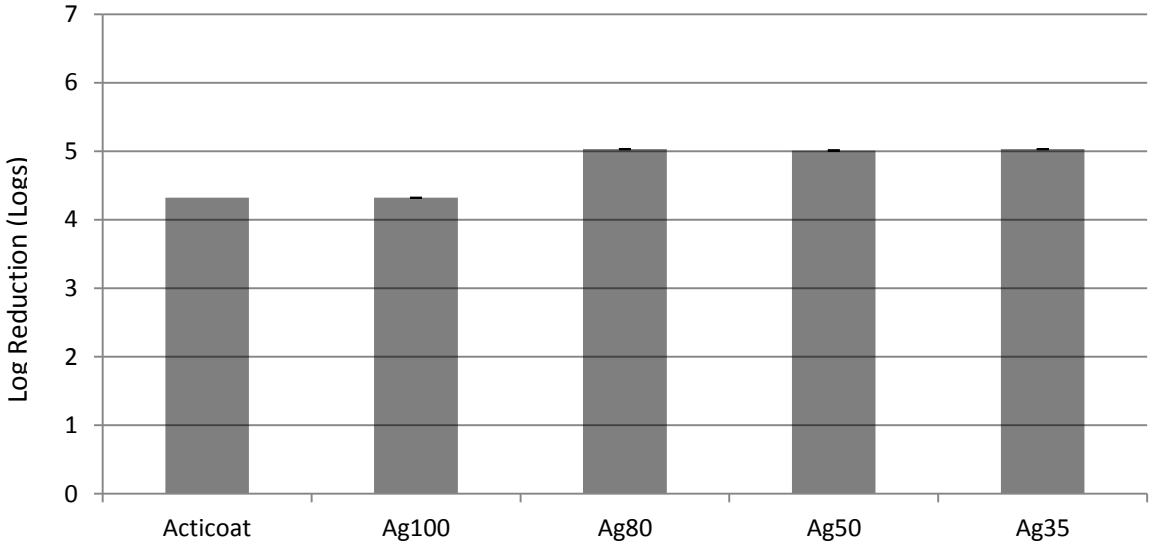

Figure 4.4. Log Reduction of S. aureus without sterilization.

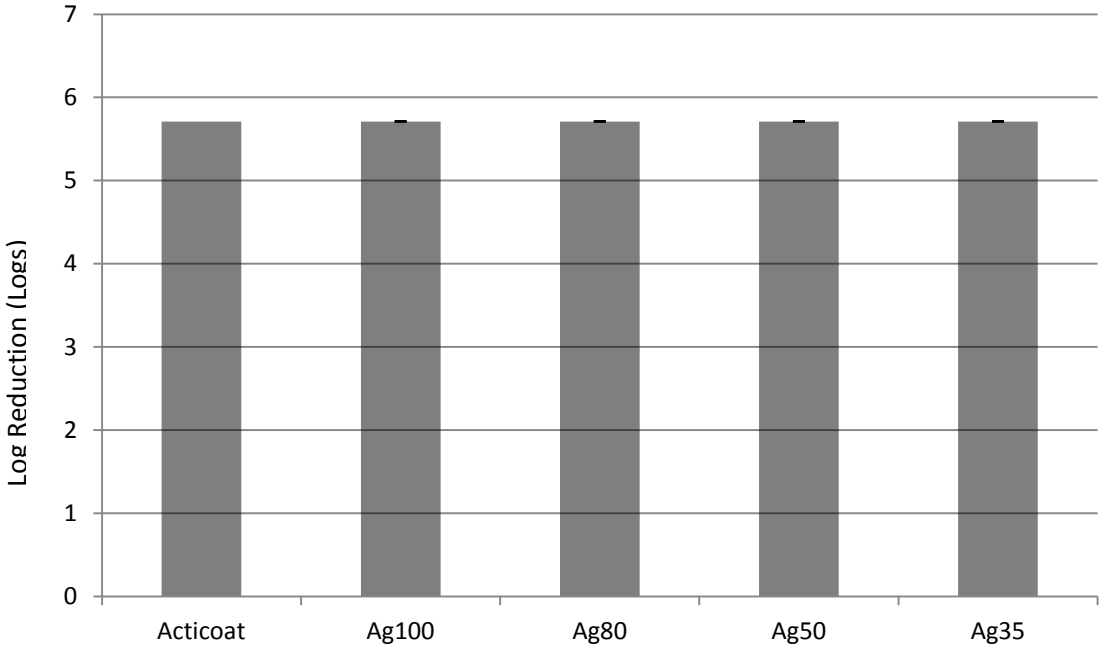

Figure 4.5. Log Reduction of P. aeurginosa after EO sterilization of the dressings.

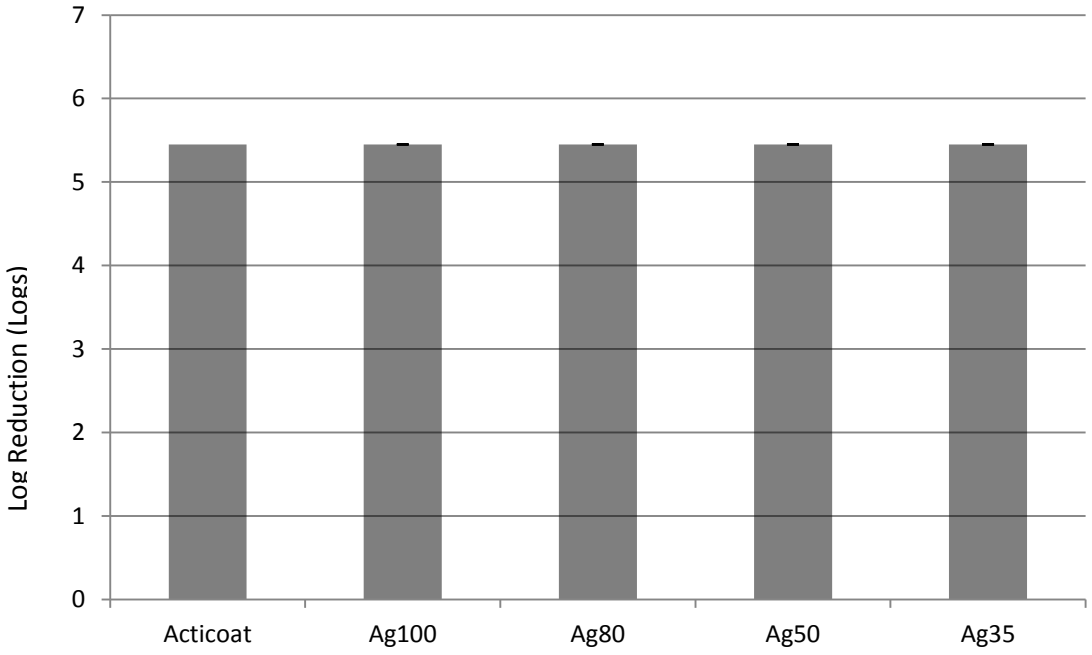

Figure 4.6. Log Reduction of P.aeruginosa after E-beam sterilization of the dressings.

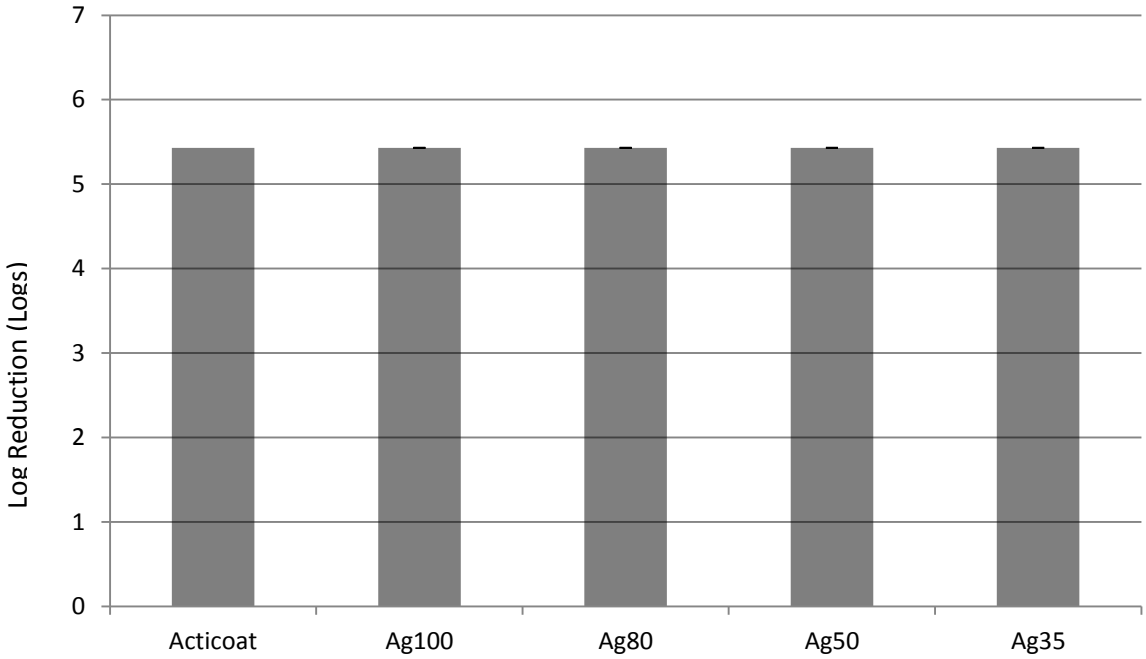

Figure 4.7. Log Reduction of P. aeurginosa after gamma irradiation of the dressings.

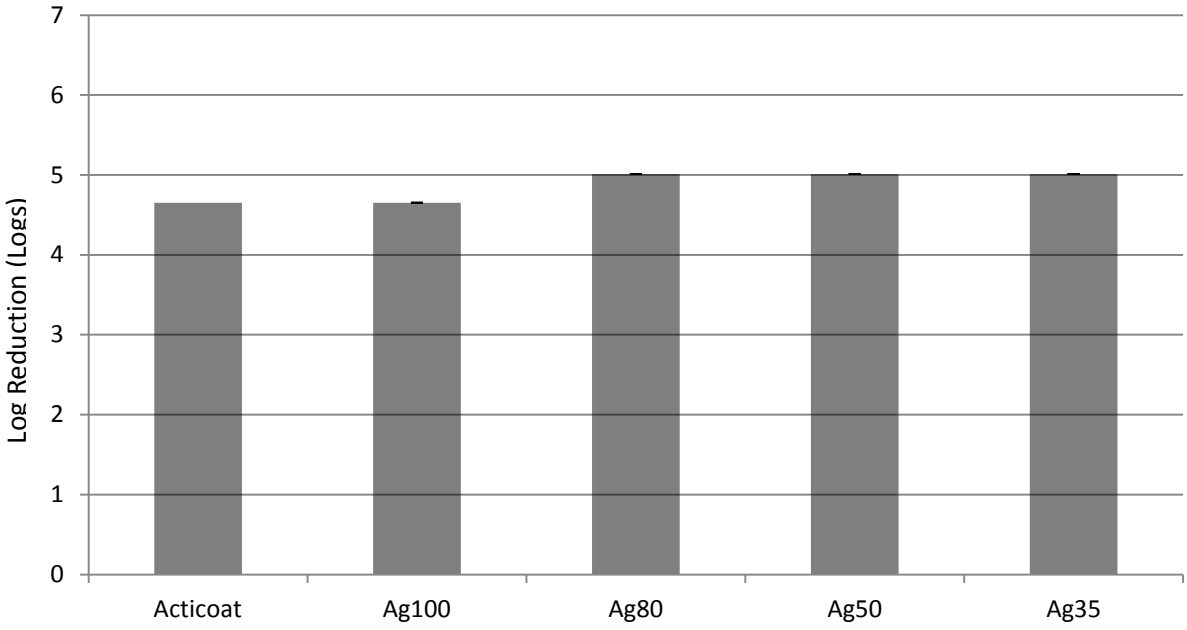

Figure 4.8. Log Reduction of P. aeruginosa without sterilization.

Figures 4.7-4.9 show the CZOI profiles for dressings sterilized with E-beam, EO and gamma sterilization, respectively. As observed previously, there were very few significant differences in the CZOIs created on Day 1, but after a few days of re-plating the dressings with more gold produced smaller zones than those with more silver. Interestingly, all dressings except for Ag_{35} showed a significant increase from Day 1 to Day 3 ($p<0.05$), where only pure silver dressings showed this phenomenon in the unsterilized data presented in Chapter 2. Furthermore, no dressing was bacteriostatic on the seventh day of the trial (all recorded a CZOI of 0 on this day). Overall, the dressings sterilized with E-beam had greater longevity than dressings sterilized with either EO or gamma irradiation. This agreed with log reduction results which showed that E-beam sterilization was the most effective sterilization method for maintaining antimicrobial properties.

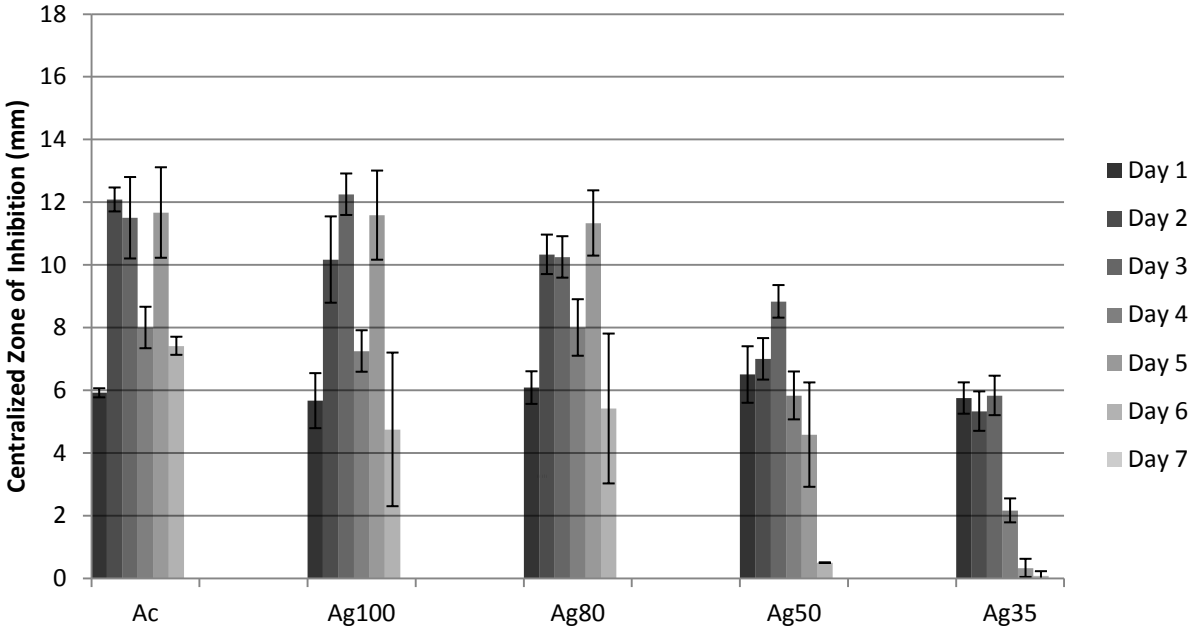

Figure 4.9. CZOI profile for all dressings sterilized with E-beam irradiation.

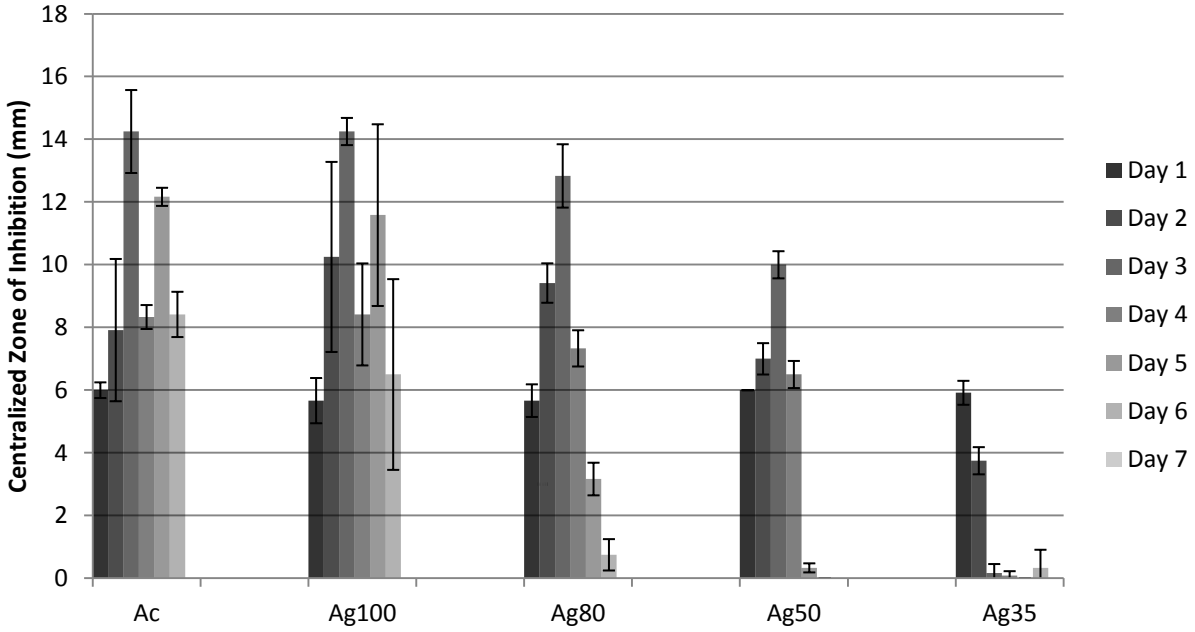

Figure 4.10. CZOI profile for all dressings sterilized with EO.

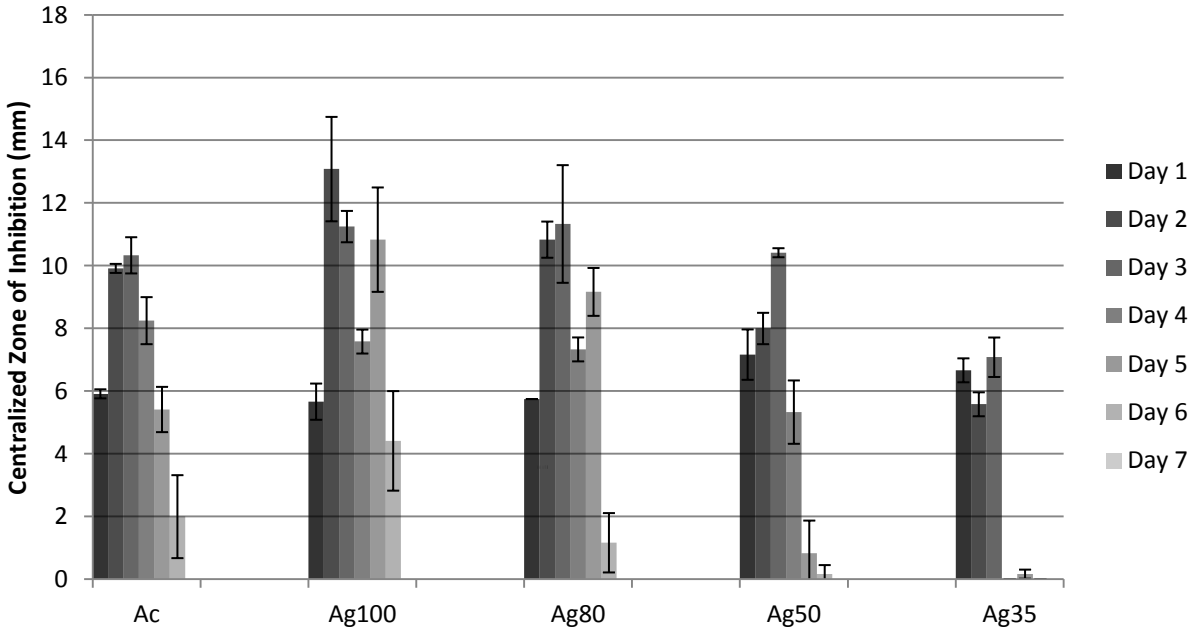

Figure 4.11. CZOI profile for all dressings sterilization with gamma irradiation.

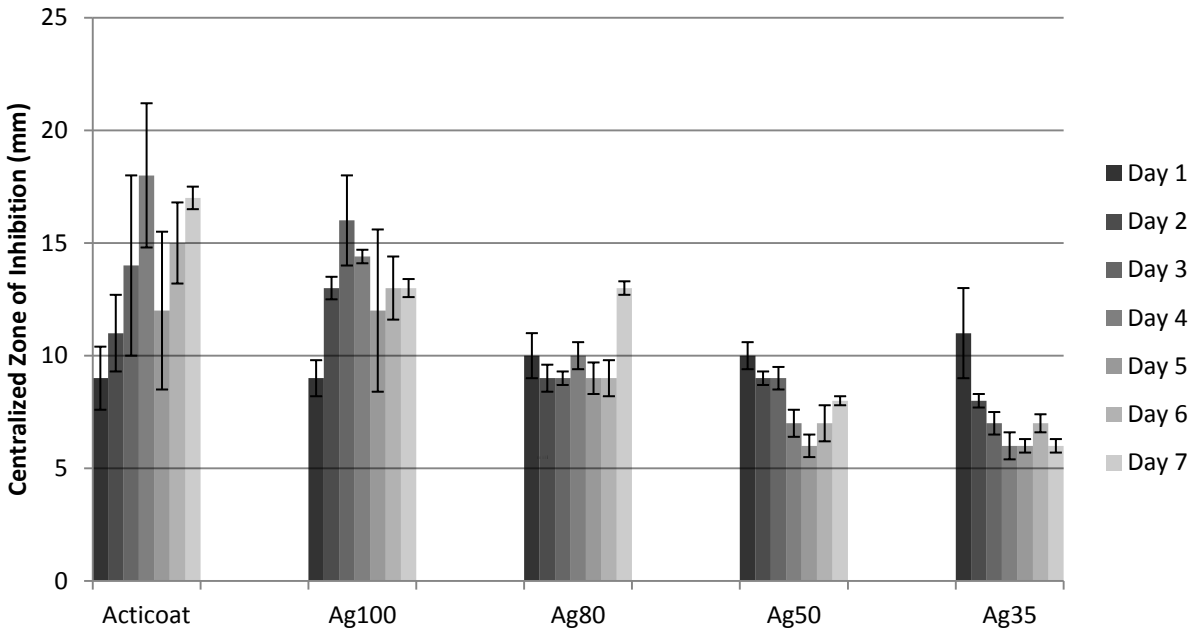

Figure 4.12. CZOI profile of all unsterilized dressings.

Conclusions

Gold silver dressing alloys were sterilized by ethylene oxide, gamma irradiation and exposure to an electron beam. Log reduction results showed that E-beam was the best sterilization method to maintain antimicrobial properties from trials with *S. aureus*; however, all sterilization methods and dressings were strongly antimicrobial again *P. aeruginosa*. Longevity studies complemented antimicrobial capacity as the E-beam was found to be the most effective sterilization method to maintain a bacteriostatic dressing. An unexplained increase in the CZOI from Day 1 to Day 3 was observed in all dressings expect for Ag_{35}. Overall, E-beam is the recommended sterilization method from this study as it maintains the dressing properties higher than other methods utilized in this study.

References

1. Rogers, WR. Sterilization of Polymer Healthcare Products. Shrewsbury: Smithers Rapra; 2005.

2. Kereluk K, Gammon RA, Lloyd RS. **Microbiological Aspects of Ethylene Oxide Sterilization.** *Appl. Microbiol.* 1970;19(1):157-62.

3. Mendes GCC, Brandao TRS, Silva CLM. **Ethylene oxide sterilization of medical decives: A review.** *Am. J. Infect. Control.* 2007;35(9):574-81.

4. Silindir M, Ozer AY. **Sterilization Methods and the Comparison of E-beam Sterilization with Gamma Radiation Sterilization.** *J.Pharm. Sci.* 2009;34:43-53.

5. Taylor PL, Ussher AL, Burrell RE. **Impact of heat on nanocrystalline silver dressings Part I: Chemical and biological properties.** *Biomaterials*. 2005;26:7221-29.

6. Wright JB, Hansen DL, Burrell RE. **The comparative efficacy of two antimicrobial barrier dressings: in vitro examination of two controlled release silver dressings.** *Wounds*. 1998;10:179–88.

Appendix 4A. EO Sterilization Report.

STERIS
Isomedix Services

ENGINEERING TEST CYCLE

EO Processing Work Instructions - STI Chambers

Customer: STERIS Isomedix Services
Customer Lot #: N/A
Chamber Number: 11

STERIS Lot #: 1124011A
Process Code: STE-777
Rev: D

SELECT CYCLE [√] **Check as Completed**

Verify Computer Date is Correct [✓]
Reset Cycle: ✓
Record Selected Cycle #: 777 Operator [signature]
Check Printer Paper Amount: [✓] Date 8.28.11

PRODUCT LOADING

Pallet ID Tag Compare [✓] CYCLE START Time: 1122
Transfer Time Specification MIN / MAX (Minutes): 0 / 60 Actual Transfer Time: 7

COMPARE AND RECORD VALUE	**Specification**	**Printout**
Jacket Temperature:	130	130
Evacuation Level:	2.0	2.0
Humidity Dwell Time:	66	66
EO Pressure Rise:	8	8
Exposure Time:	4.01	241
Number of Nitrogen Washes:	1	1
Number of Air Washes:	1	1

ODMS[RT] Entry (initials) Move from PCR to Chamber: [initials] Operator: [signature]
Date: 8.28.11

END OF CYCLE

Make Copy of Printout: [✓]
Inspect and Sign Printouts: [✓]
Check Alarms are Responded: [✓] Operator LO
Date 8.28.11

PRODUCT UNLOADING

ODMS[RT] Entry (initials) Gas Weight, Chamber to Aeration: LO End of Cycle Time: 2012
Comments: N/A

Appendix 4B. E-Beam Dosimetry Report.

Dosimetry Report / Certificate of E-Beam Processing

BeamOne®
First in electron beam services

PCN Number: S1117209T-T1

Processing Facility: SAN DIEGO

Customer: UNIVERSITY OF ALBERTA
SPSA: UNI TEST24
Product: WOUND DRESSINGS

Lot (s): N/A

Cases: 14 UNITS
Date Processed: 23-Aug-11 **Date Read:** 23-Aug-11

Calibration Curve ID: 3015-BDcombo
DSM Batch: B3 batch BD
DSM Thickness (T in mm): 0.0183
Spectrophotometer: SD8
Wavelength (nm): 554

Correlation STD:Dmin 1.32
Correlation STD:Dmax 1.42

Monitoring DSM Position	DSM Pack. Number	Absorbance Readings (OD)		Response (Ave. OD / T)	Dose kGy	Correlated Dmin, kGy	Correlated Dmax, kGy
S1117209T							
BLOCK	1	0.120	0.120	6.557	4.9	6.5	7.0
S1117209T1							
BLOCK	1	0.255	0.254	13.907	13.8	18.2	19.6
BLOCK	2	0.249	0.249	13.607	13.4	17.7	19.0
					Minimum and Maximum Doses in PCN:	24.2	26.6
					Minimum and Maximum Dose Specifications:	22.5	27.5

Prepared By _____ Date 8/23/11

Audited By _____ Date 8-23-11

Form 02-5009 Revision F

Page 1 of 1